Department of Chemical Engineering

Topological Analysis of Hydrogen Oxidation Reaction Kinetics at Ni/YSZ Anode of the Solid Oxide Fuel Cell

Yasir Rasool Dar

This thesis is presented for the Degree of
Master of Philosophy (Chemical Engineering)
of
Curtin University

May 2011

Declaration

To the best of my knowledge and belief this thesis contains no material previously published by any other person except where due acknowledgement has been made. This thesis contains no material which has been accepted for the award of any other degree or diploma in any university.

Signature:

Date:

Abstract

The understanding of the mechanisms and kinetics of reactions that occur on the electrodes hold the key to further advances in solid oxide fuel cell (SOFC) technology. The typical material widely used as anode in SOFC is Nickel/Yttria-stabilised Zirconia (Ni/YSZ). The kinetics of the hydrogen oxidation reaction mechanism at Ni/YSZ anode of the SOFC is investigated in this work using the reaction route (RR) graph method, which is a relatively new graphical method for the analysis of reaction kinetics based on the electrical analogy.

A mechanism for the hydrogen oxidation reaction consisting of the most promising elementary steps is chosen for the analysis. The RR graph for this mechanism is constructed using the standard procedures. The graph is reduced by exploiting its analogy with electrical resistive circuits. Making use of this reduced graph, an analytical expression for the overall reaction rate is derived for the first time. This rate expression was found to approximate the overall rate obtained using the conventional quasi steady state (QSS) methodology satisfactorily. The reaction pathway containing the two hydrogen spill-over reactions is identified as the dominant pathway in the mechanism. Further analysis reveals that the hydrogen spill-over to oxide ion is the slowest reaction step with highest step resistance and governs the rate of the over-all reaction.

Acknowledgement

My utmost praise goes to ***The Omniscient and Almighty GOD*** without whose guidance this work would not have come to successful completion. I would then like to extend my heartfelt gratitude to my supervisors *Professor Moses Tade* and *Dr. Vijay Periasamy* for their unreserved assistance, critical and sagacious views, inspirational and empowering advises and encouragement. Furthermore, they deserve all the due respect for dedicating their valuable time and unrestrained patience during the course of this research.

It is worth to acknowledge *Professor Datta* and his group at WPI (WORCESTER POLYTECHNIC INSTITUTE, USA) for their contributions in providing me essential technical support and for familiarizing me with RR graph. It pleases me most to offer my deepest appreciation to my chairperson *Dr. Vishnu Pareek* for his kind inspiration and orienting me to the most appropriate research field.

It gives me a great pleasure to courteously recognize *Mr. Shahin and Mr. Anteneh* for they have provided me valuable pieces of advice which I have immensely benefited from. I would also like to thank all the administrative staff of the department of chemical engineering and the faculty as well for they have always been considerately helpful and supportive. My appreciation also goes to all those whose names I failed to mention yet have contributed significantly to this research work.

My study and life would not have been so lovable and exciting without my cheering, cooperative and considerate friends.

Lastly, it is deemed to fervently pass supreme gratitude to my adorable parents and beloved brothers and sisters for their unconditional and invaluable backing which words cannot describe.

Table of Contents

List of Tables

List of Figures

Nomenclature

Symbols:

a_i	Activity of terminal species i
A_ρ	Affinity of elementary reaction ρ
$\mathcal{A}_\rho$	Dimensionless reaction affinity of elementary reaction ρ
E_f^{act}	Activation energy of the forward reaction
E_r^{act}	Activation energy of the reverse reaction
E_{OR}	Electro-motive force
ER	*Empty Route*
FR	*Full Route*
F	Faraday's constant
ΔG_ρ	Gibbs free energy change of the elementary reaction ρ
ΔH_R	Reaction enthalpy
h_i	Molar enthalpy
i_F	Fuel cell current density
$I_\rho^\bullet$	Maximum branch current
I_k	Intermediate species k
INs	intermediate Nodes
$\vec{k}_\rho$	Forward rate Constant
$\overleftarrow{k}_\rho$	Backward rate constant
$\vec{k}_{\rho,\phi_{eq}}$	Equilibrium rate constant for the forward reaction
$\overleftarrow{k}_{\rho,\phi_{eq}}$	Equilibrium rate constant for the reverse reaction

$\vec{k}_\rho^0$	Pre-exponential component of the forward reaction
$\overleftarrow{k}_\rho^0$	Pre-exponential component of the reverse reaction
l_{TBP}	Length of three phase boundary
n	Number of Terminal species
p	Number of elementary reactions
q	Number of intermediate species
r_ρ	Rate of elementary steps
r_{OR}	Rate of overall reaction
$r_\rho^\bullet$	Maximum rate of the elementary reaction ρ
R	Gas Constant
R_ρ	Resistance of elementary reaction ρ
$R_\rho^\bullet$	Resistance of elementary reaction s_ρ , when s_ρ is the RDS
S_ρ	Elementary reaction ρ
ΔS_R	Reaction entropy
S_i	Molar entropy in J/kmol
T	Temperature
TNs	Terminal Nodes
$v_{\rho i}$	Stoichiometric coefficient of species i in reaction ρ
z_{OR}	Reversibility of overall reaction
z_ρ	Reversibility of reaction s_ρ
z	Number of electrons

Greek symbols:

α	Symmetry factor
$\vec{\beta}_{\rho k}$	Stoichiometric coefficient of I_k in reaction step S_ρ
ρ	Elementary reaction

μ	Number of linearly independent reaction routes
η_{act}	Activation Over potential
σ_ρ	Stoichiometric number of elementary reaction ρ
ω_ρ	Step weight for reaction
θ_k	Surface coverage of intermediate species k
$\theta^{\bullet}_{k,\rho}$	Surface coverage of intermediate specie$k$, while considering ρ as RDS
$\Delta\phi$	Electrical potential difference between the electrode and the electrolyte
ψ	Dimensionless factor

Abbreviations:

CHP	combined heat-and power
KFL	Kirchhoff's Flux law
KPL	*Kirchhoff's Potential Law*
MARI	most abundant reactive intermediate
Ni/YSZ	Nickel/Yttria-stabilised zirconia
QE	Quasi-Equilibrium
QSS	Quasi steady state
RLS	Rate Limiting Step
RDS	Rate Determining Step
SOFC	Solid Oxide Fuel Cell

Chapter 1

Introduction and Background

1.1. Introduction

The ever increasing demand for energy will lead to rigorous problems. Green house gases emissions due to utilization of fossil fuels are in fact responsible for the negative impacts on the world's climate. This obviously leads to the idea of reducing the energy consumption. Besides this ideal solution, increasing the efficiency of energy conversion processes can result in reducing green-house gas emissions. To achieve this effervescent goal, fuel cell is a potential contender. At present, thermo-mechanical processes are being employed to generate electrical energy by primarily producing the heat by combustion or thermonuclear reactions and then converting into mechanical and finally into electrical energy. By virtue of Carnot theorem it is also evident that efficiency of such a process cannot exceed a certain limit [1, 2]. On the other hand fuel cells are the most efficient devices yet invented to generate power electrochemically directly from chemical or fuel energy are not restricted by Carnot efficiency limit [3]. In addition to that, a fuel cell operating with hydrogen as a fuel will generate only useful electricity and drinking water, which makes it a zero emission power source. Therefore, development of fuel cells not only provides the way to enhance the efficiency of energy conversion process but also can help to minimize the environmental problems of our planet.

Fuel cells have enormous potential to generate electric power for stationery, portable as well as for transport application. Fuel cells are commonly named based on the type of electrolyte [4]; at present nearly five basic type of fuel cells are under development as given in Table 1.1. Solid oxide fuel cell (SOFC) is the most prominent among them due to its higher efficiency and choice among a range of fuels at higher operating temperature. Although some prototypes are available, the commercializing stage is still facing significant challenges concerning long term stability, cost reduction and performance improvement. SOFC consists of three main components anode, cathode and electrolyte, albeit anode is the central part where fuel is oxidized and electrons for the electrical current are extorted but yet its electrochemistry is not well understood [5, 6]. Moreover, even with the availability of large body of experimental data the mechanistic details of even the simple hydrogen oxidation at anode are ambiguous and still a part of controversial

discussion and it is believed that understanding the mechanisms and kinetics of reactions that occur on the anode near the three-phase boundary is likely to be key to further advances in this area [7].

Reaction Route (RR) Graph is a promising and vigorous graph theoretic approach proposed by Datta and his students [8-11] and is useful to explore the mechanistic and kinetics details of catalytic as well as electrochemical systems. More over analogy of RR graph with electrical network provides means of pruning the mechanism in an easy fashion, which leads to the identification of the rate limiting steps. Combining the approach with Langmuir-Hinshelwood-Hougen-Watson (LHHW) methodology, an explicit rate expression can be obtained, which can be used to enhance the performance of entire system. In this study we investigate a detailed reaction mechanism taken from the work of Vogler et al. [6] for the hydrogen oxidation reaction at nickel/yttria-stabilized zirconia (Ni/YSZ) pattern anode by using the RR graph approach. The results of current study agree well with other results in the literature. In the remainder of this chapter, an introduction of the fuel cell technology along with some basics of fuel cell focusing mainly on SOFC is provided. Towards the end, a glimpse of RR graph technique is given followed by the thesis outline describing the constituents of this thesis.

1.2. Fuel Cell Basics

William Grove was the one who discovered the basic operating principle of fuel cells in 1839, by reversing water electrolysis reaction to generate power from hydrogen and oxygen. Different configuration of fuel cells can be found but the basic operating principle discovered by him still remains unchanged [1].

A fuel cell is an electrochemical “device” that continuously converts chemical energy into electrical energy (and some heat) for as long as fuel and oxidant are supplied.

Thus Fuel cells hold similarities with conventional batteries and engines. For instance, they share the electrochemical phenomena for producing power with batteries and like engines they can operate on a continuous supply of fuel. On the other hand, unlike batteries, a fuel cell does not need recharging. It can operate quietly and efficiently, and with hydrogen as fuel, it generates only power and water. Compared to thermal engines, fuel cells efficiency is not limited by Carnot theorem. Like in typical batteries, the required chemical reactants are not enclosed within the electrochemical device [12]. During the process, the fuel and oxidising agents are supplied externally. In principle, any exothermic chemical reaction that can be separated into a reduction reaction and an oxidation reaction can be exploited in a fuel cell for the generation of electrical power. A schematic diagram of an individual fuel cell is provided in Figure 1.1.

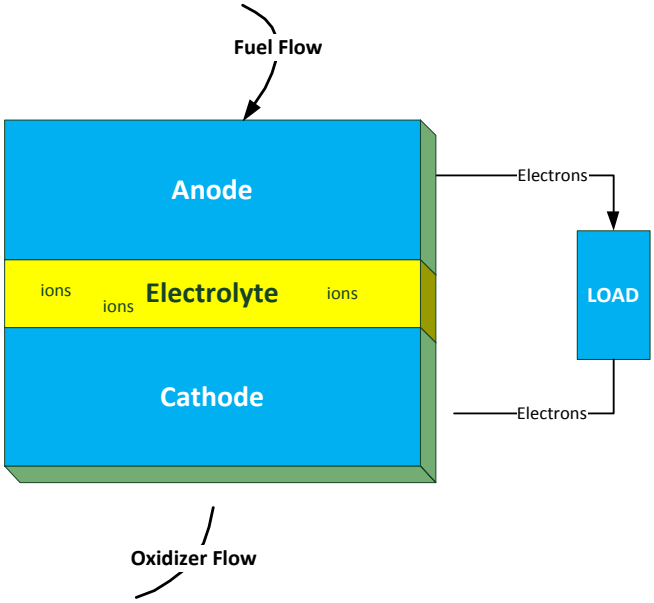

Figure 1.1: Schematic diagram of individual fuel cell [13].

1.2.1. Types of Fuel Cells

Classification of Fuel cells primarily based on the employed kind of electrolyte. This categorization defines the occurrence of different sorts of chemical reactions, implication of various catalysts, the operating temperature range of the cell, required fuel and so on. Presently, several types of fuel cells are under development, each having its own pros and cons and potential areas of applications. A list of best known fuel cells is provided along a schematic representation in Figure 1.2 and their important characteristics are arranged in Table 1.1.

- Alkaline fuel cells (AFCs)
- Polymer electrolyte membrane fuel cells (PEMFCs)
- Phosphoric acid fuel cells (PAFCs)
- Direct methanol fuel cells (DMFCs)
- Molten carbonate fuel cells (MCFCs)
- Solid oxide fuel cells (SOFCs).

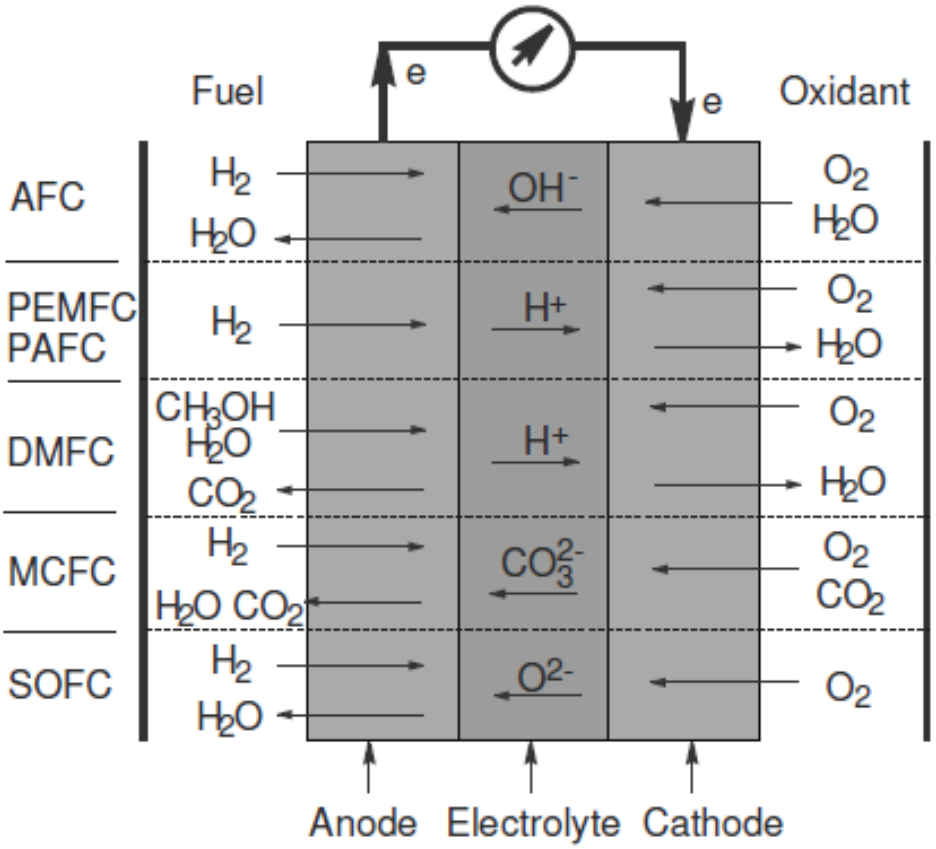

Figure 1.2: Representation of different types of Fuel Cell [14].

Table 1.1: Characteristic of different types of Fuel Cells [2, 3].

Fuel cell Type	***Fuel***	***Electrolyte***	***Charge Carrier***	***Operating Temperature***	***Electric Efficiency***	***Applications***
AFC	Pure H2	KOH	OH^-	60–120°C	35–55%	<5 kW, niche markets (military, space)
PEMFC	Pure H2 (tolerates CO2)	Solid polymer (Nafion)	H^+	50–100°C	35–45%	Automotive, CHP (5–250 kW), portable
PAFC	Pure H2 (tolerates CO2, approx. 1% CO)	Phosphoric acid	H^+	~220°C	40%	CHP (200 kW)
DMFC	Methanol (CH_3OH)	Solid polymer (higher density)	H^+	50–120°C	45%	Portable electronic systems
MCFC	H2, CO, CH4, other hydrocarbons (tolerates CO2)	Lithium and potassium carbonate	CO_2^{3-}	~650°C	>50%	200 kW–MW range, CHP and standalone
SOFC	H2, CO, CH4, other hydrocarbons (tolerates CO2)	Solid oxide electrolyte (yttria, zirconia)	O^{2-}	~1000°C	>50%	2 kW–MW range, CHP and standalone

CHP: Combined heat and power

1.2.2. Operating Principles

For the fuel cell operating at hydrogen the global reaction can be termed as hydrogen oxidation reaction such as

$$H_2 + \frac{1}{2}O_2 \rightleftharpoons H_2O \tag{1.1}$$

In a typical configuration of fuel cell the fuel and the oxidiser are separated by a gas-tight electrolyte therefore the global reaction can be divided into cathodic and anodic reactions [2, 3] i.e.

$$\frac{1}{2}O_2 + 2e^- \rightleftharpoons O^{2-} \qquad \text{Cathode reaction}$$

$$H_2 + O^{2-} \rightleftharpoons H_2O + 2e^- \qquad \text{Anodic reaction}$$

A traditional arrangement of fuel cell normally consists of fuel electrode (anode) and oxygen electrode (cathode) and these electrodes are interconnected via ion-conducting electrolyte. These electrodes are further coupled through a load with the help of external metallic wires outside the cell. The electric current is transmitted by means of electrons in the outer circuit while in the electrolyte it is due to ions. These ions could be different based on different type of electrolyte. Hence these ions conducting electrolyte builds up a concentration gradient that results in electrical voltage between the electrodes. For a fuel cell operating at hydrogen, this maximum voltage is about 1.2 V and can be calculated as (also referred as over circuit potential) [12]

$$E = -\frac{\Delta G}{zF} \tag{1.2}$$

where z is the number of electrons transferred and F is Faraday's constant. The free enthalpy of reaction (ΔG) depends on the concentrations of reactants and products in the gas-mixture actually fed to the anode and cathode. Generally the gases supplied to the electrodes are not pure (e.g., ambient air is used frequently as oxidiser), and from Eq. 1.2 the Nernst equation follows [6, 15]

$$E = -\frac{\Delta G}{zF} - \frac{RT}{zF} ln \frac{a_{H_2O}}{a_{H_2} a_{O_2}^{0.5}} \tag{1.3}$$

where ΔG is the free enthalpy of over all reaction, R the ideal gas constant, T the temperature and a_i activities of the species.

1.2.3. Efficiency

For traditionally employed thermo-mechanical processes such as steam and gas turbine, the efficiency is limited by Carnot's efficiency theorem[2, 6] i.e. for system operated between a hot state T_1 and cold state with temperature T_2, the maximum possible efficiency is

$$\text{Carnot limit} = \frac{T_1 - T_2}{T_1} \tag{1.4}$$

Unlike the above scenario, fuel cells are not subject to Carnot's efficiency limit. In fact, it is usually assumed that if there were no irreversibilities, then Fuel cell might have 100% efficiency [2]. For the reaction given in Eq. 1.1 the total amount of energy released is equal to the free enthalpy ΔH that could be converted into to electrical power. However, in an ideal fuel cell, only the free reaction enthalpy ΔG = ΔH – T ΔS can be converted into electrical energy. Therefore the maximum efficiency of fuel cell can be written as

$$\text{Maximum efficiency} = \frac{\Delta G}{\Delta H} \tag{1.5}$$

At a system temperature of 800 K and a ambient temperature of 300 K a fuel cell running on hydrogen works with a theoretical efficiency of 80% whereas a thermo-mechanical process is limited to 60% [2, 6].

1.3. Solid Oxide Fuel Cells (SOFCs)

Indeed, Solid oxide fuel cells (SOFCs) are the most capable and efficient devices yet invented for the production of electric energy through chemical fuels. The central idea and material was proposed by Nernst and his colleagues [4]. These fuel cells employ solid-ceramic oxidic electrolyte as denoted in the name and operate at high temperatures (500–1000℃). Electrolyte of this type, allows O_2 ions to pass through its crystal lattice via available vacancies. SOFCs acquire a number of dominant features because of their high operating temperature as compared to other types of fuel cells because of which it has been gaining attention of various research groups all over the world during the last two decades. They could obtain an electrical efficiency of nearly 55% and also are capable of working in hybrid systems and when coupled with gas turbines and combined heat-and power (CHP) generation, an efficiency of 70 to 90% can be achieved. Other advantages include a relatively broader spectrum of fuels e.g. hydrogen, methane or natural gas and hydrocarbon. No need of expensive catalyst to start electrochemical reaction. More over solid nature of electrolyte provides geometrical flexibility of cell designs i.e. planer, tubular and monolithic. Beside these positive attributes, need of high-temperature sealing techniques and thermal stresses due to different thermal expansion coefficient of individual materials are also prominent drawbacks. The components of SOFC are discussed below.

A Solid Oxide Fuel Cell (SOFC) is typically composed of four main components. Two porous electrodes, anode and cathode, interposed between an electrolyte made of a particular solid oxide ceramic material [4] and the interconnect that connects the anode of one cell to next cathode in a stack. These components are connected to each other in a pertinent way. A simplified diagram of SOFC is shown in Figure 1.3.

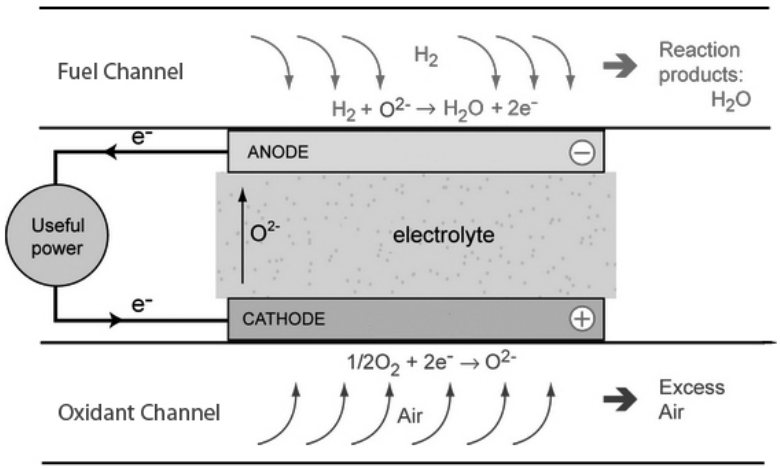

Figure 1.3: Simplified diagram showing oxygen ion and electron flow in SOFC [16].

i) Electrolyte

Due to the high ionic conductivity of electrolyte, oxygen ions can migrate from the cathode to anode and because of the dense structure of the electrolyte the cathodic gas cannot return. Yttria-stabilized zirconia (YSZ) is currently the most widely employed material for the electrolyte manufacture because of its high ionic conductivity for oxygen [4]. Some of the desiring features of a superior electrolyte are;

- Insignificant electronic conductivity
- High ionic conductivity
- Chemical stability during the operation
- Thermal expansion compatibility with other components of cell
- Thermodynamic stability over a operational range of temperature if oxygen partial pressure

ii) Electrodes

***Anode**:* is the electrode where hydrogen and oxygen ions react to produce water. The electrons released in this reaction are migrated to the cathode with the help of an external circuit as in Figure 1.3 The most widely used material for the anode is currently a composite of Ni/8YSZ (*i.e.* Ni with 8% mole of YSZ) as it is highly active for electro-chemical reactions.

***Cathode**:* receives the electrons coming from the anode and convert oxygen to oxygen ions which are then absorbed by electrolyte and ready to go towards the anode. The typical cathode material for SOFC is the strontium doped $LaMnO_3$ (LSM), and during early development, platinum and other noble metals have also been considered.

Here are some other obligatory characteristics of electrodes (anode and cathode) as

- High electron conductivity
- Adequate porosity to allow transport of reactants or/and products to or/ and from triple phase boundary (TBP)
- Compatibility with other cell components in terms of chemical, thermal and mechanical characteristics during fabrication and as in operation.

iii) Interconnect

Ceramics are most popular interconnect used in high temperature SOFC. There are two main disadvantages while using ceramics as interconnect that is high cost and relative rigidity that makes them brittle [4].

1.4. A Glimpse of Reaction Route (RR) Graph Approach

Reaction Route Graph is a relatively new graph theoretic approach, and is highly suitable to explore the kinetics of complex catalytic and electrochemical systems. The fundamental difference between RR graph approach and other graphical techniques is that the nodes or joints in the graph do not necessarily symbolize the individual species, rather just simply indicate the connectivity of different elementary reactions or steps in the reaction network [11]. This characteristic of RR graph plus its analogy with electrical circuits makes it superior for the quantitative analysis. For example the RR graph constructed for the given mechanism can be easily converted into the equivalent electrical resistive circuit. This enables the implementation of well developed laws of electrical circuits e.g. Kirchhoff laws. It eventually leads to the development of accurate and robust rate expressions, which are required for reactor design and for the enhancement of catalyst and processes.

The RR graph application to catalytic reactions basically involves the following steps.

- Determination of surface intermediates for the considered catalyst.
- Enumeration of possible set of elementary reaction pathways involved in the over-all reaction.
- Graphical illustration of the given reaction mechanism in form of reaction network (RR graph) to visualize all the reaction routes (RR).
- Conversion of reaction network into an electrical resistive network by replacing every step with equivalent resistance. This later on facilitates the vigorous flux and kinetic analysis by making use of vast variety of electrical tools available.

More over the reaction resistive network provides a way for the reduction of network by performing a numerical comparison of reaction step resistances and facilitates a rational and logical identification of dominant pathways and eventually the rate the limiting steps (RLS). In addition to this, RR graph approach also allows the development of explicit rate expression for the considered reaction system by means of principles such as quasi-equilibrium (QE) hypothesis, most abundant reactive intermediate (MARI), and LHHW formation, without considering any steps as RLS as a priori.

1.5. Objectives of this Work

The primary objective of this study is to investigate the reaction mechanism of hydrogen oxidation reaction at Ni/YSZ anode of an SOFC by using RR Graph approach. This will result in enhanced understanding of the kinetics of the reaction by pinpointing the rate limiting steps (RLS) in the mechanism. Sometimes it is more desirable to derive an explicit rate expression which is also a focus of this work.

To achieve these goals, firstly a detailed reaction mechanism of hydrogen oxidation reaction at Ni/YSZ will be selected and the required entities to draw the RR graph will be enumerated. The RR graph for the mechanism will be constructed and pruned.

Comparison of various charge transfer pathways will be made as a function of temperature and over potential, which will result in the determination of dominant pathway and rate limiting steps. An explicit rate expression would be derived in terms of the known quantities by exploiting the electrical analogy. The results will be validated by comparing with experimental results from the literature.

1.6. Organization of Thesis

Chapter 1 provides background information of Fuel Cell technology and its significance followed by a glimpse of SOFCs and RR graph approach along with the objectives of this research work.

Chapter 2 describes the quantitative and qualitative studies performed to reveal the mechanistic and kinetic details of hydrogen oxidation reaction at SOFC anode (Ni/YSZ) leading towards a selection of detailed reaction mechanism for the implementation of RR graph approach.

Chapter 3 gives the definitions of essential terminologies of RR graph. Then the reaction routes and the nodes required to draw RR graph for the selected mechanism are enumerated followed by an RR graph for chosen system.

Chapter 4 explains the basics as well as introduces the new form of electrical analogy of RR graph approach. The model equations to estimate the kinetics of surface and charge transfer reactions and consistency of hydrogen oxidation reaction network with the constraints imposed by electrical theory laws are explained. Furthermore, pruning of the graph based on the numerical simulation results is also performed along with a derivation of an explicit rate expression and towards the end a comparison between the results of this study with the published literature is given.

Chapter 5 discusses the outcome of this investigation and provides a summary of the key recommendations.

Chapter 2

Literature Review

2.1. Introduction

Even today the most widely used material as anode in Solid oxide fuel cell (SOFC) is the typical Nickel/Yttria-stabilised zirconia (Ni/YSZ). However studies on SOFC electrodes started back in 1960s and an extensive work has been published since then [5], nevertheless the mechanistic details of even the simple hydrogen oxidation reaction are still ambiguous and are still a topic of controversial discussions [5-7, 17].

Basically hydrogen oxidation reaction can be classified into two broad categories i.e. surface reactions and charge transfer reaction. In the following section, experimental and analytical studies performed to explore the mechanistic details of hydrogen oxidation reaction by most eminent research groups are discussed, bearing in mind the different possible pathways and rate determining steps (RDS). Also, a mechanism which is complete for the purpose of kinetic studies using the reaction route graph method is identified and the different steps involved in the mechanism are discussed.

2.2. Types of Reaction Steps in Hydrogen Oxidation reaction at Ni/YSZ

2.2.1. Surface Reactions

A huge amount of experimental investigations had been performed in order to improve the performance of SOFCs by understanding the kinetics of anode surface reactions. Initially, most of the researcher focused on the structural configuration of anode and primarily investigated the effect of physical parameter and significance of surface reactions. This section basically provides an overview of the previous studies performed by using different SOFC electrode configurations such as point [12, 18-20], pattern [21-26], and cermet [27-30] electrodes.

Guindet et al. [18] investigated oxidation reaction of H_2 at 960°C on a nickel ball pressed onto an YSZ disc and primarily focused at polarization curves and recorded a maximum value of the current density for anode potential of -850 mV versus air. Moreover for lower anodic polarisation between -1000 and -850 mV they suggested that hydrogen oxidation takes place at nickel. Their plots of $log(i)$ and η follows the Tafel plots in [2]. Later on, they addressed the impact of partial pressure of H_2 and H_2O at the performance of Nickel electrode and based on polarization curves, they concluded that charge transfer reaction is not rate determining step [12].

Norby et al. [19] examined the relation between performance of electrode and triple phase boundary (TPB) by using two different structural configurations of electrodes. A nickel wire wrapped around an alumina rod and an electroplated nickel layer with circular holes made by microlithography was used to investigate the influence of partial pressure of H_2 and H_20 at reaction resistance. Finally, they concluded that for the electrode having small TBP and large Ni and YSZ area per unit TBP length, the rate is limited by charge transfer reaction because of restricted TBP length. And on the other side, reaction resistance dominates for the electrodes having large TBP length, smaller accessible area of nickel and YSZ per unit TBP length. In addition to that, they suggested that for the second electrode, the rates are limited because of too small or inactive surface and not due to small TBP length [20].

On the other side, interest in simplified patterned electrodes is increasing due to various reasons. Unlike point electrodes they can be examined after heating and pattern structure also provides access to TBP for unambiguous ex situ detection of morphological changes and potential impurity effect [5, 21, 22, 26]. Furthermore due to simplified electrode, the structural influences can be reduced and this provides a comprehensive way to study the electrochemical process [6].

Mizusaki et al. [21] investigated the reaction kinetics of H_2 oxidation reaction at nickel pattern electrodes and suggested a linear relationship between the electrode conductivity and TBP length. Previously, they had suggested that rate limiting step occur at Ni surface, later on, they had examined the relationship between concentration of adsorbed species and partial pressure of H_2O and H_2. Based on the results and polarization curve, they proposed the following reaction mechanism.

$$H_2 + 2s_e \leftrightarrow 2H_{ad}$$

$$H_2O + s_e \leftrightarrow H_2O_{ad}$$

$$H_2O_{ad} + s_e \leftrightarrow H_{ad} + OH_{ad}$$

$$OH_{ad} + s_e \leftrightarrow H_{ad} + O_{ad}$$

$$O_{ad} \leftrightarrow O_{ad,Ysz} + s_e$$

$$O_{ad,Ysz} + 2e \leftrightarrow O_{o}^{x}$$

$$H_2O_{gas} + s_e \leftrightarrow H_2O_{ad}$$

Where s_e represents the vacant site at Ni, with the adsorbed species on the Ni surface are O_{ad}, OH_{ad}, H_{ad} and H_2O_{ad}. Furthermore they reported that the rate of anodic reaction can be essentially determined through the reaction of H_2O_{gas} and the adsorbed oxygen at Ni surface. Later on Mizusaki et al. [22] performed a study to compare reaction kinetics of H_2-H_20/Ni/YSZ system and H_2-H_20/Pt/YSZ system with the help of impedance measurements at 700 to 850°C, and concluded that the reaction proceeds through the (TPB) of H_2-H_2O/Ni/YSZ and the pathway of the rate-determining reaction is different from that at the TPB of H_2-H_2O/Pt/YSZ. The first one, takes place on the nickel surface close to the TPB, where as the second occur just across the TPB.

Nakagawa et al. [23] examined an intermediate electrode between pattern anode and cermet anode. One depressed arc was found in the impedance diagram by analysing a 2 µm thick nickel layer without a porous YSZ top layer and a second arc was obtained when coated with YSZ. It had been suggested that associated resistance was proportional to the thickness of the applied porous YSZ layer and it might be because of diffusion of H_2O inside the porous YSZ layer. Based on the results it was concluded that for anodic reactions under polarisation an activation process is important and not the diffusion process. De Boer et al. [5] studied nickel pattern electrodes as they prepared different patterns by using lithographic techniques and by varying the width of and the distance between adjacent nickel stripes. Impedance and polarisation measurements were utilized for characterisation purpose and they reached a conclusion that several mechanistic processes can determine the electrochemical performance of nickel pattern anodes. Nevertheless in the range of partial pressure of H_2 and H_2O covered in the experiments they found one of these was a dominated process.

Bieberle et al. [24] presented a new approach based on a combination of modelling, simulation and experiments to examine the Ni pattern structure, and proposed that two electrode processes were mainly affected with variation in length of TBP, whereas one process remain almost constant. They also recommended that polarization resistance is inversely proportional to the TBP length and the electrode process might not be limited because of charge transfer reactions. After wards in another study Bieberle et al. [25] prepared Ni pattern electrodes with well-defined triple phase boundary (TPB) lengths with the aim of investigating the reaction mechanisms. They utilized the techniques of electrochemical impedance spectroscopy to explore the impact of various important parameters like over potential, gas atmosphere, temperature, and pattern geometry on the electrochemical behaviour and compared the results of

their investigations to findings of the complex state-of-the-art Ni-YSZ cermet anodes. They suggested that in a wide range of observed experimental conditions, Ni pattern electrodes were limited by one main electrode process, which might be credited to either the adsorption/desorption of H_2 or to the removal of O_2 from the electrolyte or even both processes might also be combined with a charge transfer reaction. Moreover they proposed, the kinetics of Ni pattern anodes are not limited because of desorption of water or diffusion effects and the partial pressure of water in the fuel gas atmosphere had a catalytic effect on the anode kinetics.

The majority of the experimental studies reported common influence of gas composition and temperature at polarization resistance which might be summed up as, a decreasing trend of polarisation resistance with increase in water vapour content and temperature, whilst an almost constant polarisation resistance pattern when hydrogen content was varied [6]. De Boer suggested that over all, it can be concluded that comparison between the results is difficult, because of the use of different types of electrodes with different ranges of temperature and under different ambient conditions [5, 26, 27].

Moreover, another type of anodes is Ceramic-metal composites ("cermets"). This a typical material used as anodes for solid oxide fuel cell (SOFC). Nickel/yttria-stabilized zirconia (Ni/YSZ) cermets have mostly been used in experimental studies (e.g. [27-32]) as anodes for hydrogen oxidation in SOFCs. Cermet structure is basically used to increase the adhesion between anode and electrolyte furthermore it also provides enhanced stability as compared to nickel and increased number of reaction sites per nominal electrode area.

Mogensen et al. [27] analysed the factors controlling the performance of (SOFC) electrodes, and with the help of commonly used anodes and cathodes, Ni-YSZ and LSM-YSZ. They suggested that H_2 oxidation reaction might be limited by at least three processes and of which one or two depend upon the microstructure and concluded that the electrochemical reaction occurs on both the solid electrolyte and the electrode materials but only in a narrow zone (few μm) along the three-phase-boundary. Primdahl et al. [28] studied the oxidation of hydrogen on Ni/YSZ (cermet) anode with the help of impedance spectroscopy. They varied the temperature, anodic overvoltage, electrode potential and H_2 and H_2O partial pressure and got three distinct arcs in impedance spectra, based on this they suggested that there are at least three rate-limiting processes.

In another study, by means of the galvanostatic current interruption and electrochemical impedance spectroscopy Jiang et al. [29] addressed the H_2 oxidation reaction for Pt and Ni electrodes by varying the H_2/H_2O ratio at 1000°C in (SOFC) with YSZ electrolyte. Based on the results they concluded that catalytic activities of electrode material, electronic conductivity of the YSZ surface and H_2O

content in H_2 gas are significant factors, controlling mechanism and kinetics of H_2 oxidation reaction. They pointed out that effect of water vapours in H_2 gas on the reaction kinetics is very much dependent on the electrode materials and is related to the partial pressure of O_2. Based on polarization and electrochemical impedance spectroscopy results, they suggested two major processes are largely contributing to the reaction kinetics of hydrogen oxidation at given conditions, which are hydrogen adsorption/diffusion on the nickel surface and charge transfer from the electrolyte to the nickel electrode. In another study they inspected the hydrogen oxidation on Ni/ 3 mol% Y_2O_3–ZrO_2 (Ni /Y-TZP) cermet electrodes in moist H_2 environments and proposed the same process as the rate limiting steps as previously [30].

2.2.2. Charge transfer reactions at Ni/YSZ Anode

Because of the controversy about the actual pathway of H_2 oxidation, different researchers attempted to summarise all of the proposed pathway and different possible charge transfer reactions [6, 7, 33]. Bieberle suggested the first quantitative elementary kinetic model for this reaction and assumed oxygen spill-over, two electron charge reaction steps. Williford et al. also reported the similar mechanism at Pt/YSZ anode [34]. Bessler et al. [35] reviewed the elementary reaction steps for H_2 oxidation and primarily focused on the electron charge transfer reactions. Recently, Vogler et al. [7] proposed a quantitative kinetic modelling study to investigate the hydrogen oxidation reaction at Ni/YSZ pattern anode. They suggested a very detailed reaction mechanism primarily focusing on the so called spill over reactions given in Table 2.1 and compared their results with [25] and found that hydrogen spill over pathway can best describe the experimental results. A schematic diagram for all the available charge transfer pathways [6, 7, 35] is given in Figure 2.1 and are explained in this section.

Table 2.1: Reaction mechanism of H2 oxidation reaction at Ni/YSZ anode [6, 7, 17, 36-39]

Type of reaction	Elementary Reactions
YSZ surface reactions	
	$H_2O_{(gas)} + [\,]_{YSZ} \leftrightarrow H_2O_{YSZ}$
	$H_2O_{YSZ} + O^{-2}_{YSZ} \leftrightarrow 2OH^{-}_{YSZ}$
	$O^{x}_{O\ YSZ} + [\,]_{YSZ} \leftrightarrow O^{-2}_{YSZ} + V^{\cdot\cdot}_{o\ YSZ}$
Ni surface reactions	
	$H_2O_{(gas)} + [\,]_{Ni} \leftrightarrow H_2O_{Ni}$
	$H_{2(gas)} + 2\,[\,]_{Ni} \leftrightarrow 2H_{Ni}$
	$H_{Ni} + O_{Ni} \leftrightarrow OH_{Ni} + [\,]_{Ni}$
	$H_2O_{Ni} + O_{Ni} \leftrightarrow 2OH_{Ni}$
	$OH_{Ni} + H_{Ni} \leftrightarrow H_2O_{Ni} + [\,]_{Ni}$
Charge-transfer reactions	
	$H_{Ni} + OH^{-}_{YSZ} \leftrightarrow H_2O_{YSZ} + [\,]_{Ni} + e^{-}$
	$H_{Ni} + O^{-2}_{YSZ} \leftrightarrow OH^{-}_{YSZ} + [\,]_{Ni} + e^{-}$
	$O^{-2}_{YSZ} + [\,]_{Ni} \leftrightarrow O^{-}_{Ni} + [\,]_{YSZ} + e^{-}$
	$O^{-}_{Ni} \leftrightarrow O_{Ni} + e^{-}_{Ni}$
	$O^{-2}_{YSZ} + [\,]_{Ni} \leftrightarrow O_{Ni} + [\,]_{YSZ} + 2\,e^{-}$
	$OH^{-}_{YSZ} + [\,]_{Ni} \leftrightarrow OH_{Ni} + [\,]_{YSZ} + e^{-}$

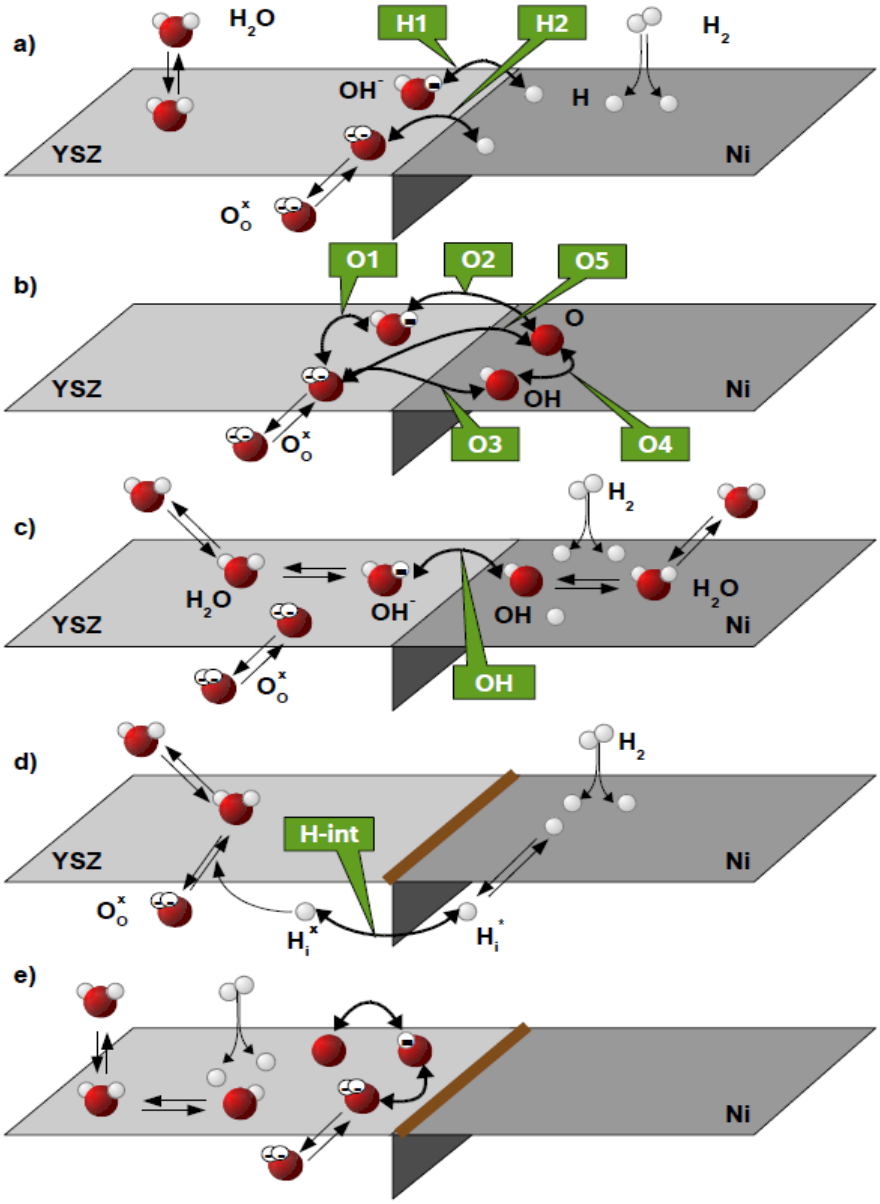

Figure 2.1: (Source: [6, 7]) Schematic representation of charge transfer reactions at Ni/YSZ TBP. a) Spill-over of H2 from the Nickel surface onto an oxygen ion or hydroxyl ion on the YSZ surface. b) Showing Charge-transfer reactions with and without spill-over of oxygen ions from the YSZ surface to the Nickel surface. c) Spill-over hydroxyl from the YSZ surface to the Ni surface. d) Charge-transfer due to an interstitial proton. e) Charge-transfer and reactions on YSZ surface only. In panels d) and e) brown walls represent the possible segregated impurities.

i) Oxygen spillover

The term spillover is often used as reference for transition of species between different surfaces. So oxygen spillover is the transfer of oxygen ions (O_{YSZ}^{2-}) from YSZ surface to Ni surface through a nickel vacant site [35].

$$\mathrm{O}_{\mathrm{YSZ}}^{-2} + [\,]_{Ni} \leftrightarrow \mathrm{O}_{\mathrm{Ni}}^{-} + [\,]_{YSZ} + e_{Ni}^{-}$$

After that, succeeding chemical reactions of hydrogen and oxygen species takes place, e.g. adsorption of molecular H_2 and desorption of H_2O, takes place on metal (Ni) surface. This path could also be found in some other studies [36, 10, 1, 3] furthermore using Pt/YSZ electrodes this charge transfer reaction had been found at cathode [40] and anode [34, 41]. Other than this, transition of hydroxyl ions from the YSZ to the Ni surface could also be the case [42] .

$$\mathrm{OH}_{\mathrm{YSZ}}^{-} + [\,]_{Ni} \leftrightarrow \mathrm{OH}_{\mathrm{Ni}} + [\,]_{YSZ} + e_{Ni}^{-}$$

Oxygen spill over has also been considered as the origin of electrochemical promotion during some studies [43, 44] and experimental verifications for oxygen spillover in Pt/YSZ electrodes through photoelectron emission microscopy and cyclovoltammerty have also been reported [45].

ii) Hydrogen Spillover.

Spillover of hydrogen from the Ni to YSZ surface [35] is another possible pathway which has been highlighted in different experimental and quantitative investigations [5, 36, 39, 46]. H_2 atoms may hop to either an oxygen ion site in an elementary charge-transfer reaction or to a hydroxyl site.

$$\mathrm{H}_{\mathrm{Ni}} + \mathrm{OH}_{\mathrm{YSZ}}^{-} \leftrightarrow \mathrm{H_2O}_{\mathrm{YSZ}} + [\,]_{Ni} + e_{Ni}^{-}$$

$$\mathrm{H}_{\mathrm{Ni}} + \mathrm{O}_{\mathrm{YSZ}}^{-2} \leftrightarrow \mathrm{OH}_{\mathrm{YSZ}}^{-} + [\,]_{Ni} + e_{Ni}^{-}$$

During this pathway H_2 first adsorb at Ni surface and H_2O desorbs at YSZ surface. However any direct experimental evidence of hydrogen spill-over has not been found [35] from the literature [37, 47] as it had been considered with the

assumption of fast surface transport of adsorbed H_2 on the Ni surface and also of protons on the YSZ surface.

iii) Interstitial Hydrogen transfer

Interstitial H_2 atoms and interstitial proton are known to be present in high concentrations and have enough diffusivities in bulk of Ni and YSZ respectively, to support the reaction at typical SOFC temperature. So charge transfer may take place at two phase boundary of Ni and YSZ as below (Kröger-Vink notation).

$$\mathrm{H}_{\mathrm{i\,Ni}}^{\mathrm{x}} \leftrightarrow \mathrm{H}_{\mathrm{i\,YSZ}}^{\cdot} + e_{Ni}^{-}$$

These species are produced via surface adsorption and surface/bulk exchange of H_2 and H_2O on Ni and YSZ respectively. This pathway was also reported by several authors [28, 48, 49] and it might produce higher currents.

iv) Reactive electrolyte

This mechanism has been offered by Brown et al. [50] and in this scenario it might be possible that O_2 ions are oxidised to form O_2 atoms on electrolyte surface (YSZ) and then atomic oxygen can proceed to a chemical reactions on YSZ. As charge transfer can take place over the complete electrolyte surface area if TBP is restricted by segregated impurities [6].

In a recent study Vogler et al. [38] addressed the role of interstitial hydrogen pathway in a 2D modelling study by assuming only this as active charge transfer pathway and suggested that in case if TBP is blocked by secondary phases [51-53] these pathways (iii & iv) might be possible but with clear TBP surface spill-over is most probable pathway. Further estimated parameters taken from the parent work used in this study did not incorporate any effect of these steps, therefore in order to maintain the thermodynamic consistency and to allow a fair comparison these steps have not been considered here. Next, no experimental validation is found for the mechanism at YSZ surface. Vogler found a quantitative similar match from two hydrogen spill over pathway by considering H_2O_{YSZ} dissociation into the mechanism or by assuming fast surface diffusion and excluding H_2O_{YSZ} dissociation reaction, both of the assumptions are chemically reasonable and he suggested the need for a clarification through experimental studies. In this case study H_2O_{YSZ} dissociation step has not been considered instead assuming fast diffusion of hydroxyl group on YSZ surface with simultaneous electro-catalytic effect of water [54].

2.3. Analytical Investigations of H_2 oxidation at Ni/YSZ Pattern Anode

To completely understand the experimental investigation of such a complex electrochemical system as given in the previous section, proper theoretical background is required. H_2 oxidation reaction has been addressed on qualitative basis. Nevertheless, to achieve an unambiguous result, quantitative models are required so that their results can be compared to the experimental findings to develop appropriate understanding of the chemical and physical processes involved in the system and to indentify the dominant reaction pathway and the rate determining steps [6].

Bieberle et al. [17] investigated a simplified anodic (SOFC) system, Ni, H_2–H_2O/YSZ, by utilizing so called state-space modelling (SSM) approach and proposed an electrochemical model for this system. They validated this model by fitting the simulation results to the experimental impedance spectra, observed under well-defined operating conditions. Moreover, they performed repeated analysis by changing the triple phase boundary (TPB) length, the partial pressure of the components, and the over-potential (η). They suggested a reaction mechanism in Kröger-Vink notation as given below;

$$\mathrm{O}_{\mathrm{O}\ \mathrm{YSZ}}^{\mathrm{x}} + [\,]_{Ni} \leftrightarrow O_{Ni} + V_{o\ YSZ}^{\cdot\cdot} + 2e^{-}$$

$$O_{Ni} + H_{\ Ni} \leftrightarrow OH_{Ni} + [\,]_{Ni}$$

$$O_{Ni} + H_2O_{Ni} \leftrightarrow 2OH_{Ni}$$

$$H_{\ Ni} + OH_{Ni} \leftrightarrow H_2O_{Ni} + [\,]_{Ni}$$

$$H_{2(gas)} + 2\,[\,]_{Ni} \leftrightarrow 2H_{Ni}$$

$$H_2O_{(gas)} + [\,]_{Ni} \leftrightarrow H_2O_{Ni}$$

where $[\,]_{Ni}$ represent vacant site at nickel surface, $V_o^{\cdot\cdot}$ and $\mathrm{O}_{\mathrm{O}}^{\mathrm{x}}$ represent vacancies and oxygen ions respectively and four species are attached to Ni surface ($O_{Ni}, H_{\ Ni}, OH_{Ni}, H_2O_{Ni}$). They suggested that to get explicit kinetics of the system, more detailed and extensive data is required and at this stage, it might be unsafe to approve any specific reaction mechanism as dominating pathway. The same mechanism can also be found in some other studies [46, 55] and was recently used to develop a thermodynamically consistent kinetic model for H_2 oxidation reaction

at anode of SOFC by Vijay et al. [55]. They also found that surface reactions may perform greater role in determining the overall rate of reaction.

Bessler et al. [56] proposed a new computational approach that could be used for simulating impedance spectra based on transient numerical simulation of dynamic behaviour of electrochemical systems. They used the same six-step surface reaction model of the hydrogen oxidation reaction at an SOFC Ni/YSZ pattern anode as given in ref [17, 55] and then compared the result with the state–space modelling study of Bieberle and Gauckler [17]. Good agreement was obtained between simulated impedance and experimental data from literature. They concluded that the overall rate is dominated by surface adsorption and desorption reactions and charge transfer reaction is not a rate limiting step. However based on some discrepancies in the model (as it cannot completely describe the anodic reaction especially the surface diffusion and electrolyte surface reaction), an ultimate conclusion about the anodic hydrogen oxidation reaction is not possible. Afterward, Bessler et al. [39] developed a framework for electrochemical simulation of solid oxide fuel cell system which was based on basic physical and chemical process involved in the system. In this study they also addressed the surface reaction at YSZ surface (considering species $\mathrm{H_2O_{YSZ}}$, $\mathrm{OH^-_{YSZ}}$ and $\mathrm{O^{-2}_{YSZ}}$ attached to YSZ) and reported a hydrogen oxidation reaction mechanism at Ni/YSZ as given below.

Charge-transfer reaction

$$\mathrm{H_{Ni}} + \mathrm{OH^-_{YSZ}} \leftrightarrow \mathrm{H_2O_{YSZ}} + [\,]_{Ni} + e^-$$

YSZ surface reactions

$$\mathrm{H_2O_{(gas)}} + [\,]_{YSZ} \leftrightarrow \mathrm{H_2O_{YSZ}}$$

$$\mathrm{H_2O_{YSZ}} + \mathrm{O^{-2}_{YSZ}} \leftrightarrow 2\mathrm{OH^-_{YSZ}}$$

$$\mathrm{O^x_{O\ YSZ}} + [\,]_{YSZ} \leftrightarrow \mathrm{O^{-2}_{YSZ}} + V_o^{\cdot\cdot}{}_{YSZ}$$

Ni surface reactions

$$O_{Ni} + H_{\ Ni} \leftrightarrow OH_{Ni} + [\,]_{Ni}$$

$$O_{Ni} + H_2O_{Ni} \leftrightarrow 2OH_{Ni}$$

$$H_{\ Ni} + OH_{Ni} \leftrightarrow H_2O_{Ni} + [\,]_{Ni}$$

$$H_{2(gas)} + 2\,[\,]_{Ni} \leftrightarrow 2H_{Ni}$$

$$H_2O_{(gas)} + [\,]_{Ni} \leftrightarrow H_2O_{Ni}$$

Vogler et al. [36] presented a combined modelling and experimental study to examine the electrochemical behaviour of Ni/YSZ anode. The model was developed based on elementary kinetic approach to charge transfer reaction and surface reaction which also enable them to compare different pathways presented in the literature. They suggested that the so called hydrogen spill over reaction from Ni to YSZ is the dominating reaction pathway and the charge transfer reaction is the rate limiting step.

$$H_{Ni} + OH^{-}_{YSZ} \leftrightarrow H_2O_{YSZ} + [\,]_{Ni} + e^{-}$$

Recently, Goodwin et al. [57] developed a model to deal with the electrochemical behaviour of pattern anode. They compared different charge transfer pathway and validate their results with the experimental findings of Muzaki at el. [21] and concluded that hydrogen spill over mechanism can explain the experimental results. Mukherjee et al. [58] investigated the electrochemical behaviour by using first principle investigation combined with Density Functional theory calculation (DFT) and statistical thermodynamics. Comparing the H_2 oxidation reaction at different metals they suggested that oxygen adsorption energy can explain the electro-catalytic activity. Rossmeisl et al. [59] calculated the thermodynamic data with the help of Quantum mechanical calculation and compared theoretical activity of hydrogen spill over and oxygen spill over pathway and concluded that surface-adsorbed oxygen play a vital role H_2 oxidation reaction which pointed out that oxygen spill over is the dominant reaction pathway under the given experimental conditions. Furthermore cermet anode has also been studied by several authors, e.g. [32, 49, 60, 61] using different theoretical approaches and the results do not lead to a unique view of hydrogen oxidation reaction.

2.4. Shortlisted reaction steps for further investigation using the RR graph approach

Based on previous literature a list of most promising reaction steps is selected as in Table 2.2, to further investigate with the help of RR graph approach.

Table 2.2: Shortlisted steps of hydrogen oxidation reactions for further study

Elementary Reaction (ERs)	References
YSZ Surface Reactions	
$\mathrm{H_2O_{(gas)}} + [\,]_{YSZ} \leftrightarrow \mathrm{H_2O_{YSZ}}$	[6, 7, 37-39, 57]
$\mathrm{O^X_{O\ YSZ}} + [\,]_{YSZ} \leftrightarrow \mathrm{O^{-2}_{YSZ}} + V_o^{\cdot\cdot}{}_{YSZ}$	[6, 7, 17, 37-39, 55, 57]
Ni Surface Reactions	
$H_2O_{(gas)} + [\,]_{Ni} \leftrightarrow H_2O_{Ni}$	[6, 7, 17, 22, 38, 39, 55, 57, 58, 62]
$H_{2(gas)} + 2\,[\,]_{Ni} \leftrightarrow 2H_{Ni}$	[6, 7, 17, 22, 38, 39, 55, 57, 58, 62]
$H_{Ni} + O_{Ni} \leftrightarrow OH_{Ni} + [\,]_{Ni}$	[6, 7, 17, 22, 38, 39, 55, 57, 58, 62]
$H_2O_{Ni} + O_{Ni} \leftrightarrow 2OH_{Ni}$	[6, 7, 17, 22, 38, 39, 55, 57, 58, 62]
$OH_{Ni} + H_{Ni} \leftrightarrow H_2O_{Ni} + [\,]_{Ni}$	[6, 7, 17, 22, 38, 39, 55, 57, 58, 62]
Charge-Transfer Reactions	
$\mathrm{H_{Ni}} + \mathrm{OH^-_{YSZ}} \leftrightarrow \mathrm{H_2O_{YSZ}} + [\,]_{Ni} + e^-$	[6, 7, 35, 36, 39, 57]
$\mathrm{H_{Ni}} + \mathrm{O^{-2}_{YSZ}} \leftrightarrow \mathrm{OH^-_{YSZ}} + [\,]_{Ni} + e^-$	[6, 7, 35, 36, 57]
$\mathrm{O^{-2}_{YSZ}} + [\,]_{Ni} \leftrightarrow \mathrm{O^-_{Ni}} + [\,]_{YSZ} + e^-$	[6, 7, 35, 36, 57, 58]
$\mathrm{O^-_{Ni}} \leftrightarrow \mathrm{O_{Ni}} + e^-_{Ni}$	[6, 7, 35, 36, 57, 58]
$\mathrm{O^{-2}_{YSZ}} + [\,]_{Ni} \leftrightarrow \mathrm{O_{Ni}} + [\,]_{YSZ} + 2\,e^-$	[6, 7, 35, 36, 57]
$\mathrm{OH^-_{YSZ}} + [\,]_{Ni} \leftrightarrow \mathrm{OH_{Ni}} + [\,]_{YSZ} + e^-$	[6, 7, 35, 36, 57]

Chapter 3

Construction of RR Graph for the Hydrogen Oxidation Reaction Mechanism at Ni/YSZ Anode

3.1. Introduction

The most widely used material as anode for Solid oxide fuel cell (SOFC) is nickel/yttria-stabilized zirconia (Ni/YSZ). Even though a large quantity of experimental data is available yet the mechanistic details of hydrogen oxidation reaction at Ni/YSZ surface are ambiguous [5]. Recently, Voglar et al. [7] proposed a modelling study for the hydrogen oxidation reaction at Ni/YSZ surface; they reported that, the hydrogen oxidation reaction can be formulated globally as in Eq. 3.1 using Kröger-Vink notation for bulk species.

$$H_{2(gas)} + \mathrm{O}^{\mathrm{x}}_{\mathrm{O\ YSZ}} \leftrightarrow \mathrm{H_2O_{(gas)}} + V_o^{\cdot\cdot}{}_{YSZ} + 2\,e^- \tag{3.1}$$

Reaction Route (RR) graph is an incredibly robust and emerging tool, that can potentially be utilized to reveal the mechanistic and kinetic details of catalytic as well as electrochemical reaction system developed by Datta and his students [8-11] . This chapter starts with a brief introduction of RR graph theory in order to explain the basics of this approach. After that a detailed reaction mechanism of hydrogen oxidation at Ni/YSZ pattern anode is demonstrated involving different charge transfer pathways. Later on by using the concept of RR graph approach reaction routes (RRs) and nodes required to obtain RR graph for the selected mechanism are enumerated and eventually a RR graph for the hydrogen oxidation reaction at Ni/YSZ anode is assembled through which all the conceivable pathways resulting in overall reaction (OR) as given in Eq. (3.1) can be topologically traced as *Walks*. In this chapter, the basic reaction route graph theory is discussed. Followed by this a reaction mechanism for the hydrogen oxidation reaction on Ni/YSZ surface is identified and finally the RR graph for this mechanism is obtained.

3.2. Reaction Route Graph Theory

There are two distinctive goals of any type of kinetic analysis [8-11] namely,

1. To evaluate the rates of elementary steps (r_ρ) for a given reaction mechanism, by first determining the unknown concentration of intermediate species in terms of step rate constants and terminal species (reactant & product) activities (concentrations).
2. To develop a relationship between the rate of overall reaction (r_{OR}) and elementary reaction or step rates (r_ρ)

Reaction route graph is a potential tool and robust approach through which these goals can be achieved. The graph drawn for a given reaction mechanism can clarify how various steps are connected to each other forming a reaction network. Furthermore RR graph can be directly converted into an equivalent electrical network by simply substituting the branches signifying the elementary reaction by resistor and the OR by a battery with an EMF related to affinity, or Gibbs free energy of the OR.

3.2.1. Basic Definitions

In order to explain the RR Graph approach important terminologies have been defined by Datta and his students [8-11] as given below;

Reaction Route (RR): or a reaction pathway, or a reaction sequence, is a linear combination of elementary reactions i.e. $\sum_{\rho=1}^{p} \sigma_{g\rho}$ so that, it can eliminate a particular number of intermediate and/or terminal species to produce a reaction. Whereas;

p = Total number of reactions involved in a particular combination

$\sigma_{g\rho}$ = Stoichiometric number (normally, 0, ±1 or ±2) of step S_ρ in the gth RR

Full Route (FR): If a reaction route (RR) can eliminate all the intermediate species such as

$$\sum_{\rho=1}^{p} \sigma_{g\rho}\, S_\rho = OR$$

Where, OR = Over all reaction; then it is termed as a Full Route (FR).

Empty Route (ER): In the same way, if a linear combination or reaction route can eliminate all the species (intermediate and/or terminal) then it is referred as empty route (ER).

$$\sum_{\rho=1}^{p} \sigma_{g\rho}\, S_{\rho} = 0$$

Walk: is an alternating sequence of nodes and branches, starting from one node and proceeding to an ending node in such a way that a given node may not be crossed more than once. A walk starting and ending at the same node is referred to as a cycle, on the other hand, a walk starting from one terminal node and finishing at the other terminal node, is termed as a full route [11].

For a selected mechanism thus an infinite number of combinations of elementary steps can be generated through the linear combination of any two or more RRs but here we are only concerned with the so called direct RRs following the concept of directness or minimality proposed by Milner et al. This means that any direct FR and ER cannot involve more than $q+1$ and $q+2$ steps, respectively. Where q is the number of linearly independent intermediate species, I_k, and by utilizing this concept we can get a finite and unique RRs. A formal stoichiometric algorithm can be employed to enumerate complete set of (direct) FRs and ERs [63].

However, to construct the RR graph for a given mechanism, in fact we are not required to have the whole set of RRs but only a set of linearly independent RRs ($\mu = p - q\ RRs$) are needed that can include both FRs and ERs. Even though, all the other direct RR of unique set can be topologically traced as *walks* on the finally constructed RR graph. Furthermore to draw the RR graph we will also be in need of intermediate nodes (INs) and terminal nodes (TNs) which are based on Quasi-Steady State assumption and also satisfy network laws (e.g. Kirchhoff's Laws) as explained below.

Quasi-Steady-State Assumption: According to the QSS assumption, the rates of formation and consumption of the intermediates species are approximately equal, and can be expressed as

$$\Delta r_i = \sum_{\rho=1}^{p} v_{\rho i}\, r_{\rho} = 0$$

where $v_{\rho i}$ is the stoichiometric coefficient of species i in reaction ρ. So for a selected mechanism the QSS condition can written for all the involved intermediate and terminal species in the system and their linear combination may generate the

whole list of intermediate and terminal nodes or otherwise stoichiometric algorithm can also be used to enumerate whole set of INs and TNs. However, elementary steps are interconnected by INs and elementary steps are connected to OR through TNs. These nodes satisfy the concept of minimality of incidence or directness, in a way that by eliminating a reaction step QSS conditions cannot be fulfilled and are also consistent with Kirchhoff's Flux (or Current) Law (KFL or KCL).

Kirchhoff's Flux (or Current) Law: states that the sum of step rate r_ρ (similar to branch current I_ρ) of all branches going into and out of a node *j* is equal to zero (from mass conservation, same as $V_{\text{node}} = 0$).

$$\Delta r_j \equiv \sum_{\rho=1}^{p} m_{\rho j}\, r_\rho = 0$$

Where as $m_{\rho j} = 1$ if a branch is going into the node and $m_{\rho j} = -1$ if a branch is leaving the node also $m_{\rho j}$ are the elements of the so called incidence matrix of the RR graph. In addition, RR Graphs are also thermodynamically consistent, as they also coincides with Kirchhoff's Potential Law (KPL)

Kirchhoff's Potential Law (KPL): states that the branch affinity, i.e. negative of Gibbs free energy change for a reaction step, $A_\rho = -\Delta G_\rho$ (same as branch voltage V_ρ) of all branches in a cycle or closed walk, sum up to zero,

$$\sum_{\rho=1}^{p} \sigma_{g\rho}\, A_\rho = 0$$

Where the stoichiometric number $\sigma_{g\rho} = 1$ or -1 depending upon the direction of branch and of *walk* in a concerned closed path or cycle. All the estimated (or measured) kinetics should be consistent with this KPL condition and also by using this analogy there is no need to calculate all the rate constant instead some can also be predicted using the KPL relations.

Finally Datta and his students [8-11] have described two main features of a properly drawn RR graph for a given OR and its corresponding reaction mechanism.

1) The directed (with arrows) branches representing the individual elementary steps S_ρ are interconnected through intermediate nodes (INs) in a way that all of the reaction routes (RRs) can be traced on it simply as walks between terminal nodes (TNs), with the overall reaction (OR) depicted as a branch between the TNs.

2) The connectivity of the branches at the INs and TNs is consistent with the QSS condition for the intermediates and terminal species respectively and which are also equivalent to Kirchhoff's Flux (or Current) Law (KFL or KCL) in electrical circuits.

3.3. A Reaction mechanism for Hydrogen oxidation reaction

The reaction mechanism considered for this case study is comprised of 13 elementary reaction steps given in Table 3.1 taken from the work of Vogler et al. [6, 7]. The overall reaction at Ni/YSZ anode considered is given in equation 3.1. This anode half cell reaction mechanism is assumed to have two gas phase species ($H_{2(gas)}$and $\mathrm{H_2O_{(gas)}}$), two bulk lattice YSZ species ($\mathrm{O^X_{O\ YSZ}}$ and $V_{o\ YSZ}^{\cdot\cdot}$), five species attached to Ni surface ($H_{\ Ni}$, O_{Ni}, OH_{Ni}, H_2O_{Ni} and $[\ ]_{Ni}$), four species attached to YSZ surface ($[\ ]_{YSZ}$, $\mathrm{H_2O_{YSZ}}$, $\mathrm{O^{-2}_{YSZ}}$ and $\mathrm{OH^{-}_{YSZ}}$) where as $[\ ]_{Ni}$ and $[\ ]_{YSZ}$ denotes a free surface site at Ni and YSZ surface respectively.

Basically, hydrogen oxidation reaction at Ni/YSZ can be characterized into three categories e.g. Ni surface reactions, YSZ surface reaction and charge transfer reactions. The work of Deutschmann et al. [62] is considered for Ni surface reactions, which was developed using the combination of theory and available surface science and catalysis experiments. Furthermore, it was validated through specifically designed experiment consisting of single cermet anode (no electrolyte or Cathode) in a flow reactor with gas analysis under various conditions of steam reforming and dry reforming. For YSZ surface reaction mechanism (step S_1 and S_2 in Table 3.1) Vogler et al. [6] did not find any experimentally validated literature. Bessler was the one who first demonstrated the different charge reaction pathways [35] which have been focused in various quantitative modelling studies [36, 38] and are also considered in this study. However, the so called interstitial charge transfer is not considered here as it is out of the scope of this study.

Table 3.1: A Reaction Mechanism for Hydrogen Oxidation at Ni/YSZ Pattern Anode [6, 7].

Symbol	Elementary Reaction (ERs)
YSZ Surface Reactions	
S_1	$H_2O_{(gas)} + [\,]_{YSZ} \leftrightarrow H_2O_{YSZ}$
S_2	$O^{X}_{O\ YSZ} + [\,]_{YSZ} \leftrightarrow O^{-2}_{YSZ} + V^{\cdot\cdot}_{o\ YSZ}$
Ni Surface Reactions	
S_3	$H_2O_{(gas)} + [\,]_{Ni} \leftrightarrow H_2O_{Ni}$
S_4	$H_{2(gas)} + 2\,[\,]_{Ni} \leftrightarrow 2H_{Ni}$
S_5	$H_{Ni} + O_{Ni} \leftrightarrow OH_{Ni} + [\,]_{Ni}$
S_6	$H_2O_{Ni} + O_{Ni} \leftrightarrow 2OH_{Ni}$
S_7	$OH_{Ni} + H_{Ni} \leftrightarrow H_2O_{Ni} + [\,]_{Ni}$
Charge-Transfer Reactions	
S_8	$H_{Ni} + OH^{-}_{YSZ} \leftrightarrow H_2O_{YSZ} + [\,]_{Ni} + e^{-}$
S_9	$H_{Ni} + O^{-2}_{YSZ} \leftrightarrow OH^{-}_{YSZ} + [\,]_{Ni} + e^{-}$
S_{10}	$O^{-2}_{YSZ} + [\,]_{Ni} \leftrightarrow O^{-}_{Ni} + [\,]_{YSZ} + e^{-}$
S_{11}	$O^{-}_{Ni} \leftrightarrow O_{Ni} + e^{-}_{Ni}$
S_{12}	$O^{-2}_{YSZ} + [\,]_{Ni} \leftrightarrow O_{Ni} + [\,]_{YSZ} + 2\,e^{-}$
S_{13}	$OH^{-}_{YSZ} + [\,]_{Ni} \leftrightarrow OH_{Ni} + [\,]_{YSZ} + e^{-}$

3.4. Enumeration of (Reaction Routes) RRs and Nodes

The first step to draw the RR graph is to enumerate all, full routes (FRs), empty routes (ERs), intermediate nodes (INs) and terminal node (TNs). Datta and his students [8-11] have developed a detailed stoichiometric algorithm for the enumeration of FRs, ERs, INs, and TNs or alternatively one may evaluate them by doing the simple inspection of the mechanism as described earlier, that knowledge of linearly independent RRs is enough to define the topological features of RR graph [11]. In this case study of hydrogen oxidation electrochemical reaction system at Ni/YSZ anode the considered mechanism includes 13 elementary reaction steps (p=13) and 8 intermediate species (q=8). Following the concept of minimality, a direct FR cannot involve more than q+1 elementary reaction and similarly a direct ER cannot have more than q+2 steps. All the full routes and empty routes for this system obtained by using the stoichiometric algorithm are given in Table 3.4; however a FR or reaction path way can also be represented in a more usual format as $\sum_{\rho=1}^{p} \sigma_\rho S_\rho = OR$ e.g. a FR comprised of steps S_1, S_2, S_4, S_8 and S_9 is illustrated in Table 3.2.

Table 3.2: Illustration of Full Route (FR_1: S_1+ S_2+ S_4+ S_8+ S_9)

		σ_ρ
S_1	$H_2O_{(gas)} + [\,]_{YSZ} \leftrightarrow H_2O_{YSZ}$	1
S_2	$O^{X}_{O\ YSZ} + [\,]_{YSZ} \leftrightarrow O^{-2}_{YSZ} + V_{o\ YSZ}^{\cdot\cdot}$	1
S_4	$H_{2(gas)} + 2\,[\,]_{Ni} \leftrightarrow 2H_{Ni}$	1
S_8	$H_{Ni} + OH^{-}_{YSZ} \leftrightarrow H_2O_{YSZ} + [\,]_{Ni} + e^{-}$	1
S_9	$H_{Ni} + O^{-2}_{YSZ} \leftrightarrow OH^{-}_{YSZ} + [\,]_{Ni} + e^{-}$	1
Net OR	$\boldsymbol{H_{2(gas)} + O^{X}_{O\ YSZ} \leftrightarrow H_2O_{(gas)} + V_{o\ YSZ}^{\cdot\cdot} + 2e^{-}}$	

In the same way an ER involving steps S_5, S_6 and S_7 (Table 3.3) can also be represented as

$\sum_{\rho=1}^{p} \sigma_\rho S_\rho = 0$ i.e.

Table 3.3: Illustration of Empty Route (ER_1: S_5- S_6- S_7)

		σ_ρ
S_5	$H_{Ni} + O_{Ni} \leftrightarrow OH_{Ni} + [\,]_{Ni}$	1
S_6	$2OH_{Ni} \leftrightarrow H_2O_{Ni} + O_{Ni}$	-1
S_7	$H_2O_{Ni} + [\,]_{Ni} \leftrightarrow OH_{Ni} + H_{Ni}$	-1
Net: 0=0		

Table 3.4: Lists of Enumerated FRs and ERs

List of all Full Routes:		**List of all Empty Routes:**	
FR 1	$S_1+S_2+S_4+S_8+S_9$	ER 1	$S_5-S_6-S_7$
FR 2	$S_2+S_4-S_3+S_7+S_9+S_{13}$	ER 2	$-S_1-S_3+S_7-S_8+S_{13}$
FR 1	$S_2-S_3+S_4+2S_5-S_6+S_{12}$	ER 3	$S_{10}+S_{11}-S_{12}$
FR 2	$S_2-S_3+S_4+2S_5-S_6+S_{10}+S_{11}$	ER 4	$S_5-S_9+S_{12}-S_{13}$
FR 3	$S_2-S_3+S_4+S_5+S_7+S_{12}$	ER 5	$-S_1-S_3+S_5-S_6-S_8+S_{13}$
FR 4	$S_2-S_3+S_4+S_5+S_7+S_{10}+S_{11}$	ER 6	$S_5-S_9+S_{10}+S_{11}-S_{13}$
FR 5	$S_1+S_2+S_4+S_5+S_8+S_{10}+S_{11}-S_{13}$	ER 7	$S_1+S_3-2S_5+S_6+S_8+S_9-S_{10}-S_{11}$
FR 6	$S_1+S_2+S_4+S_5+S_8+S_{12}-S_{13}$	ER 8	$S_1+S_3-2S_5+S_6+S_8+S_9-S_{12}$
FR 7	$S_2-S_3+S_4+S_6+2S_7+S_{10}+S_{11}$	ER 9	$S_1+S_3-S_5-S_7+S_8+S_9-S_{10}-S_{11}$
FR 8	$S_2-S_3+S_4+S_6+2S_7+S_{12}$	ER 10	$S_1+S_3-S_5-S_7+S_8+S_9-S_{12}$
FR 9	$2S_1+S_2+S_3+S_4+S_6+2S_8+S_{10}+S_{11}-2S_{13}$	ER 11	$S_1+S_3-S_6-2S_7+S_8+S_9-S_{10}-S_{11}$
		ER 12	$S_1+S_3-S_6-2S_7+S_8+S_9-S_{12}$
FR 10	$2S_1+S_2+S_3+S_4+S_6+2S_8+S_{12}-2S_{13}$	ER 13	$-S_6-S_7+S_9-S_{10}-S_{11}+S_{13}$
FR 11	$S_2-S_3+S_4-S_6+2S_9-S_{10}-S_{11}+2S_{13}$	ER 14	$-S_6-S_7+S_9-S_{12}+S_{13}$
FR 12	$S_2-S_3+S_4-S_6+2S_9-S_{12}+2S_{13}$	ER 15	$-S_1-S_3-S_6-S_8+S_9-S_{10}-S_{11}+2S_{13}$
FR 13	$S_1+S_2+S_4+S_6+S_7+S_8+S_{10}+S_{11}-S_{13}$	ER 16	$-S_1-S_3-S_6-S_8+S_9-S_{12}+2S_1$
FR 14	$S_1+S_2+S_4+S_6+S_7+S_8+S_{12}-S_{13}$		

According to Horituti-Temkin theorem, only $\mu = p\text{-}q$=13-8=5 are the linearly independent RRs which may include FRs and ERs and the remaining are the linear combination of one or more RRs. Moreover only $p-(q+1)$ = 13-(8+10) = 4 of the ERs are linearly independent [10]. The interconnectivity of elementary steps and OR is based at Quasi Steady State (QSS) assumptions of intermediate and terminal species respectively. So INs (intermediate nodes) are enumerated stoichiometrically based on the QSS (Quasi steady state) conditions of the linearly independent intermediate species. And by definition, a direct QSS condition at any node, cannot involve more than $p-(q-1)$ = 13-8+1= 6 rates. QSS condition for the intermediate and terminal species are given in Table 3.5.

Table 3.5: QSS condition for intermediate and terminal species involved in hydrogen oxidation at Ni/YSZ anode.

Intermediate Species		
Q_1	$-r_1+r_8=0$	H_2O_{YSZ}
Q_2	$r_3-r_6+r_7=0$	H_2O_{Ni}
Q_3	$r_2-r_9-r_{10}-r_{12}=0$	O^{-2}_{YSZ}
Q_4	$-r_5-r_6+r_{11}+r_{12}=0$	O_{Ni}
Q_5	$r_{10}-r_{11}=0$	O^{-}_{Ni}
Q_6	$-r_8+r_9-r_{13}=0$	OH^{-}_{YSZ}
Q_7	$r_5+2r_6-r_7+r_{13}=0$	OH_{Ni}
Q_8	$2r_4-r_5-r_7-r_8-r_9=0$	H_{Ni}
Terminal Species		
	$r_2 = r_{OR}$	$O^{X}_{O\ YSZ}$
	$r_4 = r_{OR}$	$H_{2(gas)}$
	$r_1-r_3= r_{OR}$	$H_2O_{(gas)}$
	$r_2 = r_{OR}$	$V^{\cdot\cdot}_{o\ YSZ}$
	$r_8+r_9+r_{10}+r_{11}+2r_{12}+r_{13}= 2r_{OR}$	e^-

3.5. Construction of RR graph

From previous work [11, 63-66], it can be observed that different approaches had been utilized to construct the RR graph. In some cases, a set of linearly independent RRs was selected and the shortest FR was identified. All the ERs were then added on it in such a way that the final form of RR graph was achieved. But in others, construction of RR graph was started by making a cyclic graph first, with the help of linearly independent ERs. Later, the remaining steps (adsorption/desorption) were added into the cyclic graph until the final form of the graph was obtained. Moreover, some examples can also be found in which intermediate nodes have been used as a starting point to which the ERs were added and finally FRs were satisfied. Therefore, different methods could be used to draw the graph, but the obtained RR graph should follow the constraints set by the conservation principles.

Once the FRs, ERs, INs and TNs have been obtained, the RR graph can be constructed. By analysing the enumerated lists of FRs and ERs a set of five linearly independent RRs has been selected from Table 3.2 to start with as given below.

FR 1 $S_1+ S_2+ S_4+ S_8+ S_9$
ER 1 $S_5-S_6-S_7$
ER 2 $-S_1-S_3+S_7-S_8+S_{13}$
ER 3 $S_{10}+S_{11}-S_{12}$
ER 4 $S_5-S_9+S_{12}-S_{13}$

In this case, we will start constructing the RR graph by first making a cycle graph and with the help of linearly independent ERs (i.e. ER_1, ER_2, ER_3, ER_4) given in Figure 3.1 and then we will add the other remaining steps in the cycle graph so that all the FR can be satisfied and traced as *Walks* on the final form of RR graph. From the Figure 3.1 it can be observed that some ERs have a few common steps, e.g. ER_4 and ER_2 have S_{13} as common step and so on. With the help of these common steps these two ERs can be fused to get a bigger cycle graph. So we started from ER_2 and ER_4 by combining these two ERs we can get another cycle graph as shown in fig 3.2. It can be observed that this new cycle graph and ER_3 has S_{12}, common, so by taking advantage of this similarity we can enlarge the cycle graph. At this stage we are still left with ER_4 which needs to be added into the graph so that we can complete the whole cyclic graph. Now this is a bit of tricky step, as we can see in the Figure 3.2, S_5 and S_7 are in same direction but in fact according to ER_1 $S_5-S_6-S_7$, these steps should be in opposite directions. An important characteristic of non minimal graph that needs to be mentioned here is upon examination of the enumerated list of the direct FRs and ERs, it can be realized that there are non-unit stoichiometric numbers in several of the FRs; especially, it can be seen that some FRs have stoichiometric numbers of ±2, suggesting that the RR graph will have each step S_ρ twice including

the OR, which must also be symmetrical. This can be achieved by duplicating the cycle graph as shown in Figure 3.3 and fusing the two nodes together to shape a symmetric cyclic graph. The characteristics associated with each of the unfused nodes will be the same but now they are represented collectively as a fused node in Figure 3.4. It can also be observed from Figure 3.3 that after fusing the nodes represented in yellow colour, it is now possible to add the ER_1 in the graph by adding step S_6. And in fact, this will also satisfy the node requirement according to the QSS conditions. Finally, at this stage our cyclic graph is complete as all the ERs can be traced as walks shown in Figure 3.4 and also ready for the addition of the adsorption/desorption steps. So we added the S_2 and S_4 twice in the graph to get a balanced graph. Which also helped to satisfy the linearly independent full route FR_1 and also at the same time it can be seen that all the nodes (intermediate and terminal) satisfy the QSS condition for the intermediate and terminal species. At the end we connect the terminal node in order to add two overall reactions ($2r_{OR}=2r_2=2r_4$). The final RR graph for the hydrogen oxidation reaction for the 13 steps reaction mechanism is given in Figure 3.5 and it should be noted that all the enumerated FRs and ERs can be traced as paths on the resulting RR graph.

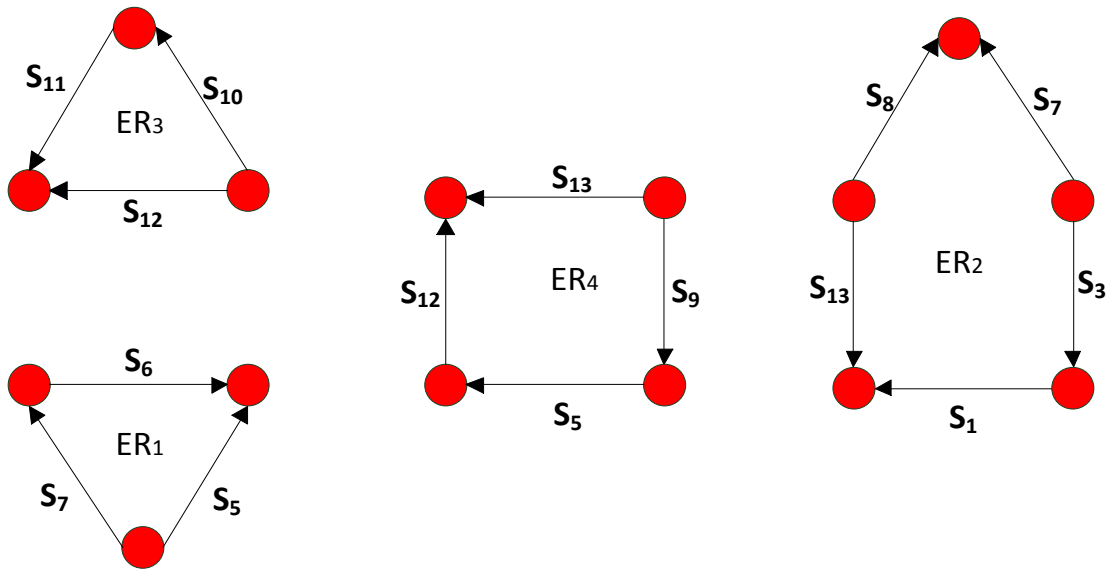

Figure 3.1: linearly independent (Empty Routes) ERs.

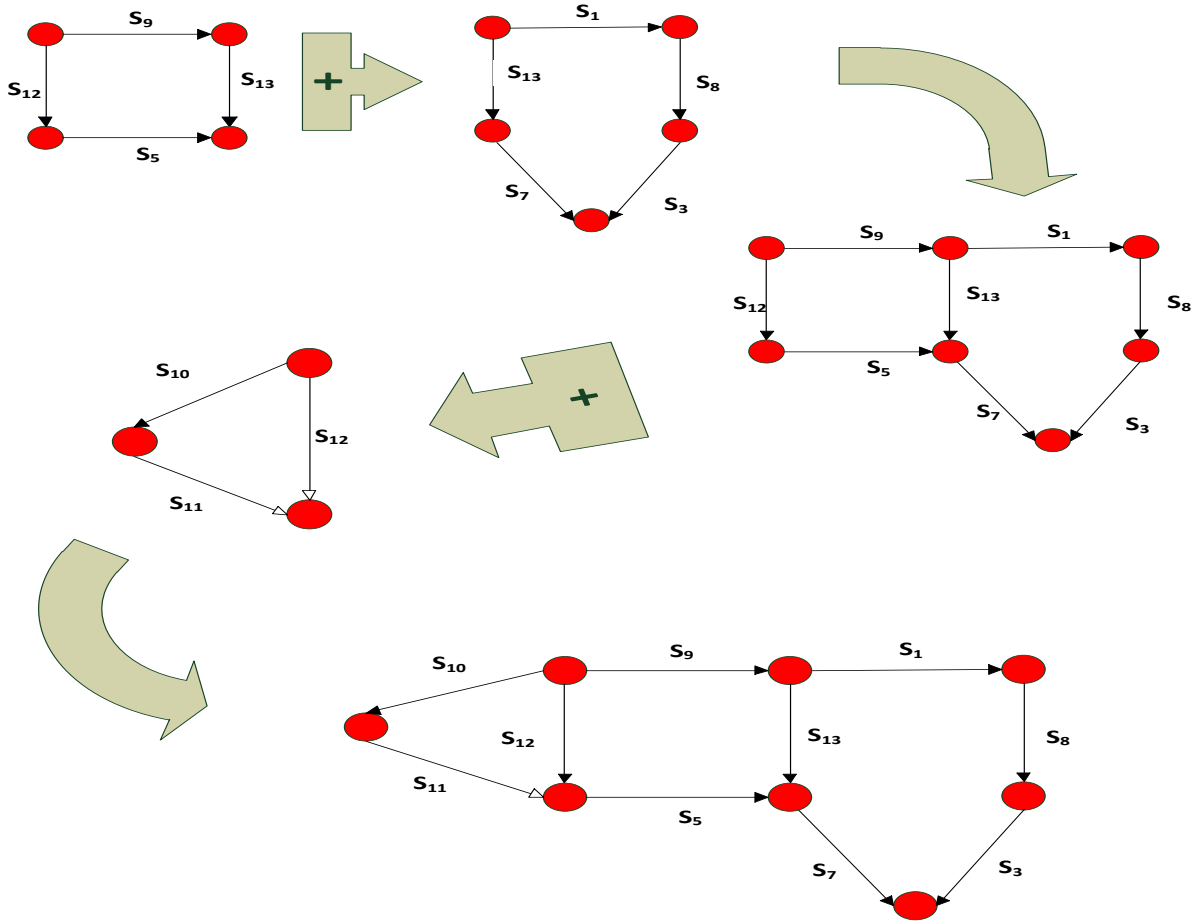

Figure 3.2: Merging of ERs based on common steps

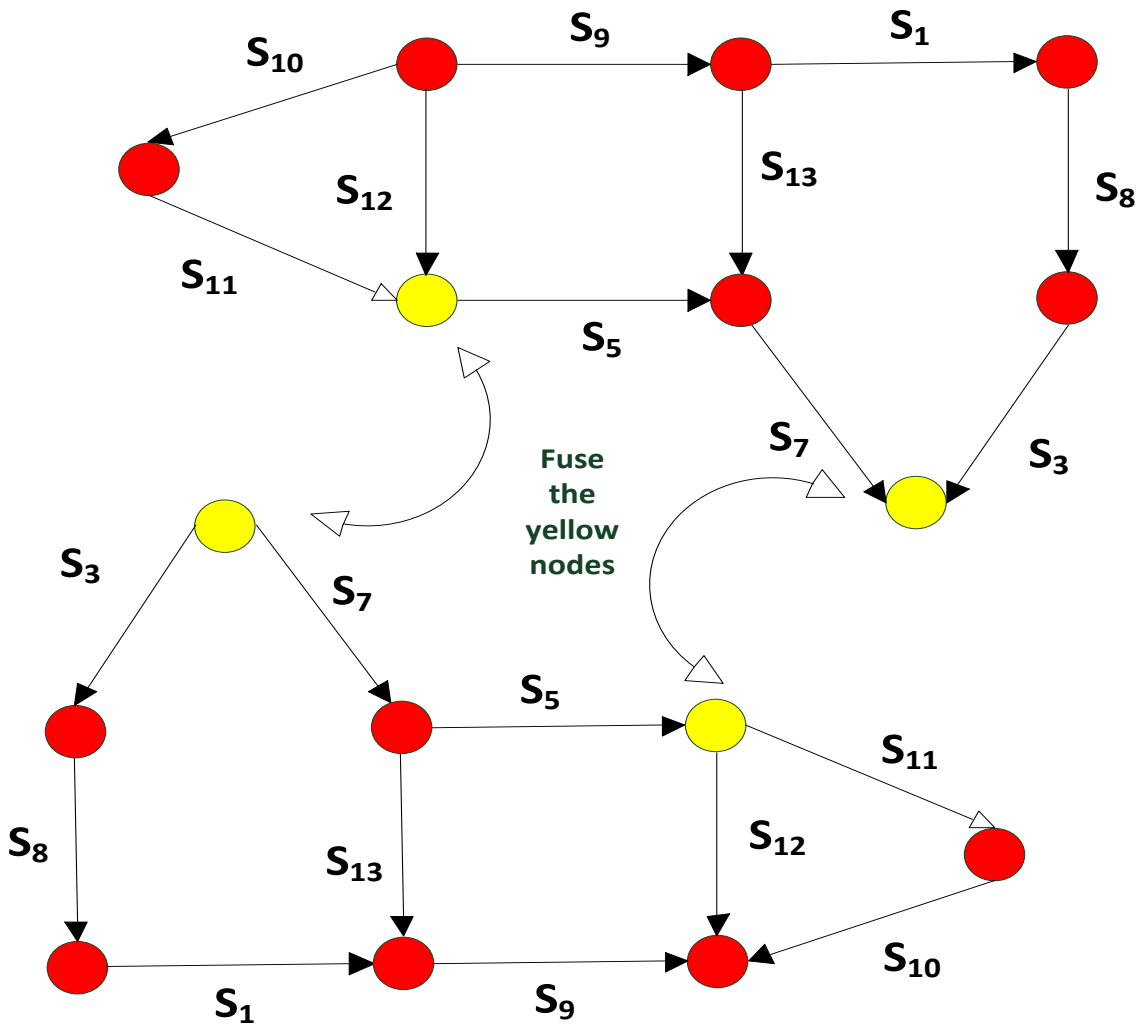

Figure 3.3: Fusing two Cyclic Graphs.

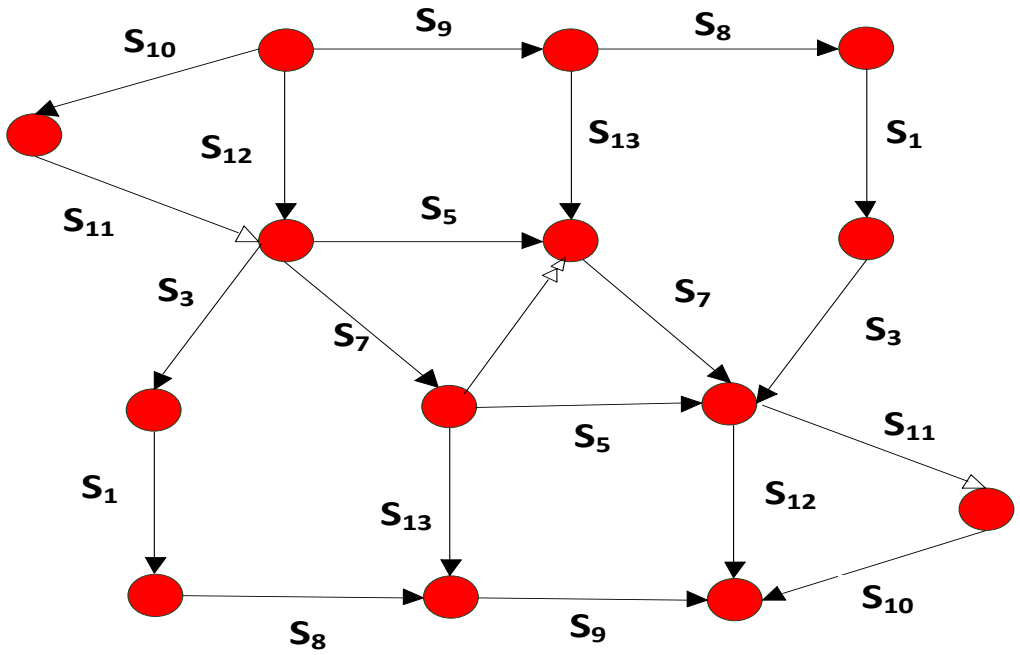

Figure 3.4: Final Form of Cyclic Graph after fusing.

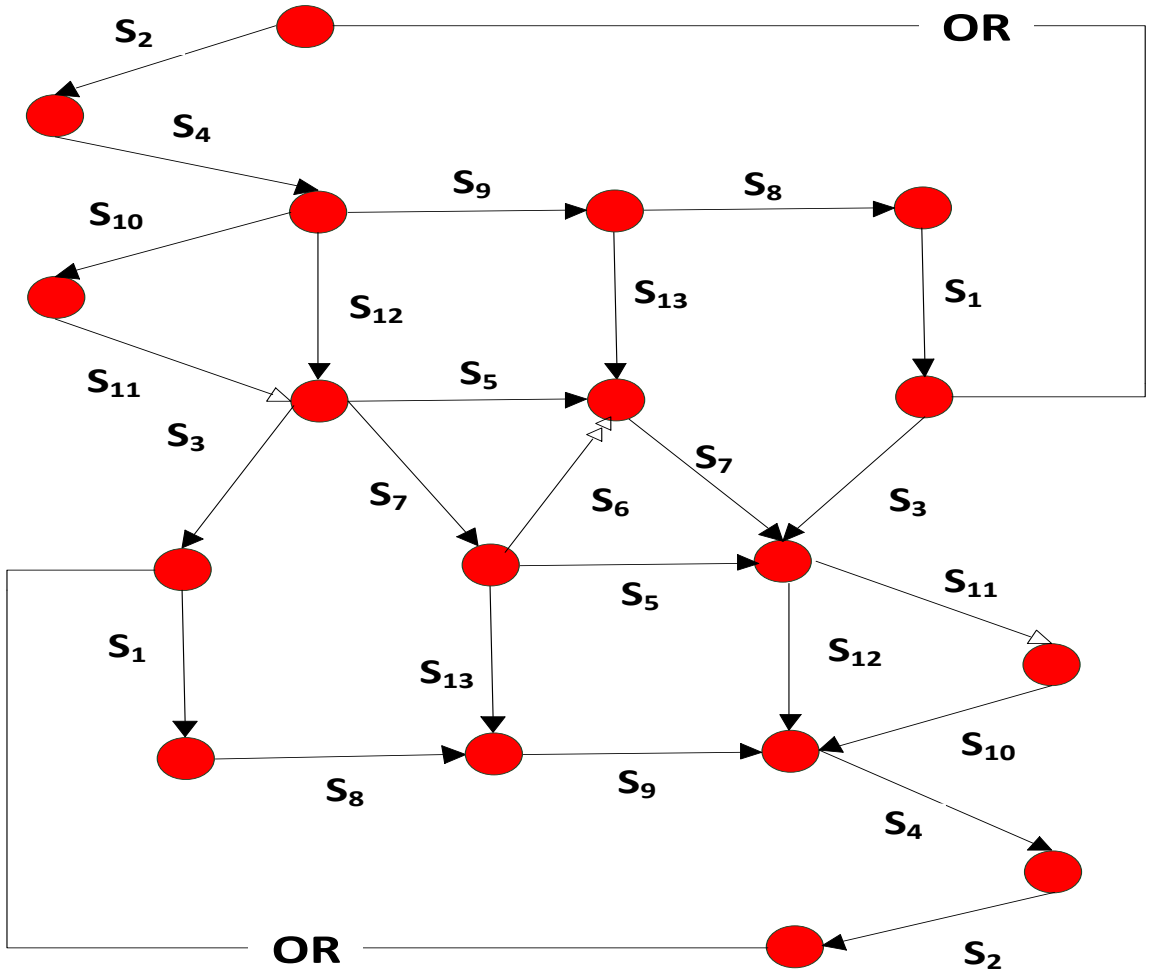

Figure 3.5: RR Graph for Hydrogen Oxidation Reaction at Ni/YSZ Pattern Anode.

3.6. Conclusions

In order to draw the RR graph for the hydrogen oxidation reaction mechanism at Ni/YSZ anode utilizing the stoichiometric algorithm, the constituents to draw the RR graph were first enumerated. Using these, a cyclic graph is first constructed and then remaining steps which are not part of any cycle, are added. Thus a final structure of RR graph for the selected system was achieved. This fulfils the entire set of requirements as explained in RR graph theory, i.e., the reaction routes can be traced as walks on the graph and all the intermediate nodes concur with the QSS approximations for intermediate species as well as for terminal species.

Chapter 4

Topological Analysis and Discussion of the Results

4.1. Introduction

At the start of this chapter the basic terminologies describing the analogy of RR Graph with electrical networks and of the new form of electrical analogy suggested by Datta and his students [8-11] are explained. An equivalent electrical circuit diagram is drawn for RR Graph of 13 step hydrogen oxidation reaction mechanism as constructed in previous chapter by substituting each branch representing a step reaction with equivalent resistance and the one representing the overall reaction with a voltage source. Next, the thermodynamic consistency of estimated kinetic data is explained with the help of constraints imposed by the concurrence of RR graph approach with Kirchhoff laws.

Moreover topological analysis of RR network has been performed by comparing the resistance of alternative paths between any two given nodes as function of temperature and over-potential due to the dependence of kinetics of system upon both of the stated variables. This eventually provides the means to investigate the contribution of various pathways in the determining the overall rate of reaction at Ni/YSZ anode. Based on the numerical simulation analysis results we conclude that FR1 is a dominant pathway which involves the two hydrogen spill-over reaction (step S_8 and S_9) and which also coincides with the findings of Vogler et al. [6, 7]. To further validate the results a simulation of RR circuit is performed in Pspice [67]. Continuing the process of investigation for the predicted dominant pathway (FR_1) reveals that step the S_9 is rate limiting step (RLS) and govern the rate of over all reaction. In addition to all above, an explicit rate expression for hydrogen oxidation reaction mechanism is developed and compared with the QSS numerical simulation results and a good agreement is found. Finally, the results of this study are compared with the findings of a recent modelling study by Vogler et al. [6, 7] and also with experimental results [25] in the form of polarization curves, and good agreement is found, which demonstrates an effective way for the characterization of electrochemical systems.

4.2. Basic introduction of Electrical analogy

The basic terminologies required for establishing the analogy of RR graph with electrical networks are described in this section [8-11].

Reaction or steps affinity A_ρ: is equal to negative of Gibbs free energy, $A_\rho = -\Delta G_\rho$, which is related to rate of forward $\overrightarrow{r_\rho}$ and backward $\overleftarrow{r_\rho}$ reaction through, $\mathcal{A}_\rho = \ln(\overrightarrow{r_\rho}/\overleftarrow{r_\rho})$, where $\mathcal{A}_\rho$ is dimensionless affinity and can be written as , $\mathcal{A}_\rho \equiv A_\rho/RT$.

Reaction or step resistance R_ρ: is defined as the mean value of the inverse of the total step rate, $r_\rho = \overrightarrow{r_\rho} - \overleftarrow{r_\rho}$, with in the boundary values i.e. $\overrightarrow{r_\rho}$ and $\overleftarrow{r_\rho}$, mathematically can be expressed as

$$R_\rho \equiv \frac{1}{\overrightarrow{r_\rho} - \overleftarrow{r_\rho}} \int_{\overleftarrow{r_\rho}}^{\overrightarrow{r_\rho}} \frac{1}{r_\rho} dr_\rho = \frac{\ln(\overrightarrow{r_\rho}/\overleftarrow{r_\rho})}{\overrightarrow{r_\rho} - \overleftarrow{r_\rho}} \tag{4.1}$$

And indeed we do not know the reaction resistance a priori unlike electrical circuits as it comprises unknown intermediate species and in addition, reaction resistances are not a constant, rather this depend on reaction conditions, i.e. as temperature and composition that have direct impact on $\overrightarrow{r_\rho}$ and $\overleftarrow{r_\rho}$.

Ohm's Law Form of step Kinetics: It can be perceived from the given explanations of branch affinity and branch resistance that step rate is consistent with Ohm's Law as

$$r_\rho = \frac{\mathcal{A}_\rho}{R_\rho} \tag{4.2}$$

Because of the consistency of RR graph with Kirchhoff laws, a quantitative relation can be observed between RR graph and its corresponding electrical circuit. So the overall resistance can be evaluated in terms of step resistance and the rate of over-all reaction may be expressed as;

$$r_{OR} = \frac{\mathcal{A}_{OR}}{R_{OR}} \tag{4.3}$$

Next, we will be discussing some important terminologies of so called new form of electrical analogy proposed by Datta and his students [8-11] that basically provides an explicit rate expression.

4.3. New Form of Electrical Analogy

Reversibility: It is the ratio of rate of reverse to forward direction of an elementary step i.e. $z_\rho \equiv \overleftarrow{r_\rho} / \overrightarrow{r_\rho}$, it is also related to step affinity as $z_\rho = exp^{(\mathcal{A}_\rho)}$. So for the overall reaction can be expressed as

$$z_{OR} = \overleftarrow{r_{OR}} / \overrightarrow{r_{OR}} = \exp(\mathcal{A}_{OR}) = \frac{1}{K_{OR}} \prod_{i=1}^{n} a_i^{v_i} \tag{4.4}$$

As it is a thermodynamic property and by virtue of KPL;

$$z_{OR} = \frac{\overleftarrow{r_{OR}}}{\overrightarrow{r_{OR}}} = \prod_{\rho=1}^{q+1} \left(\frac{\overleftarrow{r_\rho}}{\overrightarrow{r_\rho}} \right)^{\sigma_\rho} = \prod_{\rho=1}^{q+1} (z_\rho)^{\sigma_\rho} \tag{4.5}$$

In a combination of elementary steps that results in a FR, all the intermediate species will be cancelled so

$$z_{OR} = \prod_{\rho=1}^{q+1} \left(\frac{\overleftarrow{\omega_\rho}}{\overrightarrow{\omega_\rho}} \right)^{\sigma_\rho} \tag{4.6}$$

where ω_ρ is the so called reaction step weights ω_ρ which involves known quantities i.e. rate constants and activities of terminal species.

Intermediate Reaction Route: is a combination of elementary steps, such that in the resultant reaction, all the intermediate species are removed by keeping the one intermediate of interest I_k .

Quasi-Equilibrium (QE): if for a particular step $z_\rho \to 1$, or otherwise it affinity $\mathcal{A}_\rho \to 0$, then it is termed as Quasi-Equilibrated. At real equilibrium, $z_\rho = 1$ and $\mathcal{A}_\rho = 0$

Rate Limiting Step (RLS): it is the one in a considered sequence, whose resistance R_ρ contributes prominently to the R_{OR}. And in a sequence, it could be more than one.

Rate Determining Step (RDS):

This is the rate $r_\rho^\bullet$ ($I_\rho^\bullet$) or current of the branch $S_\rho(R_\rho)$ assuming that all the other resistors present in the circuit are short-circuited so the entire motive force $\mathcal{A}_{OR}$ (E_{OR}) will occur across a chosen step (resistor), which will then be the maximum step rate (current) for the given motive force.

4.4. Elementary Kinetics and Thermodynamic Data

The model equations used to describe the kinetics of different types of reactions i.e. surface reaction and charge transfer reactions can be found in electrochemical books [15, 68]and has been widely used in published literature. The total rate of reaction can be written as $r_\rho = \vec{r}_\rho - \overleftarrow{r}_\rho$.

$$\vec{r}_\rho = \vec{k}_\rho \prod_{i=1}^{n} a_i^{-\vec{v}_{\rho i}} \prod_{k=1}^{q} \theta_k^{-\vec{\beta}_{\rho k}}$$

$$\overleftarrow{r}_\rho = \overleftarrow{k}_\rho \prod_{i=1}^{n} a_i^{\overleftarrow{v}_{\rho i}} \prod_{k=1}^{q} \theta_k^{\overleftarrow{\beta}_{\rho k}} \tag{4.7}$$

Here θ_k is the unknown activities of intermediate species, I_k, a_i is the given or known activities of terminal species. $\vec{\beta}_{\rho k}$ is the stoichiometric coefficient of I_k in reaction step S_ρ as a reactant and as a product it is $\overleftarrow{\beta}_{\rho k}$ whereas for terminal species it is $\vec{v}_{\rho i}$ and $\overleftarrow{v}_{\rho i}$ respectively. Moreover for the convenience of calculations, it's better to combine the product of known rate parameters together with the activities of terminal species into reaction weights ω_ρ given in mass –action kinetics, and representing the rate explicitly in terms of unknown intermediate species concentrations and known ω_ρ as given below.

$$\vec{\omega}_\rho = \vec{k}_\rho \prod_{i=1}^{n} \theta_k^{-\vec{\beta}_{\rho k}}$$

$$\overleftarrow{\omega}_\rho = k_\rho \prod_{i=1}^{n} \theta_k^{\overleftarrow{\beta}_{\rho k}} \tag{4.8}$$

For example for S_1; $\vec{\omega}_1 = \vec{k}_1 \; and \; \overleftarrow{\omega}_1 = \overleftarrow{k}_1 p_{H_2O}$.

4.4.1. Surface Reaction

The model equations to calculate the reaction kinetics for the surface reaction at Ni and YSZ reactions are given below [6, 7, 39].

$$\vec{k}_\rho = k_f^o T^\beta \exp\left(-\frac{E_f^{act}}{RT}\right)$$

$$\overleftarrow{k}_\rho = k_r^o \exp\left(\frac{\Delta G}{RT}\right) \tag{4.9}$$

4.4.2. Electrochemical reactions

The model equations used to evaluate the reaction kinetics of electrochemical reactions are given here. The corresponding thermodynamic data is provided in Table 4.1.

$$\vec{k}_\rho = \vec{k}_{\rho,\phi_{eq}} \exp\left(\alpha \frac{zF}{RT}\eta_{act}\right) \tag{4.10}$$

Here $\vec{k}_\rho$ represents the forward rate constant and $\vec{k}_{\rho,\phi_{eq}}$ is the equilibrium rate constant and can be evaluated as given

$$\vec{k}_{\rho,\phi_{eq}} = \vec{k}_\rho^0 \exp\left(\frac{-E_f^{act}}{RT}\right) \exp\left(\alpha \frac{zF}{RT}\Delta\phi_{eq}\right)$$

Similarly

$$\overleftarrow{k}_{\rho,\phi_{eq}} = \overleftarrow{k}_\rho^0 \exp\left(\frac{-E_r^{act}}{RT}\right) exp\left(-(1-\alpha)\frac{zF}{RT}\Delta\phi_{eq}\right) \tag{4.11}$$

For the electrochemical reaction the kinetics will also be used in term of steps weights e.g. for steps S_8 , $\overrightarrow{\omega}_8 = \vec{\omega}_{8,eq}\, e^{\psi}$ and $\overleftarrow{\omega}_8 = \overleftarrow{\omega}_{8,eq}\, e^{-\psi}$

and $\vec{\omega}_{8,eq} = \vec{k}_{8,\phi_{eq}} and\ \overleftarrow{\omega}_{8,eq} = \overleftarrow{k}_{8,\phi_{eq}}$

Where $\eta_{act} = \Delta\phi - \Delta\phi_{eq}$, $\psi = 1/2\left(\frac{zF\eta_{act}}{RT}\right)$ is a dimensionless factor, R is gas constant, T is temperature, z is no of electrons and $\vec{k}_\rho^0$ are pre-exponential factors, E_f^{act} and E_r^{act} is the thermal activation energy for forward and backward reaction respectively, α is symmetry factor and $\Delta\phi$ is electrical potential difference between the electrode and the electrolyte. The pre-exponential factor and activation energies are not independent of each other, but are related through thermodynamic consistency conditions.

$$E_f^{act} - E_r^{act} = \Delta H_R \tag{4.12}$$

$$k_f^0 / k_r^0 = exp(\Delta S_R / R) \tag{4.13}$$

ΔH_R And ΔS_R are the reaction enthalpy and entropy respectively.

$$\Delta G_R = \Delta H_R - T\Delta S_R \tag{4.14}$$

For a general electrochemical reaction as given below, $\Delta\phi_{eq}$ and current density can be estimated as.

$$n_1R_1 + n_2R_2 + \cdots \ldots \leftrightarrow m_1P_1 + m_1P_1 + \cdots \ldots + \boldsymbol{z_{e^-}} \tag{4.15}$$

$$\Delta\phi_{eq} = \frac{\Delta G}{zF} + \frac{RT}{zF}\ln\left(\prod_j \left[P_j^{eq}\right]^{n_j} / \prod_i \left[R_i^{eq}\right]^{m_j}\right) \tag{4.16}$$

$$i_F = zF\, l_{TBP}\left(k_f \prod_i [R_i]^{n_j} - k_r \prod_j \left[P_j\right]^{m_j}\right) \tag{4.17}$$

Table 4.1: Thermodynamic Data for gas-phase, surface, and bulk species given as molar entropies S_i in J/kmol and molar enthalpies h_i in kJ/mol at 973 K [6, 7, 39].

Species	h_i(kJ/mol)	S_i(J/K mol)	
Gas			
$\boldsymbol{H_{2(gas)}}$	20	156	a
$\boldsymbol{H_2O_{(gas)}}$	-217	222	a
$\boldsymbol{O_{2(gas)}}$	22	233	a
Nickel Surface			
$\boldsymbol{H_{Ni}}$	-32	41	b
$\boldsymbol{O_{Ni}}$	-222	39	b
$\boldsymbol{OH_{Ni}}$	-193	106	b
$\boldsymbol{H_2O_{Ni}}$	-273	130	b
$[\,]_{Ni}$	0	0	C
Bulk Species			
$\boldsymbol{V_{o\,YSZ}^{\cdot\cdot}}$	0	0	c
$\mathbf{O_{O\,YSZ}^{X}}$	-236	0	b
YSZ Surface			
$\mathbf{OH_{YSZ}^{-}}$	-283	67	b
$\mathbf{O_{YSZ}^{-2}}$	-236	0	b
$\mathbf{H_2O_{YSZ}}$	-273	98	b
$[\,]_{YSZ}$	0	0	c

[a] Temperature dependent.

[b] Data obtained from fit to experimental data and not temperature dependent.

[c] Parameters set to zero, taken a reference.

Table 4.2: Estimated Rate constants for the elementary reactions [6, 7].

Elementary Reaction	$\vec{k}$	$\overleftarrow{k}$
S_1	7526412	2544.94
S_2	2.85E+08	2.85E+08
S_3	53.98357	159651.2
S_4	23.05098	5.230753
S_5	1.89E+09	1.56E+11
S_6	19830.75	80500156.27
S_7	8.91E+09	181258708
S_8	0.077512	48484.5
S_9	0.009183	0.066076
S_{10}	0.00426	0.23057
S_{11}	0.014637	15.29335
S_{12}	0.001416	3797.167
S_{13}	0.058629	1803446.791

Table 4.3: Specified Parameters [6, 7].

Parameters	**Values**
$p_{H_{2(gas)}}$	2.5E4 Pa
$p_{H_2O_{(gas)}}$	50 Pa
Temperature (T)	973K
η_{act}	0-400mV
Length of TBP l_{TBP}	3.7 m/cm^2

4.5. Reaction Route network & Consistency with Kirchhoff's Laws

Since a RR graph can be directly converted into an equivalent electrical circuit, the RR graph constructed with the help of enumerated FRs, ERs, INs and TNs in the previous chapter is represented as electrical network in Figure 4.1 by replacing each step or branch with a resistor and the branch representing the OR with a voltage source.

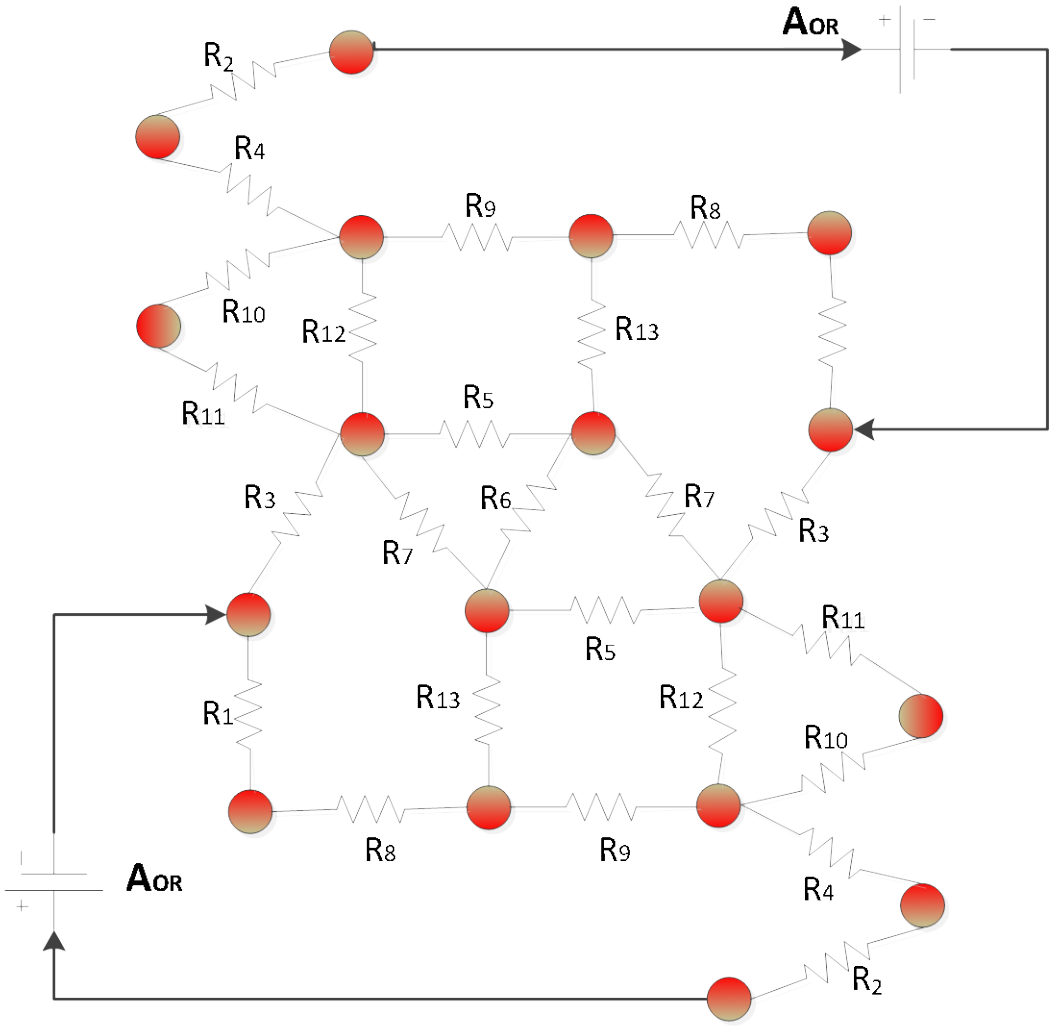

Figure 4.1: Electrical Network diagram for Hydrogen Oxidation Reaction.

Moreover RR graph or RR electrical network concurs with the Kirchhoff laws via its electrical analogy explained in the following section.

4.5.1. Kirchhoff's Potential Law

As described before, in a RR network, every cycle or ER should follow the KPL (Kirchhoff's Potential Law). For example KPL for the ER_1 can be written as S_5- S_6-S_7= 0. In the same way the corresponding linear combination of affinities should be equal to zero. A_5-A_6-A_7= 0. Correspondingly,

$$\left(\frac{\vec{r}_5}{\overleftarrow{r}_5}\right)\left(\frac{\overleftarrow{r}_6}{\vec{r}_6}\right)\left(\frac{\overleftarrow{r}_7}{\vec{r}_7}\right) = 1 \tag{4.18}$$

And it is evident that the species activities will nullify in an empty route, so for all the estimated rate constants a thermodynamic consistency check has been made, i.e.

$$\left(\frac{\vec{k}_5}{\overleftarrow{k}_5}\right)\left(\frac{\overleftarrow{k}_6}{\overleftarrow{k}_6}\right)\left(\frac{\overleftarrow{k}_7}{\vec{k}_7}\right) = 1 \tag{4.19}$$

Similarly, there are three more constraints to other linearly independent ERs, so the predicted rate constants are required to follow these constraints of thermodynamic consistency. Alternatively it is not required to calculate all the rate constants some of them might be found through KPL equations. Moreover, in a RR graph, the affinities of the elementary reactions forming FR are related to the affinity of the OR via KPL relation, e.g. for FR_1 (S_1+ S_2+ S_4+ S_8+ S_9), the affinities are related as

$$A_1 + A_2 + A_4 + A_8 + A_9 = A_{OR}$$

Similarly;

$$K_1 + K_2 + K_4 + K_8 + K_9 = K_{OR} \tag{4.20}$$

where K_{OR} and K_ρ are the equilibrium rate constant of overall reaction and elementary step respectively.

4.5.2. Kirchhoff's Flux Law (KFL)

In the same way every node follows the KFL. As, KPL confirms thermodynamic consistency and KFL is analogous to QSS analysis for intermediate species and can potentially be used to evaluate the network kinetics [11, 63]. Applying the KFL to linearly independent nodes, the following equations can be generated.

$$\begin{aligned} r_2 - r_4 &= 0 & -r_8 + r_9 - r_{13} &= 0 \\ r_{10} - r_{11} &= 0 & r_1 - r_2 - r_3 &= 0 \\ r_1 - r_8 &= 0 & r_5 + 2r_6 - r_7 + r_{13} &= 0 \\ r_3 - r_6 + r_7 &= 0 & r_3 + r_5 + r_7 - r_{10} - r_{12} &= 0 \end{aligned} \tag{4.21}$$

For each of these nodes, the equation corresponding mass action kinetics can be written as below.

$$\left(\vec{k}_{10}\theta_{O_{YSZ}^{-2}}\,\theta_{Ni}^{\circ} - \overleftarrow{k}_{10}\theta_{O_{Ni}^{-}}\theta_{YSZ}^{\circ}\right) - \left(\vec{k}_{11}\theta_{O_{Ni}^{-}} - \overleftarrow{k}_{11}\theta_{O_{Ni}}\right) = 0$$

$$\left(\vec{k}_{2}\theta_{O_{YSZ}^{ox}}\,\theta_{YSZ}^{\circ} - \overleftarrow{k}_{2}\theta_{O_{YSZ}^{-2}}\,\theta_{V_{YSZ}^{\circ\circ}}\right) - \left(\vec{k}_{4}p_{H_2}\theta_{Ni}^{\circ 2} - \overleftarrow{k}_{4}\theta_{H_{Ni}}^{2}\right) = 0$$

$$\left(\vec{k}_{1}\theta_{H_2O_{YSZ}} - \overleftarrow{k}_{1}p_{H_2O}\theta_{YSZ}^{\circ}\right) - \left(\vec{k}_{8}\theta_{H_{Ni}}\theta_{OH_{YSZ}}^{-1} - \overleftarrow{k}_{8}\theta_{H_2O_{YSZ}}\,\theta_{Ni}^{\circ}\right) = 0$$

$$\left(\vec{k}_{3}p_{H_2O}\,\theta_{Ni}^{\circ} - \overleftarrow{k}_{3}\theta_{H_2O_{Ni}}\right) - \left(\vec{k}_{6}\theta_{H_2O_{Ni}}\theta_{O_{Ni}} - \overleftarrow{k}_{6}\theta_{OH_{Ni}}^{2}\right) + \left(\vec{k}_{7}\theta_{OH_{Ni}}\theta_{H_{Ni}} - \overleftarrow{k}_{7}\theta_{H_2O_{Ni}}\theta_{Ni}^{\circ}\right) = 0$$

$$\left(\vec{k}_{5}\theta_{H_{Ni}}\theta_{O_{Ni}} - \overleftarrow{k}_{5}\theta_{OH_{Ni}}\theta_{Ni}^{\circ}\right) + 2\left(\vec{k}_{6}\theta_{H_2O_{Ni}}\theta_{O_{Ni}} - \overleftarrow{k}_{6}\theta_{OH_{Ni}}^{2}\right) - \left(\vec{k}_{7}\theta_{OH_{Ni}}\theta_{H_{Ni}} - \overleftarrow{k}_{7}\theta_{H_2O_{Ni}}\theta_{Ni}^{\circ}\right) + \left(\vec{k}_{13}\theta_{OH_{YSZ}}^{-1}\,\theta_{Ni}^{\circ} - \overleftarrow{k}_{13}\theta_{OH_{Ni}}\theta_{YSZ}^{\circ}\right) = 0$$

$$\left(\vec{k}_{1}\theta_{H_2O_{YSZ}} - \overleftarrow{k}_{1}p_{H_2O}\,\theta_{YSZ}^{\circ}\right) - \left(\vec{k}_{2}\theta_{O_{YSZ}^{ox}}\,\theta_{YSZ}^{\circ} - \overleftarrow{k}_{2}\theta_{O_{YSZ}^{-2}}\,\theta_{V_{YSZ}^{\circ\circ}}\right) - \left(\vec{k}_{3}p_{H_2O}\,\theta_{Ni}^{\circ} - \overleftarrow{k}_{3}\theta_{H_2O_{Ni}}\right) = 0$$

$$-\left(\vec{k}_{8}\theta_{H_{Ni}}\theta_{OH_{YSZ}}^{-1} - \overleftarrow{k}_{8}\theta_{H_2O_{YSZ}}\,\theta_{Ni}^{\circ}\right) + \left(\vec{k}_{9}\theta_{H_{Ni}}\theta_{O_{YSZ}}^{-2} - \overleftarrow{k}_{9}\theta_{OH_{YSZ}}^{-1}\,\theta_{Ni}^{\circ}\right) - \left(\vec{k}_{13}\theta_{OH_{YSZ}}^{-1}\,\theta_{Ni}^{\circ} - \overleftarrow{k}_{13}\theta_{OH_{Ni}}\theta_{YSZ}^{\circ}\right) = 0$$

$$\left(\vec{k}_{3}p_{H_2O}\,\theta_{Ni}^{\circ} - \overleftarrow{k}_{3}\theta_{H_2O_{Ni}}\right) + \left(\vec{k}_{5}\theta_{H_{Ni}}\theta_{O_{Ni}} - \overleftarrow{k}_{5}\theta_{OH_{Ni}}\theta_{Ni}^{\circ}\right) + \left(\vec{k}_{7}\theta_{OH_{Ni}}\theta_{H_{Ni}} - \overleftarrow{k}_{7}\theta_{H_2O_{Ni}}\theta_{Ni}^{\circ}\right) - \left(\vec{k}_{10}\theta_{O_{YSZ}^{-2}}\,\theta_{Ni}^{\circ} - \overleftarrow{k}_{10}\theta_{O_{Ni}^{-}}\theta_{YSZ}^{\circ}\right) - \left(\vec{k}_{12}\theta_{O_{YSZ}^{-2}}\,\theta_{Ni}^{\circ} - \overleftarrow{k}_{12}\theta_{O_{Ni}^{-}}\theta_{YSZ}^{\circ}\right) = 0$$

The site balance equation can be written as;

$$\theta_{H_{Ni}} + \theta_{OH_{Ni}} + \theta_{H_2O_{Ni}} + \theta_{O_{Ni}} + \theta_{O_{Ni}^{-}} + \theta_{Ni}^{\circ} = 1$$

$$\theta_{OH_{YSZ}^{-1}} + \theta_{H_2O_{YSZ}} + \theta_{O_{YSZ}^{-2}} + \theta_{YSZ}^{\circ} = 1 \qquad (4.22)$$

The above 8 non-linear algebraic KFL equation along with two site balance equations can be solved simultaneously for the input condition of the reactants and the unknown concentrations of the intermediate species can be evaluated. Once we have the site fractions, the rates and reaction resistances of each elementary reaction step can be calculated. Furthermore, with the help of TNs the rate of over all reaction (OR) can also be estimated. The estimated rate constants for the elementary reactions are given in Table 4.2 which follows the thermodynamic constraints as discussed previously.

4.6. Network Analysis and Pruning

The simplification and reduction of RR graph can be performed by comparing the resistance along parallel paths over a broad range of temperature and over-potential between any two given nodes having the same affinity drop based on the analogy with KPL. i.e., by considering each ER having different parallel paths and making a comparison of the total resistance associated to each path. So if one path is having higher resistance than others then it would be safe to conclude that this particular path contributes very little to the total flux and may be eliminated.

By simultaneously solving the eight linearly independent KFL equations along two site balance equations (Eq. 4.22) for the surfaces of YSZ and Ni, the concentrations of intermediate species namely ($H_{Ni}, O_{Ni}, OH_{Ni}, H_2O_{Ni}, [\,]_{Ni}, [\,]_{YSZ}, \mathrm{H_2O_{YSZ}}, \mathrm{O^{-2}_{YSZ}}$ and $\mathrm{OH^{-}_{YSZ}}$), are calculated. Using these, the rates, dimensionless affinities and resistance of each elementary step can be calculated from Eqs. 4.1 to 4.3. A solved electrical circuit diagram for the 13 step hydrogen oxidation mechanism is given in Figure 4.2.

4.6.1. Comparison of Alternative Pathways and Reduced Graph

Pruning of the RR graph might be started from ER_1 which basically provides two pathways for the formation of OH_{Ni} species, one is through S_6: $H_2O_{Ni} + O_{Ni} \leftrightarrow 2OH_{Ni}$ the direct reaction between adsorbed water and oxygen at Ni surface and the other is a combination S_5 and S_7 given below;

Table 4.4: Example of cycle for description of alternative pathways.

		$\boldsymbol{\sigma_\rho}$
S_5	$H_{Ni} + O_{Ni} \leftrightarrow OH_{Ni} + [\,]_{Ni}$	1
S_7	$H_2O_{Ni} + [\,]_{Ni} \leftrightarrow OH_{Ni} + H_{Ni}$	-1
Net:	$\boldsymbol{H_2O_{Ni} + O_{Ni} \leftrightarrow 2OH_{Ni}}$	

The equivalent resistances for the 1st and 2nd pathways are R_6 and R_5+R_7 respectively. Numerical simulation results of comparison for both of the pathways resistances is given in Figures 4.3a and 4.3b as a function of temperature and over-potential, respectively. As we know that reaction will proceed through a pathway having minimum resistance so it might be safe to remove S_6 from the mechanism.

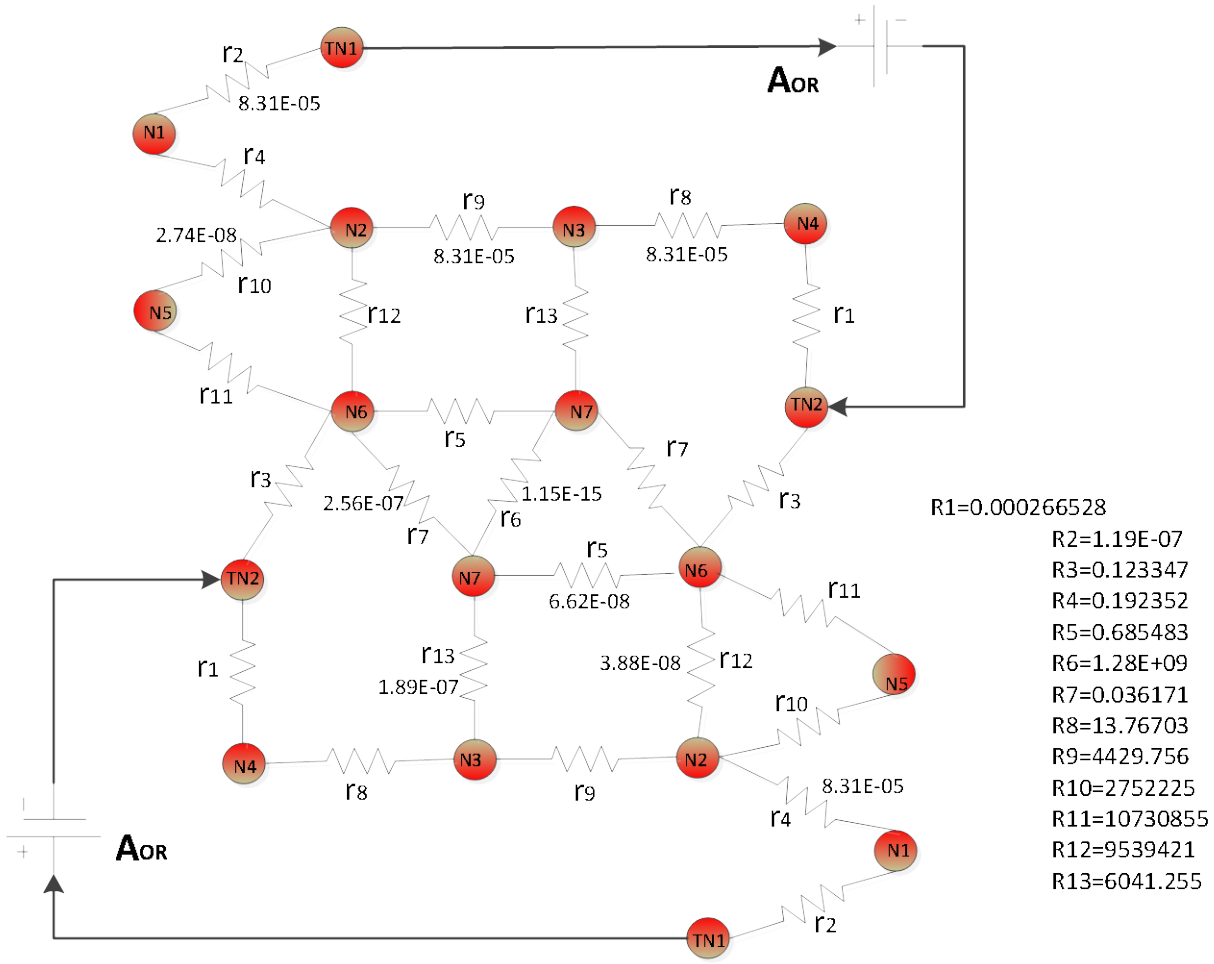

Figure 4.2: Solved network diagram for Hydrogen oxidation reaction at Ni/YSZ.

Continuing the process of pruning we now consider ER_3, S_{10}+S_{11}-S_{12} which facilitate two alternative pathways for the formation of O_{Ni}. The first one is simply S_{12} while the second is via S_{10} and S_{11} and the corresponding resistances to these pathways are R_{12} and R_{10}+ R_{11} situated between nodes N_2 and N_6 (Refer to Fig 4.1). A comparison of resistance for both paths is shown in Figure 4.4a as a function of temperature which depicts that there is not much difference between the values of the two. Numerical results for the comparison as a function of over potential are given in Figure 4.4b which also point out more or less a similar trend so at this stage it might not be safe to drop any of these pathways. After removing S_6 the graph can be reduced to a minimal form as showed in Figure 4.5 and can now facilitate a robust analysis of possible pathways which differs in selection charge transfer reactions but results in the same overall reaction.

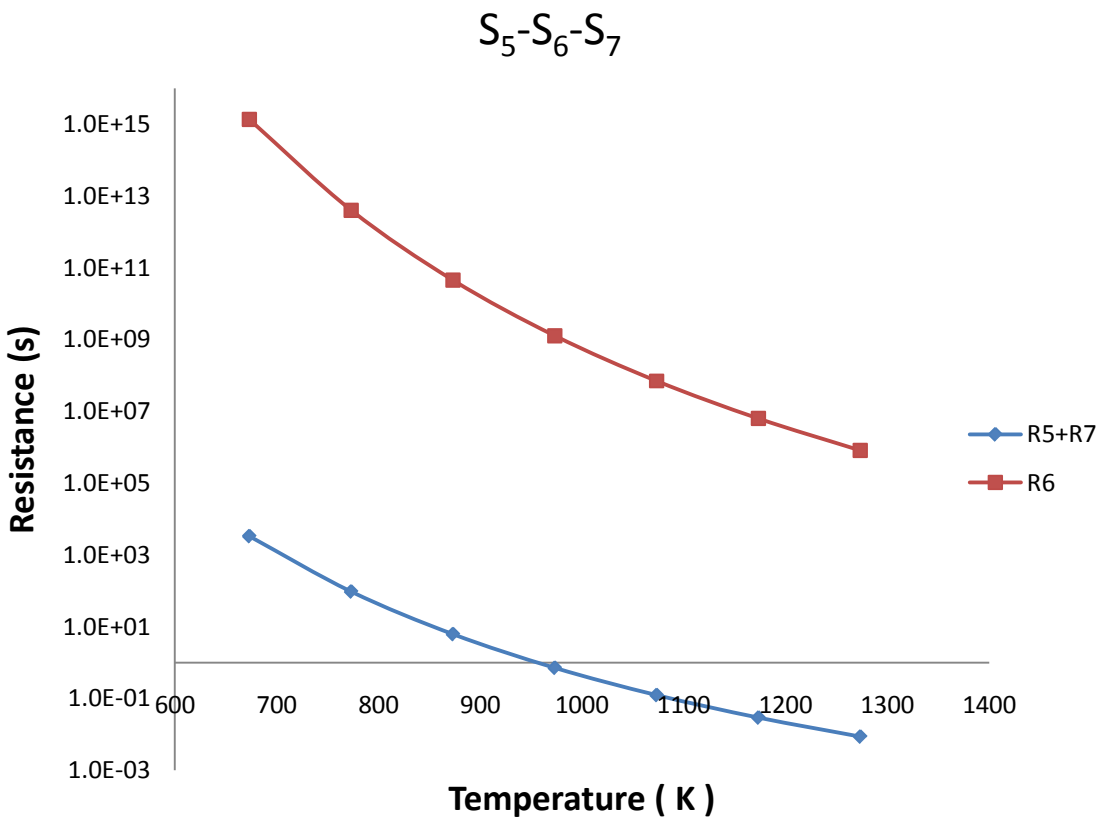

Figure 4.3a: Comparison of alternative pathways along a range of temperature for ER_1

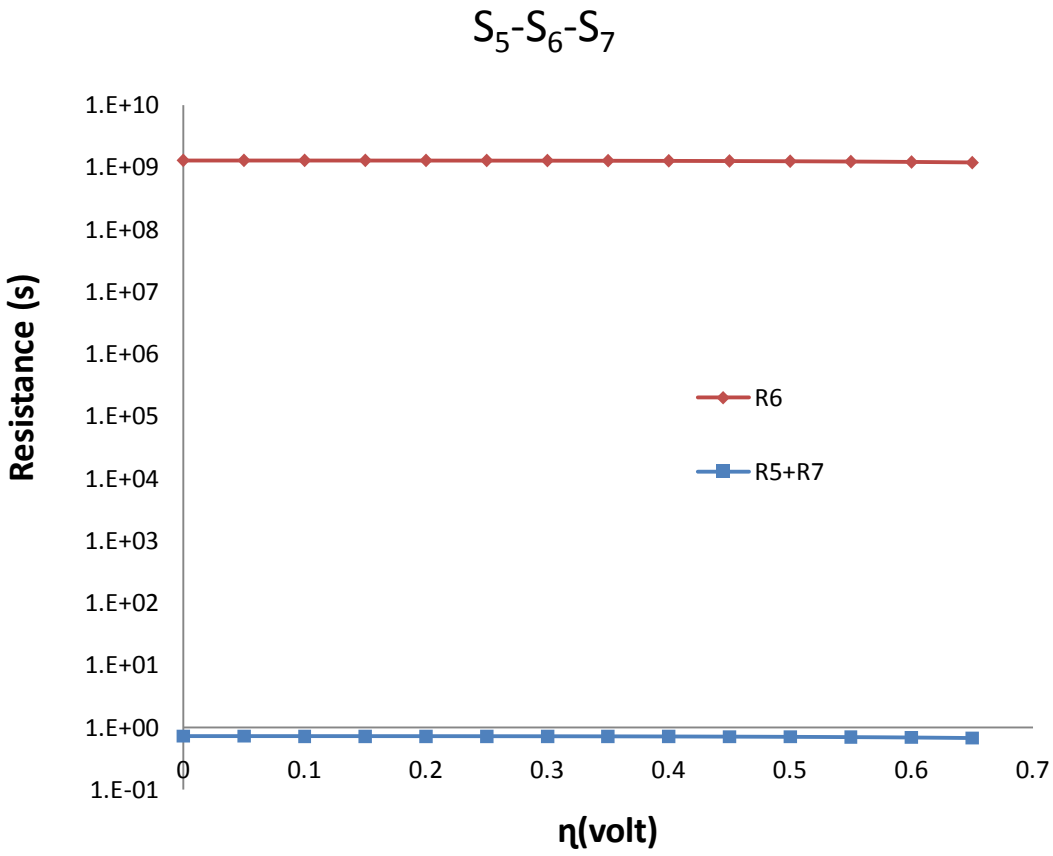

Figure 4.3b: Comparison of alternative pathways along a range of over potential for ER_1

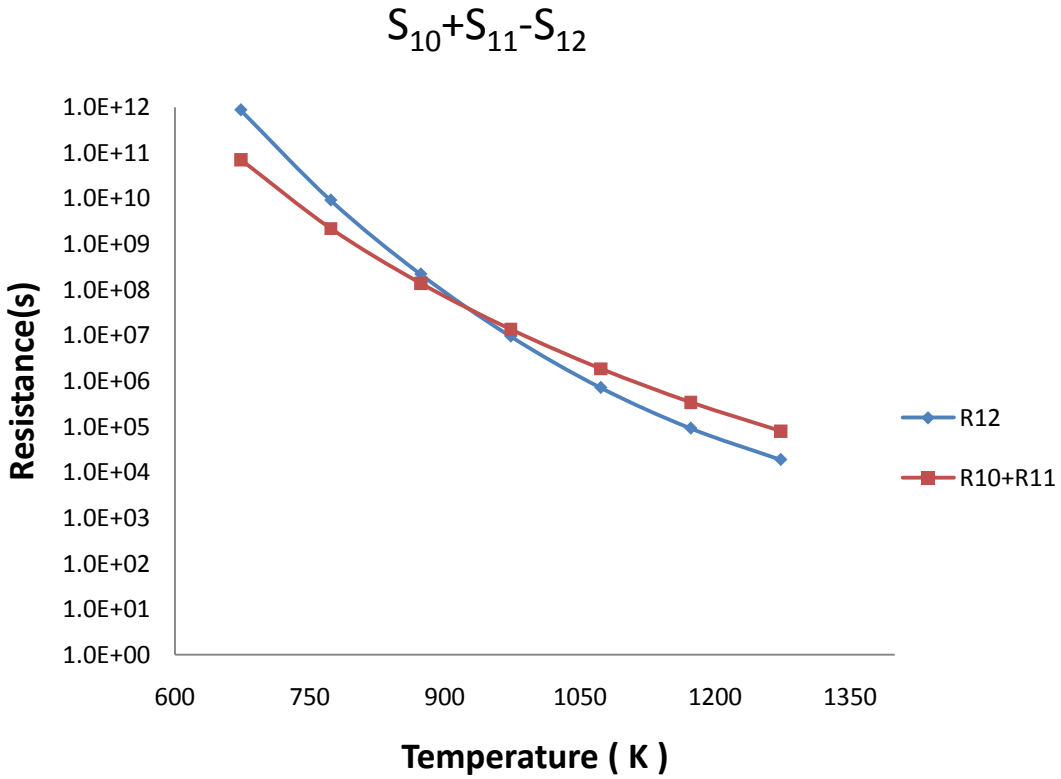

Figure 4.4a: Comparison of alternative pathway along a range of temperature for ER_3

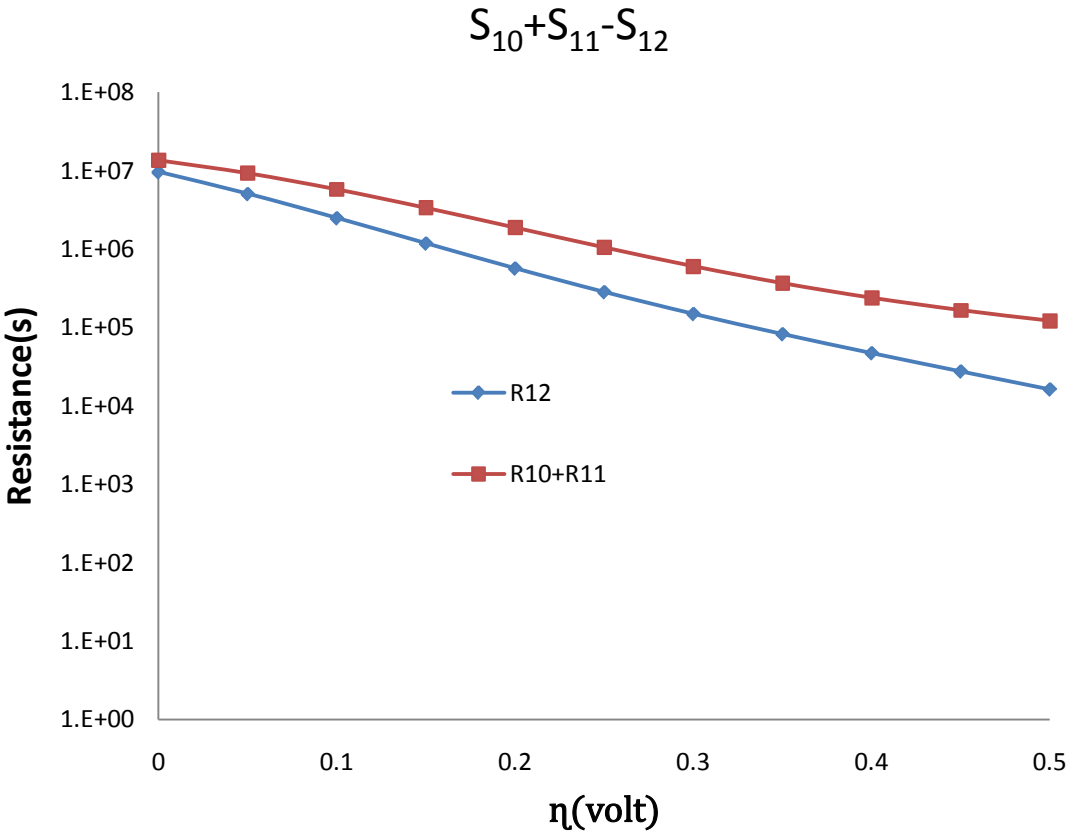

Figure 4.4b: Comparison of alternative pathway along a range of over potential for ER_3

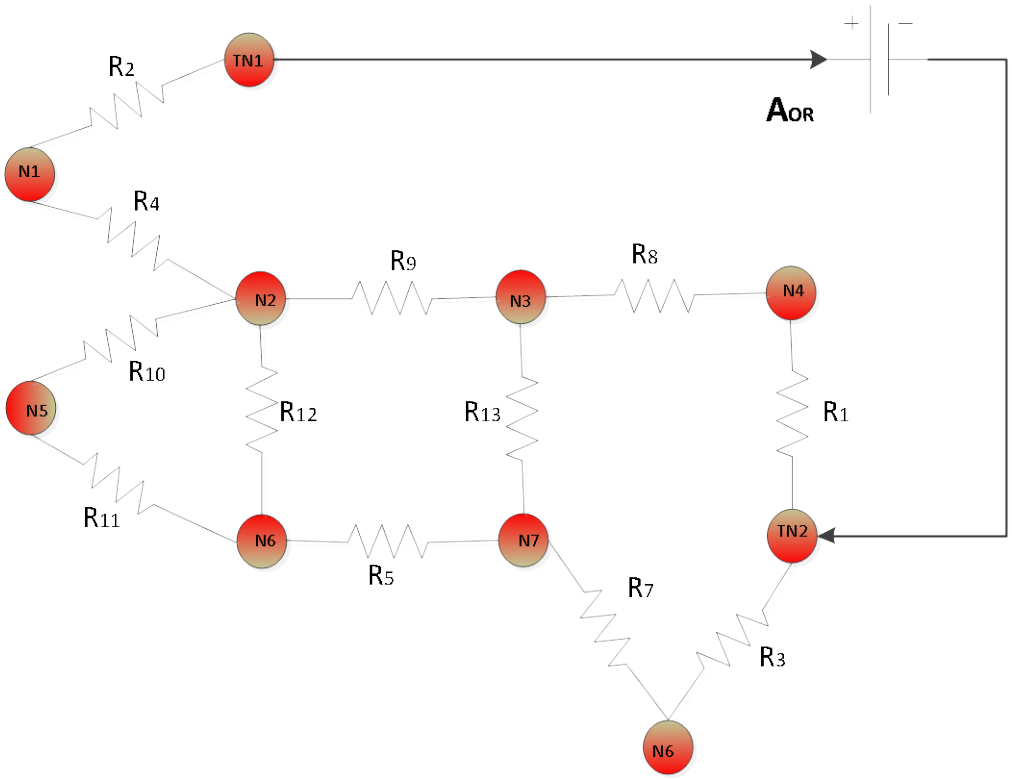

Figure 4.5: Minimal electrical circuit diagram

4.6.2. Comparison of Different Charge Transfer Mechanisms

As at this stage the RR circuit of hydrogen oxidation reaction mechanism is pruned enough to visualize the various pathways comprised of different charge transfer steps as given in Table 4.5. To identify which is the dominant pathway, a comparison of the resistance of alternative paths between nodes over a range of applied over potential η_{act} can be made. In a similar fashion a comparison of resistance can also be made over a range of temperature of the operating system as done by Datta and his students [11, 63, 65]. Furthermore, the comparison over the temperature and over-potential are equally important as the reaction rates and resistances are functions of both.

In order to investigate the significance of FR_1 and FR_2, we examined the alternative pathways between the nodes N_3 and TN_2 i.e., S_1+S_8 and S_3+S_7+S_{13}. Which is basically the reason of the occurrence of different charge transfer reactions in these full routes, as in FR_1 two hydrogen spill over reactions are involved but in FR_2 one hydrogen spill over is accompanied by hydroxyl spill-over reaction (Figure 4.5). The corresponding resistances of these alternative pathways R_1+R_8 and R_3+R_7+R_{13} are plotted as a function of time and over potential in Figure 4.6a and 4.6b respectively. It clearly shows that S_1+S_8 has lower resistance which means most of the current (flux) will pass through this pathway and hence it would be safe to eliminate the other path. In Figures 4.7a and 4.7b simulation results of alternative paths between nodes N_2 and TN2 is given to investigate the importance of pathways (S_9+S_8+S_1 & S_3+S_5+S_7+S_{12}). In other words, it gives the comparison between FR1 and FR_5 involving two hydrogen spill over and oxygen spill over reactions, respectively. Based on the results it is concluded that S_1+S_8+S_9 is a dominant pathway between the nodes N_2 and TN_2. Next a comparison of resistances of alternative path located between node N_2 and N_3 is given in Figures 4.8a and 4.8b as function of temperature and over-potential respectively, which also revealed that S_9 has lower resistance and should be kept in the final form of RR graph. After analysing the alternative paths between nodes, the final reduced form of the graph is given in Figure 4.10. To further validate the removal of S_3, S_5, S_7, S_{10}, S_{11}, S_{12} and S_{13} from the mechanism we simulate the electrical circuit (Figure 4.5) in Pspice for the considered condition given in Table 4.3 by varying η_{act}. Two values of η_{act} are simulated; $\eta_{act} = 0mv \; and \; \eta_{act} = 200mv$ shown in Figures 4.9a and 4.9b, respectively. Simulation results of both of the scenarios clearly show that most of the flux (current) is passing from FR_1 (S_1+ S_2+ S_4+ S_8+ S_9) which involves two hydrogen spill over charge transfer reactions and the steps

which are eliminated as mentioned above contributes very little to the total current or flux.

Table 4.5: Possible Charge Transfer Pathways.

Name	Expression	Active charge transfer steps
FR_1	$S_1+ S_2+ S_4+ S_8+ S_9$	Double hydrogen spill over ($S_8+ S_9$)
FR_2	$S_2+ S_4- S_3+ S_7+ S_9+S_{13}$	One hydrogen spill over along with hydroxyl spill over(S_9+S_{13})
FR_5	$S_2-S_3+S_4+S_5+S_7+S_{12}$	Single Oxygen spill over(S_{12})
FR_6	$S_2-S_3+S_4+S_5+S_7+S_{10}+S_{11}$	Combination of two oxygen spill over reactions($S_{10}+S_{11}$)

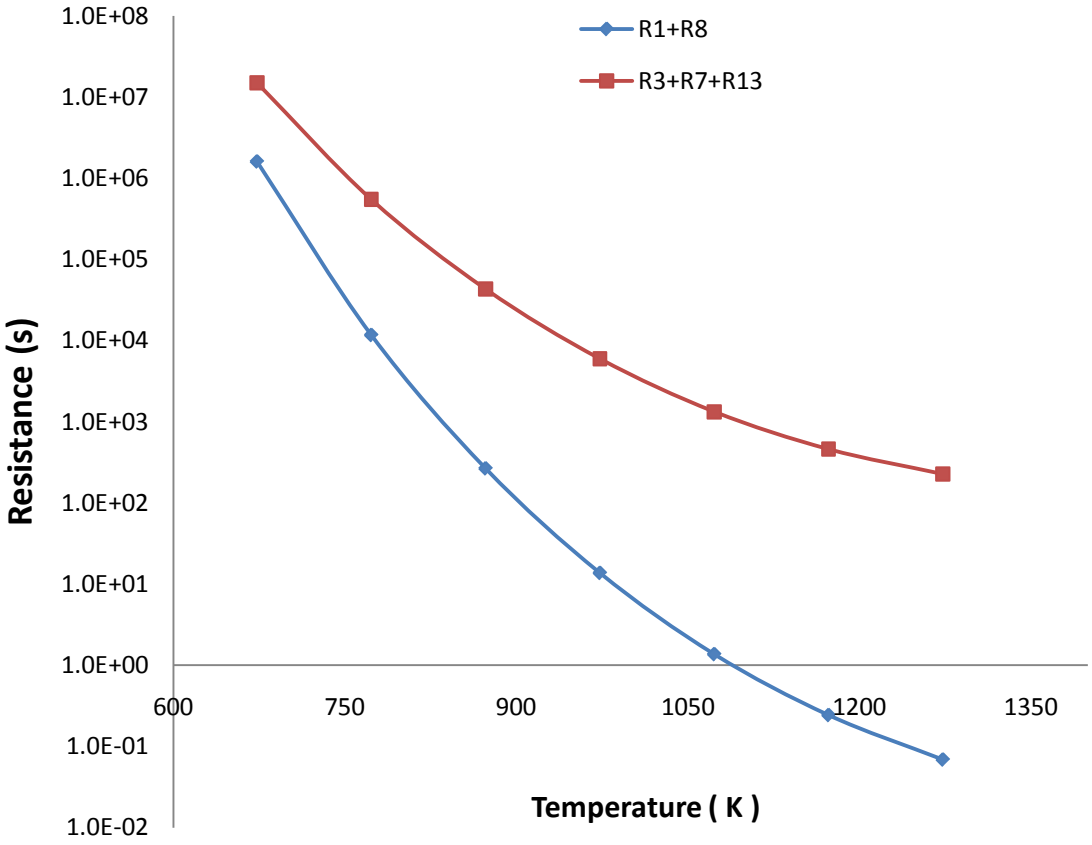

Figure 4.6a: Comparison of the resistance of alternative paths between N_3 and TN_2 as a function of temperature.

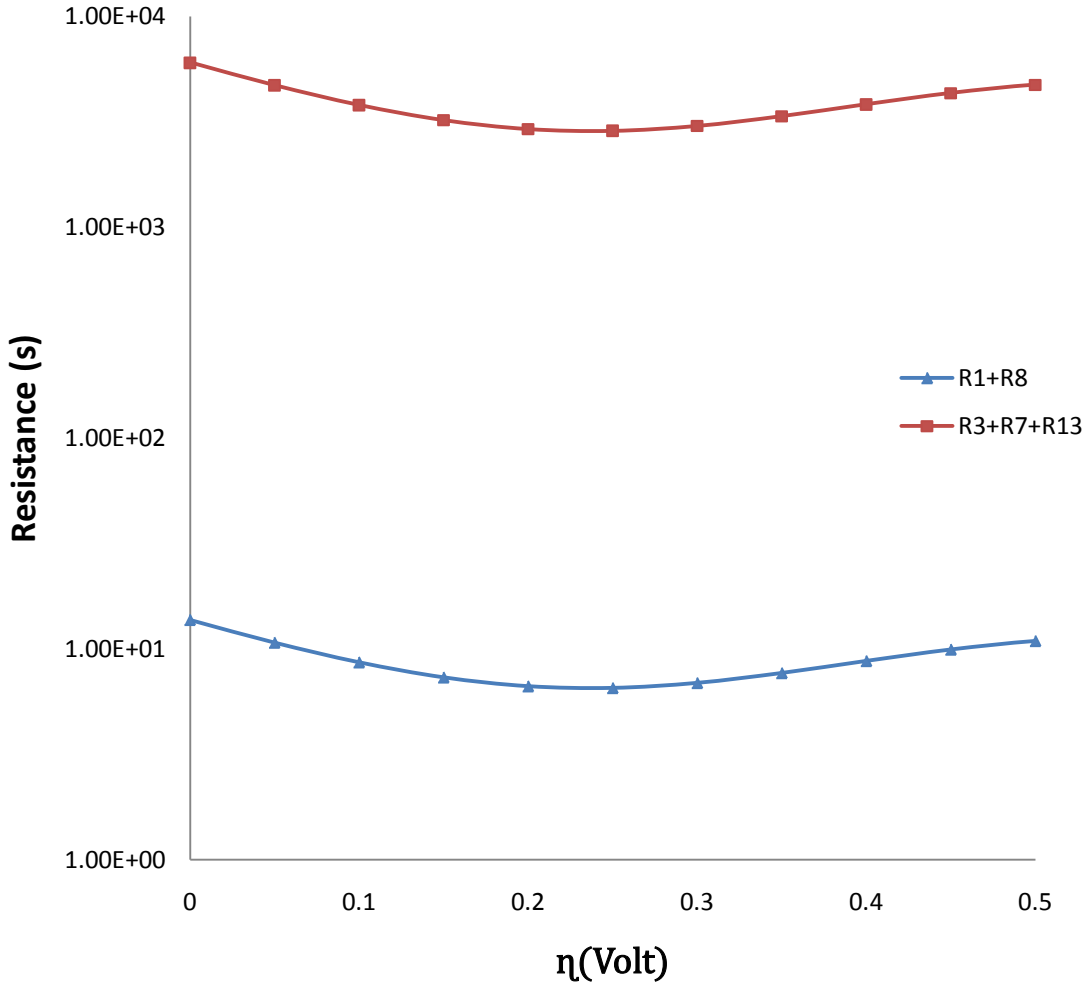

Figure 4.6b: Comparison of the resistance of alternative paths between N_3 and TN_2 as a function of over-potential.

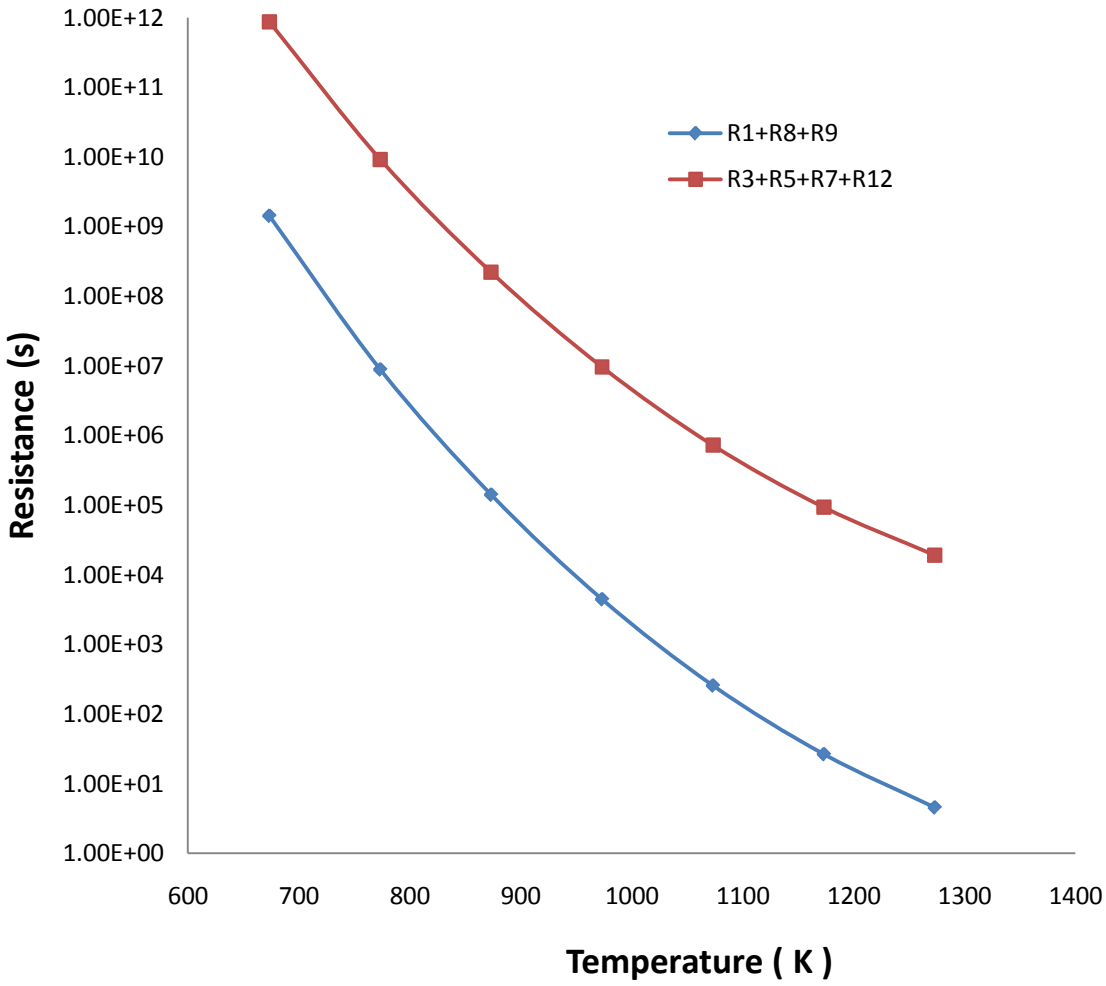

Figure 4.7a: Comparison of the resistance of alternative paths between N_2 and TN_2 as a function of temperature.

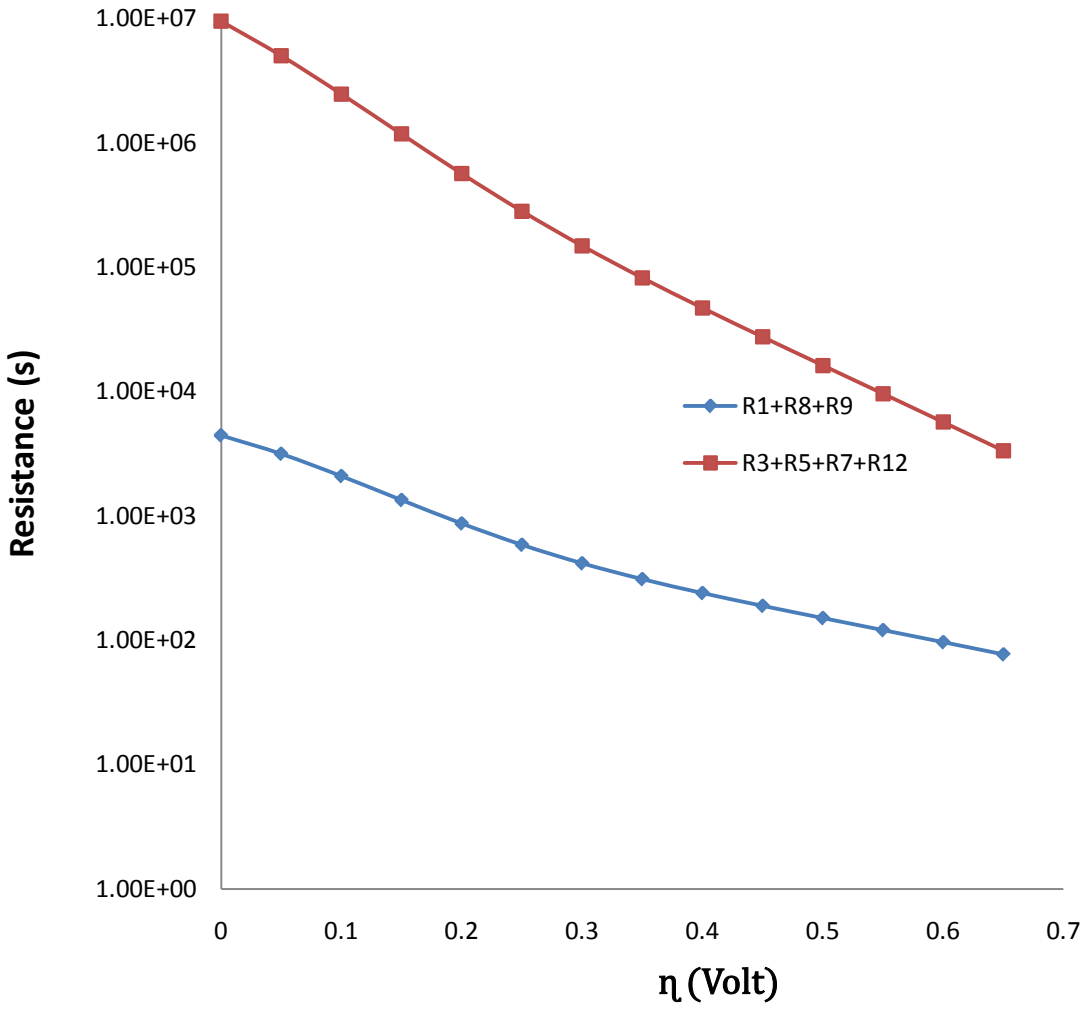

Figure 4.7b: Comparison of the resistance of alternative paths between N_2 and TN_2 as a function of over-potential.

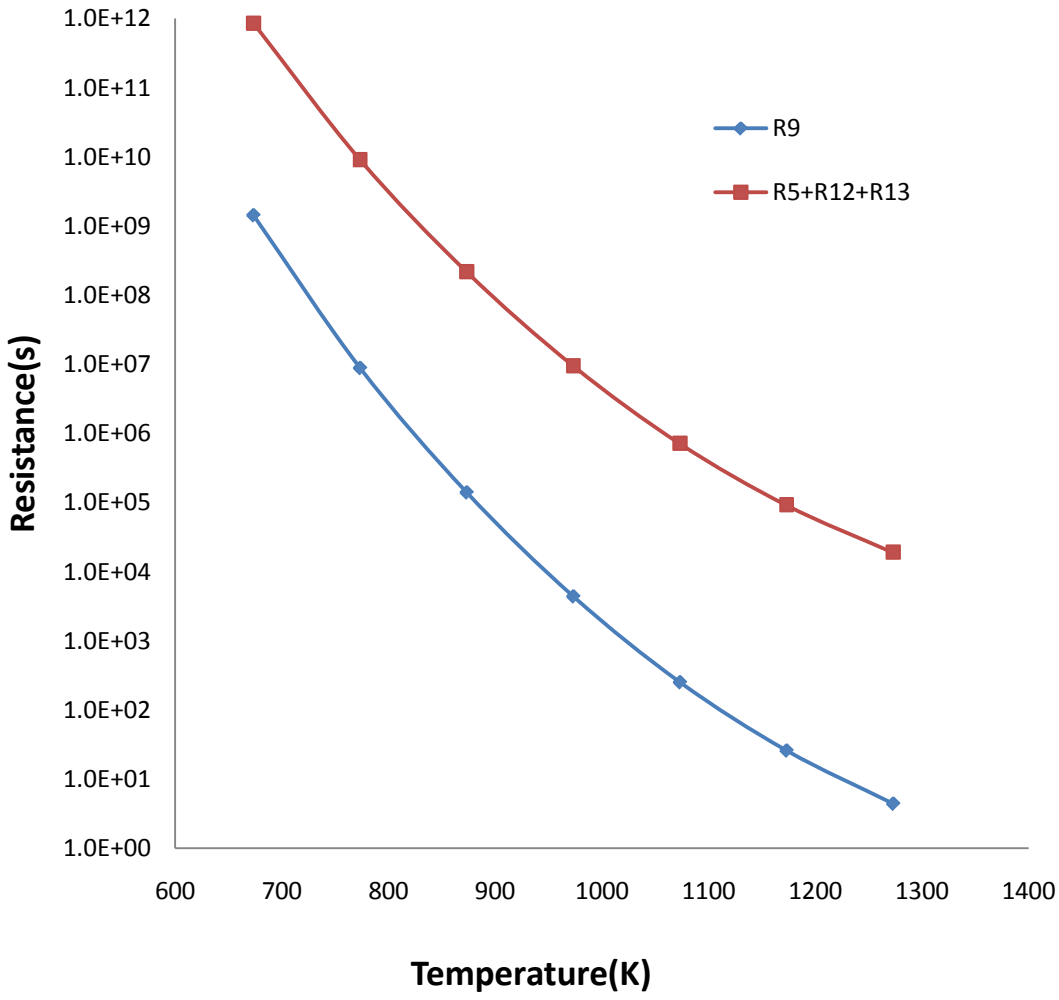

Figure 4.8a: Comparison of the resistance of alternative paths between N_2 and N_3 as a function of temperature.

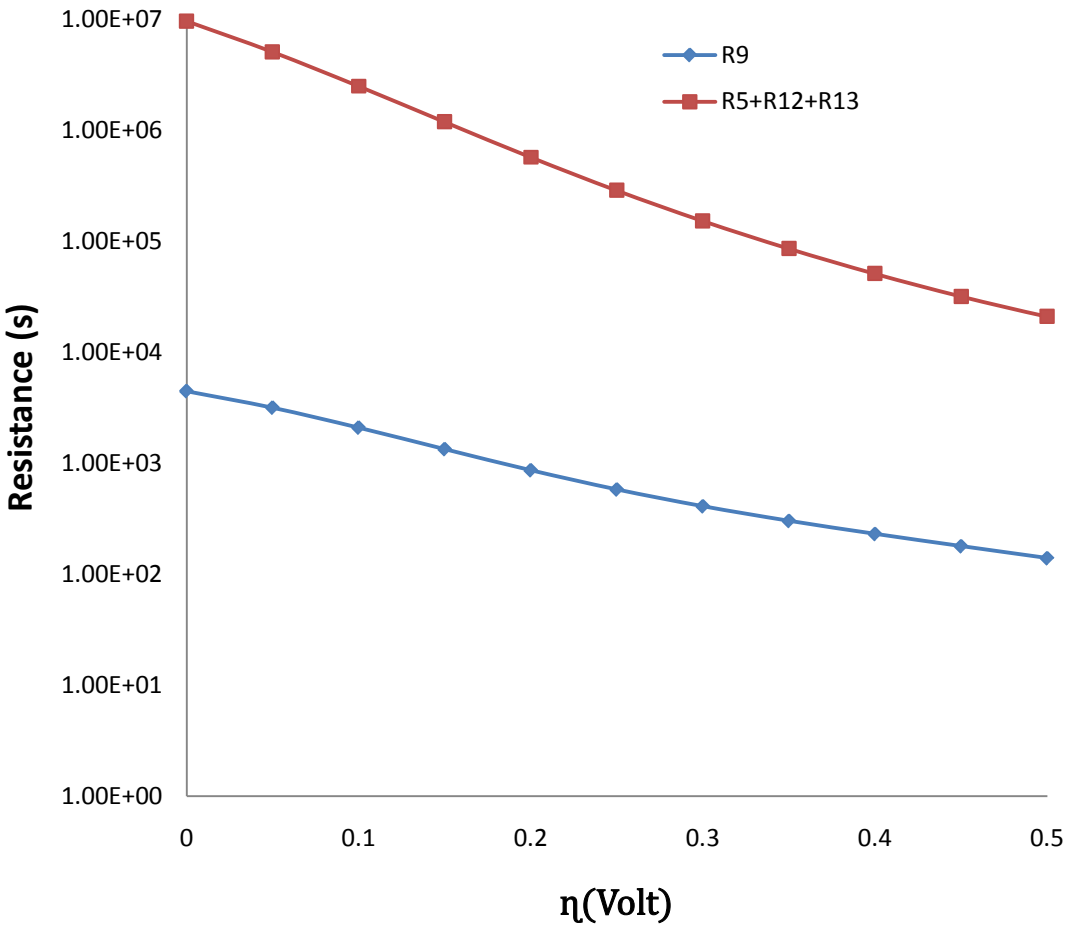

Figure 4.8b: Comparison of the resistance of alternative paths between N_2 and N_3 as a function of over-potential.

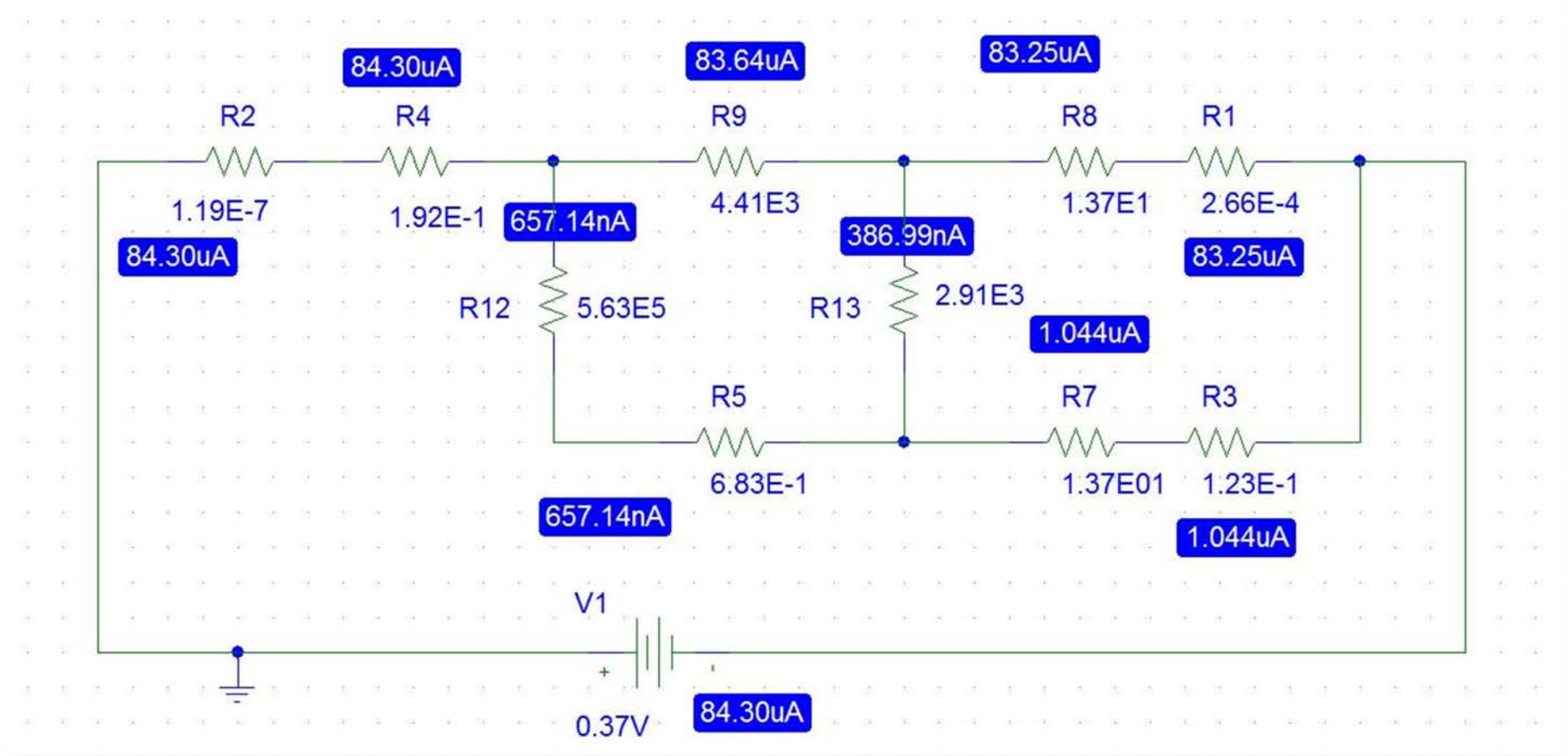

Figure 4.9a: Simulation of electrical network in Pspics with input parameters specified in text and $\eta_{act} = 0V$

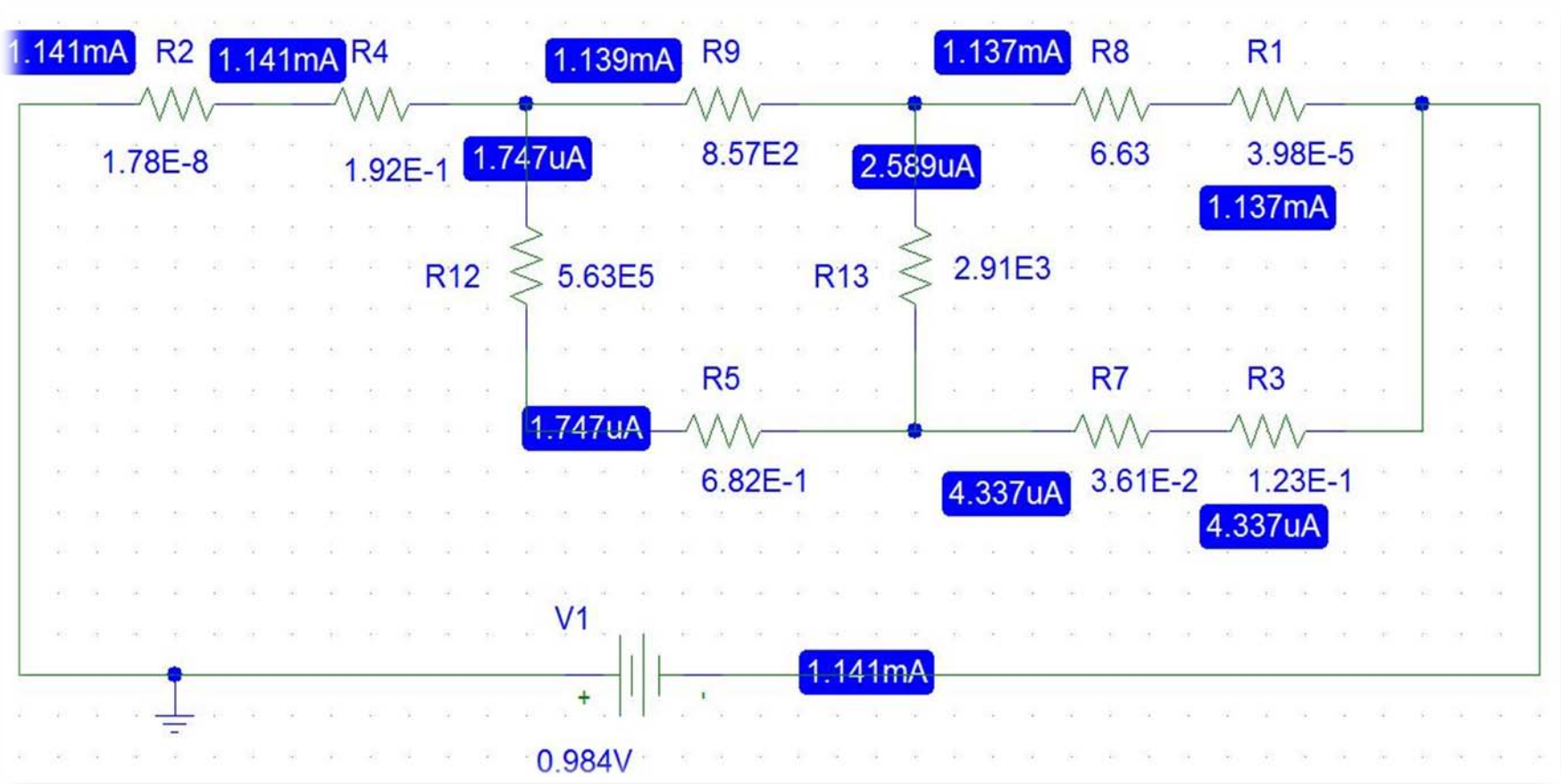

Figure 4.9b: Simulation of electrical network in Pspics with input parameters specified in text and $\eta_{act} = 0.2\ V$

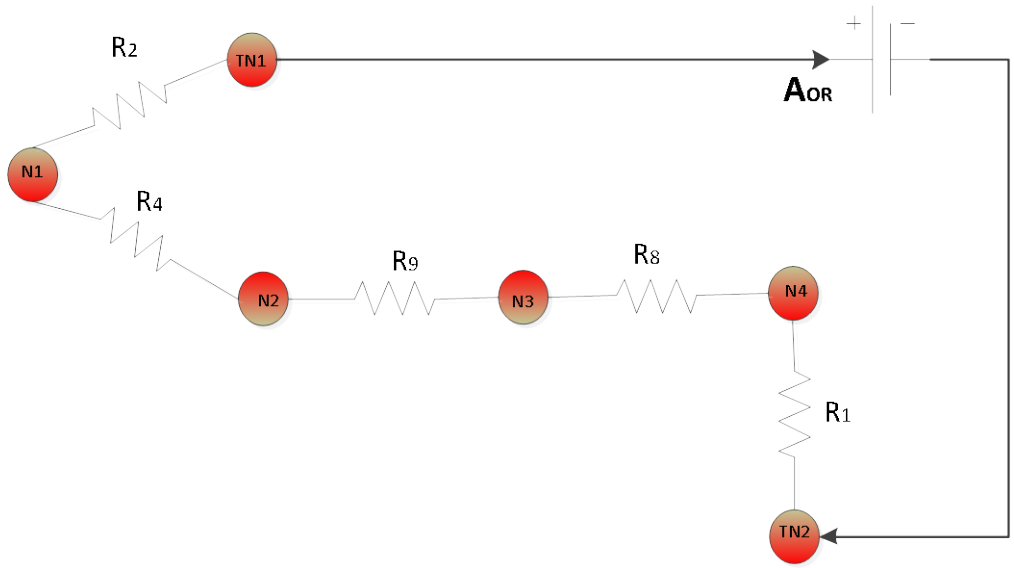

Figure 4.10: Final reduced form of RR graph for the Hydrogen oxidation reaction at Ni/YSZ indentifying FR1 as a dominant pathway.

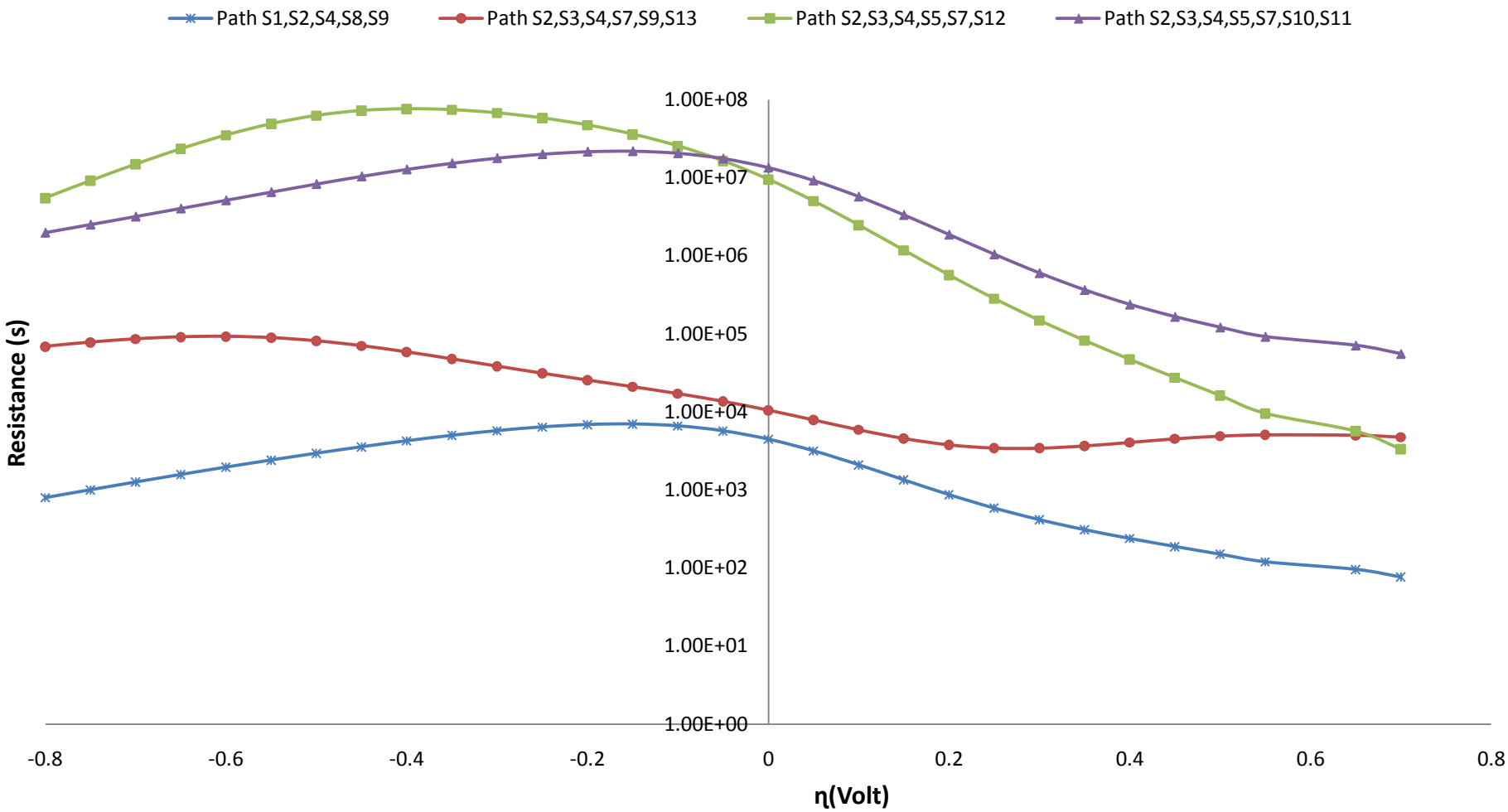

Figure 4.11: Comparison of resistances of various pathways as functions of over-potential

4.7. Explicit Rate Expression via Electrical Analogy

After the simplification process, the mechanism has also been reduced enough so that we are in a position to consider the rate of the overall reaction. By virtue of electrical circuit analogy and the linear rate law analogous to Ohm's law, a formal rate equation for the kinetics of the reduced reaction network can be developed. Therefore from the reduced graph given in Figure 4.9 the overall rate (overall current) is the ratio of the affinity of the *OR* and the overall resistance of the reaction network. The overall resistance of the reduced reaction network is

$$R_{OR} = R_1 + R_2 + R_4 + R_8 + R_9 = FR1 \tag{4.22}$$

As we know,

$$r_{OR} = \frac{\mathcal{A}_{OR}}{R_{OR}} \tag{4.23}$$

So, it can be written as

$$r_{OR} = \frac{\mathcal{A}_{OR}}{R_1 + R_2 + R_4 + R_8 + R_9} \tag{4.24}$$

Furthermore it can be seen from Figures 4.12, 4.13a and 4.13b that R_9 is a dominant step in the above sequence (FR_1), therefore;

$$r_{OR} \approx \frac{\mathcal{A}_{OR}}{R_9} \tag{4.25}$$

Although the above equations are sufficient for the numerical analysis, usually it is more advantageous to formulate an explicit rate expression in terms of terminal species i.e. reactants and products.

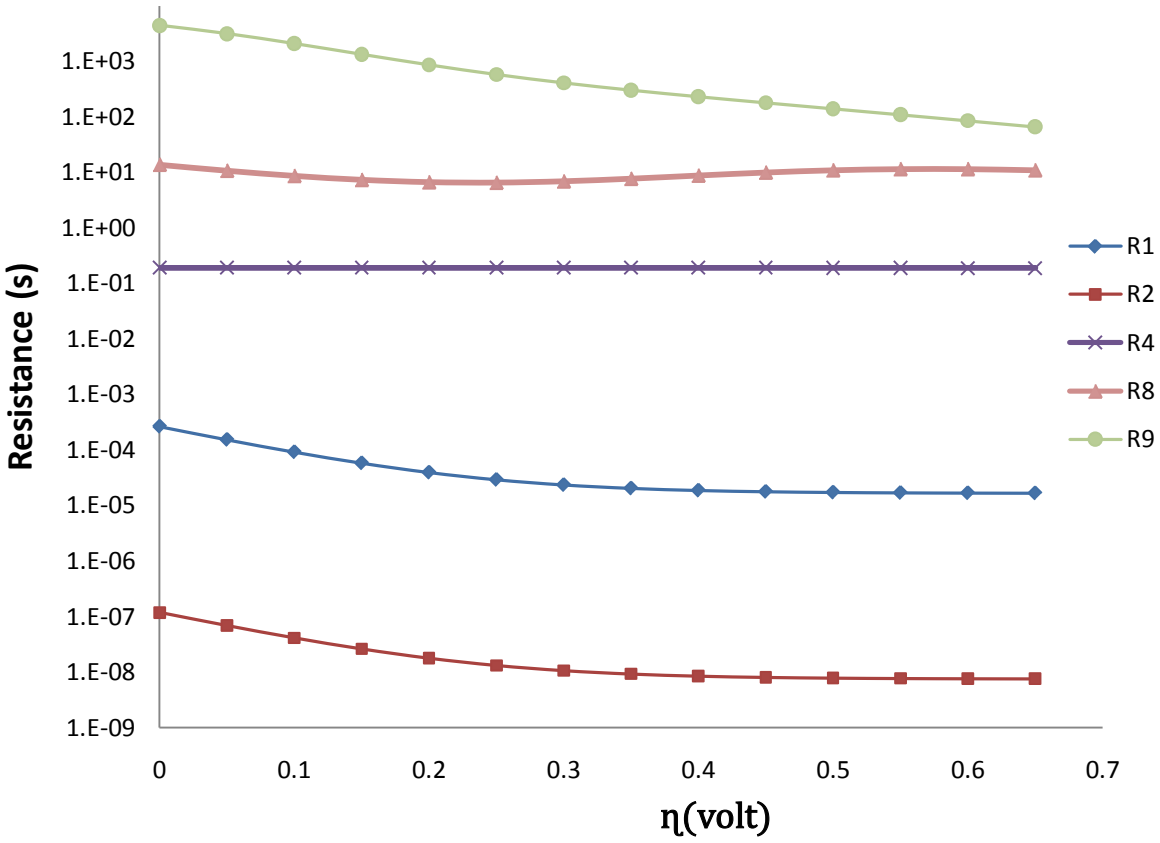

Figure 4.12: Representation of step resistance in FR_1

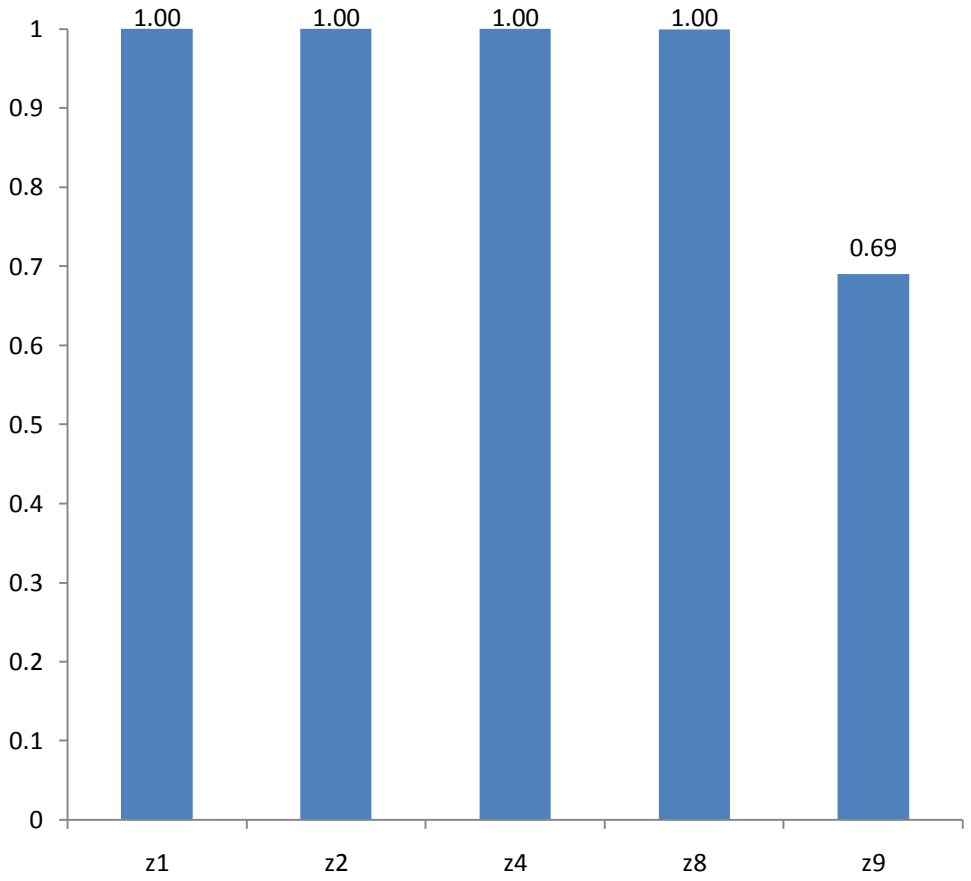

Figure 4.13a: Comparison of step reversibilities in FR_1 at $\eta_{act} = 0V$

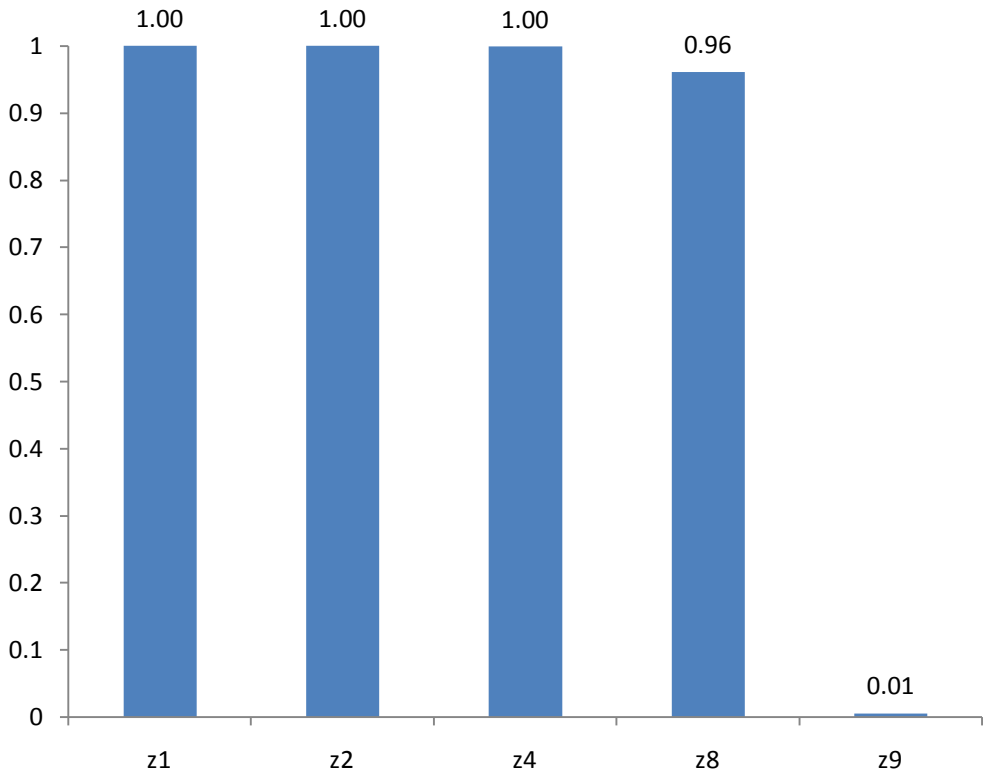

Figure 4.13b: Comparison of step reversibilities in FR_1 at $\eta_{act} = 0.2V$

This can be achieved by using so called new form of electrical analogy recently developed by Professor Datta and his co-workers [8-11]. It's important terminologies were given previously. By using that approach the rate of over all reaction can be represented as

$$r_{OR} \approx \frac{E_{OR}}{R_{OR}^{\bullet}} = \frac{E_{OR}}{R_{9}^{\bullet}} \tag{4.26}$$

Also based on the comparison of step reversibilities as given in Figures 4.13a and 4.13b, it can be perceived that in FR_1 the flux is governed by steps S_9 and all the other steps of FR_1 i.e. S_1,S_2,S_4,S_8 are quasi equilibrated. Thus

$$r_{OR} \approx \frac{E_{OR}}{R_{9}^{\bullet}} = r_9 \tag{4.27}$$

$R_9^{\bullet}$ can be achieved a priori by using the LHHW approach [11] to calculate $R_9^{\bullet}$ we assume S_9 as RDS and all the other step as QE. Therefore,

$$R_9^{\bullet} = \frac{1}{\vec{r_9^{\bullet}}} = \frac{1}{\overrightarrow{\omega_9}\theta_{H_{Ni,9}}^{\bullet}\theta_{O_{YSZ,9}^{-2}}^{\bullet}} = \frac{1}{\left(\frac{\theta_{H_{Ni,9}}^{\bullet}}{\theta_{Ni,9}^{\bullet}}\right)\left(\frac{\theta_{O_{YSZ,9}^{-2}}^{\bullet}}{\theta_{YSZ,9}^{\bullet}}\right)\left(\theta_{Ni,9}^{\bullet}\right)\left(\theta_{YSZ,9}^{\bullet}\right)} \tag{4.28}$$

In the above relation $\theta_{k,\rho}^{\bullet}$,$\theta_{Ni,\rho}^{\bullet}$ and $\theta_{YSZ,\rho}^{\bullet}$ represent the site fraction of intermediate species and of vacant site at Ni and YSZ surface respectively when a particular step S_ρ have been considered as RDS. Next the intermediate routes (IRs) for the formation of four linearly independent intermediate species involved in reduced reaction mechanism are given by

$IR_{H_2O_{YSZ}} : (-1\ S_1)$ $\qquad$ $\mathrm{H_2O_{(gas)} + [\,]_{YSZ} \leftrightarrow H_2O_{YSZ}}$

$IR_{O_{YSZ}^{-2}} : (+1\ S_2)$ $\qquad$ $\mathrm{O_{O\ YSZ}^{X} + [\,]_{YSZ} \leftrightarrow O_{YSZ}^{-2} + V_{o}^{\cdot\cdot}{}_{YSZ}}$

$IR_{OH_{YSZ}^{-1}} : \left(S_1 + \frac{1}{2}S_4 + S_8\right)$ $\qquad$ $H_2O_{(gas)} + [\,]_{YSZ} + e_{Ni}^{-} \leftrightarrow \frac{1}{2}H_{2(gas)} + \mathrm{OH_{YSZ}^{-}}$

$IR_{H_{Ni}} : \left(\frac{1}{2}S_4\right)$ $\qquad$ $\frac{1}{2}H_{2(gas)} + [\,]_{Ni} \leftrightarrow H_{Ni}$

(4.29)

For the QE steps it can written as

$$\left.\begin{aligned} \frac{\theta^{\bullet}_{H_2O_{YSZ,9}}}{\theta^{\bullet}_{YSZ,9}} &= \left(\frac{\vec{\omega}_1}{\overleftarrow{\omega}_1}\right)^{-1} \\ \frac{\theta^{-2^{\bullet}}_{O_{YSZ,9}}}{\theta^{\bullet}_{YSZ,9}} &= \left(\frac{\vec{\omega}_2}{\overleftarrow{\omega}_2}\right) \\ \frac{\theta^{-1^{\bullet}}_{OH_{YSZ,9}}}{\theta^{\bullet}_{YSZ,9}} &= \left(\frac{\vec{\omega}_1}{\overleftarrow{\omega}_1}\right)\left(\frac{\vec{\omega}_4}{\overleftarrow{\omega}_4}\right)^{\frac{1}{2}}\left(\frac{\vec{\omega}_{8,\phi_{eq}}}{\overleftarrow{\omega}_8,\phi_{eq}}\right)e^{2\psi} \\ \frac{\theta^{\bullet}_{H_{Ni,9}}}{\theta^{\bullet}_{Ni,9}} &= \left(\frac{\vec{\omega}_4}{\overleftarrow{\omega}_4}\right)^{\frac{1}{2}} \end{aligned}\right\} \quad (4.30)$$

The site balance equations are

$$\frac{1}{\theta^{\bullet}_{YSZ,9}} = 1 + \frac{\theta^{-1^{\bullet}}_{OH_{YSZ,9}}}{\theta^{\bullet}_{YSZ,9}} + \frac{\theta^{\bullet}_{H_2O_{YSZ,9}}}{\theta^{\bullet}_{YSZ,9}} + \frac{\theta^{-2^{\bullet}}_{O_{YSZ,9}}}{\theta^{\bullet}_{YSZ,9}}$$

$$\frac{1}{\theta^{\bullet}_{Ni,9}} = 1 + \frac{\theta^{\bullet}_{H_{Ni,9}}}{\theta^{\bullet}_{Ni,9}} + \frac{\theta^{\bullet}_{OH_{Ni,9}}}{\theta^{\bullet}_{Ni,9}} + \frac{\theta^{\bullet}_{H_2O_{Ni,9}}}{\theta^{\bullet}_{Ni,9}} + \frac{\theta^{\bullet}_{O_{Ni,9}}}{\theta^{\bullet}_{Ni,9}} + \frac{\theta^{\bullet}_{O^{-}_{Ni,9}}}{\theta^{\bullet}_{Ni,9}} \quad (4.31)$$

Using equations 4.28-4.31 we have

$$R^{\bullet}_9 = \frac{1}{\vec{\omega}_9\left(\frac{\vec{\omega}_4}{\overleftarrow{\omega}_4}\right)^{\frac{1}{2}}\left(\frac{\vec{\omega}_2}{\overleftarrow{\omega}_2}\right)}\left\{\left(1+\left(\frac{\vec{\omega}_4}{\overleftarrow{\omega}_4}\right)^{\frac{1}{2}}\right)\left(1+\left(\frac{\vec{\omega}_1}{\overleftarrow{\omega}_1}\right)\left(\frac{\vec{\omega}_4}{\overleftarrow{\omega}_4}\right)^{\frac{1}{2}}\left(\frac{\vec{\omega}_{8,\phi_{eq}}}{\overleftarrow{\omega}_8,\phi_{eq}}\right)e^{2\psi}+\left(\frac{\vec{\omega}_1}{\overleftarrow{\omega}_1}\right)^{-1}+\left(\frac{\vec{\omega}_2}{\overleftarrow{\omega}_2}\right)\right)\right\} \quad (4.32)$$

$$E_{OR} = 1 - z_{OR} = \frac{\overleftarrow{\omega}_1 \overleftarrow{\omega}_2 \overleftarrow{\omega}_4 \overleftarrow{\omega}_{8,\phi_{eq}} \overleftarrow{\omega}_{9,\phi_{eq}}}{\vec{\omega}_1 \vec{\omega}_2 \vec{\omega}_4 \vec{\omega}_{8,\phi_{eq}} \vec{\omega}_{9,\phi_{eq}}} e^{4\psi} \tag{4.33}$$

By using equations 4.17, 4.27, 4.32 and 4.33, an expression for current density can be developed as given below;

$$i = zl_{TBP}\left[\frac{\left(1-\frac{\overleftarrow{\omega}_1\overleftarrow{\omega}_2\overleftarrow{\omega}_4\overleftarrow{\omega}_{8,\phi_{eq}}\overleftarrow{\omega}_{9,\phi_{eq}}}{\vec{\omega}_1\vec{\omega}_2\vec{\omega}_4\vec{\omega}_{8,\phi_{eq}}\vec{\omega}_{9,\phi_{eq}}}e^{4\psi}\right)}{\frac{1}{\vec{\omega}_{9,\phi_{eq}}e^{\psi}\left(\frac{\vec{\omega}_4}{\overleftarrow{\omega}_4}\right)^{\frac{1}{2}}\left(\frac{\vec{\omega}_2}{\overleftarrow{\omega}_2}\right)}\left\{\left(1+\left(\frac{\vec{\omega}_4}{\overleftarrow{\omega}_4}\right)^{\frac{1}{2}}\right)\left(1+\left(\frac{\vec{\omega}_1}{\overleftarrow{\omega}_1}\right)\left(\frac{\vec{\omega}_4}{\overleftarrow{\omega}_4}\right)^{\frac{1}{2}}\left(\frac{\vec{\omega}_{8,\phi_{eq}}}{\overleftarrow{\omega}_{8,\phi_{eq}}}\right)e^{2\psi}+\left(\frac{\vec{\omega}_1}{\overleftarrow{\omega}_1}\right)^{-1}+\left(\frac{\vec{\omega}_2}{\overleftarrow{\omega}_2}\right)\right)\right\}}\right] \tag{4.34}$$

At equilibrium as $\eta_{act} \rightarrow 0$ so that the $\psi \rightarrow 0$ and the net current $i \rightarrow 0$ and i_{eq} (exchange current density) can be written as

$$i_{eq} = zl_{TBP}\left[\frac{\left(1-\frac{\overleftarrow{\omega}_1\overleftarrow{\omega}_2\overleftarrow{\omega}_4\overleftarrow{\omega}_{8,\phi_{eq}}\overleftarrow{\omega}_{9,\phi_{eq}}}{\vec{\omega}_1\vec{\omega}_2\vec{\omega}_4\vec{\omega}_{8,\phi_{eq}}\vec{\omega}_{9,\phi_{eq}}}\right)}{\frac{1}{\vec{\omega}_{9,\phi_{eq}}\left(\frac{\vec{\omega}_4}{\overleftarrow{\omega}_4}\right)^{\frac{1}{2}}\left(\frac{\vec{\omega}_2}{\overleftarrow{\omega}_2}\right)}\left\{\left(1+\left(\frac{\vec{\omega}_4}{\overleftarrow{\omega}_4}\right)^{\frac{1}{2}}\right)\left(1+\left(\frac{\vec{\omega}_1}{\overleftarrow{\omega}_1}\right)\left(\frac{\vec{\omega}_4}{\overleftarrow{\omega}_4}\right)^{\frac{1}{2}}\left(\frac{\vec{\omega}_{8,\phi_{eq}}}{\overleftarrow{\omega}_8,\phi_{eq}}\right)+\left(\frac{\vec{\omega}_1}{\overleftarrow{\omega}_1}\right)^{-1}+\left(\frac{\vec{\omega}_2}{\overleftarrow{\omega}_2}\right)\right)\right\}}\right] \tag{4.35}$$

With the reaction conditions used in this study, equation 4.35 provides a value of $i_{eq} = 8.3E-5$ A/cm^2, which compares well with the simulation results of Vogler et al. and Bieberle et al. [6, 7, 25]. Moreover accuracy of both equations 4.34 and 4.35 have been demonstrated in the next section by comparing the results with the published literature.

4.8. Comparison of the results

Based on the analysis given in section 4.5 it is evident that FR_1 is a dominant pathway, it involves two hydrogen spill-over charge transfer reactions. This conclusion also concurs with the finding of Voglar et al. [6, 7] who suggested that hydrogen spill-over reactions (S_8 and S_9) can best describe the experimental data [39]. However, previously the steps that govern the rate of overall reaction had not been pointed out. Based on this mechanistic analysis through RR Graph approach, it is concluded that both of the hydrogen spill-over reaction are active in the considered reaction condition as given in Table 4.3. But S_9 contributes more towards the overall rate of reaction at Ni/YSZ surface. To further validate the results, we make a comparison of numerical simulation results of this study and the result of Vogler et al. [6, 7] (for two hydrogen spill-over reactions) and experimental results of Bieberle et al. [25] in the form of polarization curves, which is an efficient method to characterize the performance of electrochemical systems. The curves are shown in Figure 4.14. Based on the similarity of results, we conclude that FR_1 composed of steps S_1, S_2, S_4, S_8 and S_9 is the overall rate governing sequence as compared to other pathways. The results of this study also demonstrate efficacy of RR graph approach and confirm that it is robust tool for the analysis of electrochemical systems. Furthermore we also make a comparison between the results obtained from QSS numerical simulation and that of rate expression derived using the so called new form of electrical analogy given in Figure 4.14, which are in very good agreement and again endorse the efficacy and usefulness of rate expression developed using electrical analogy of RR graph.

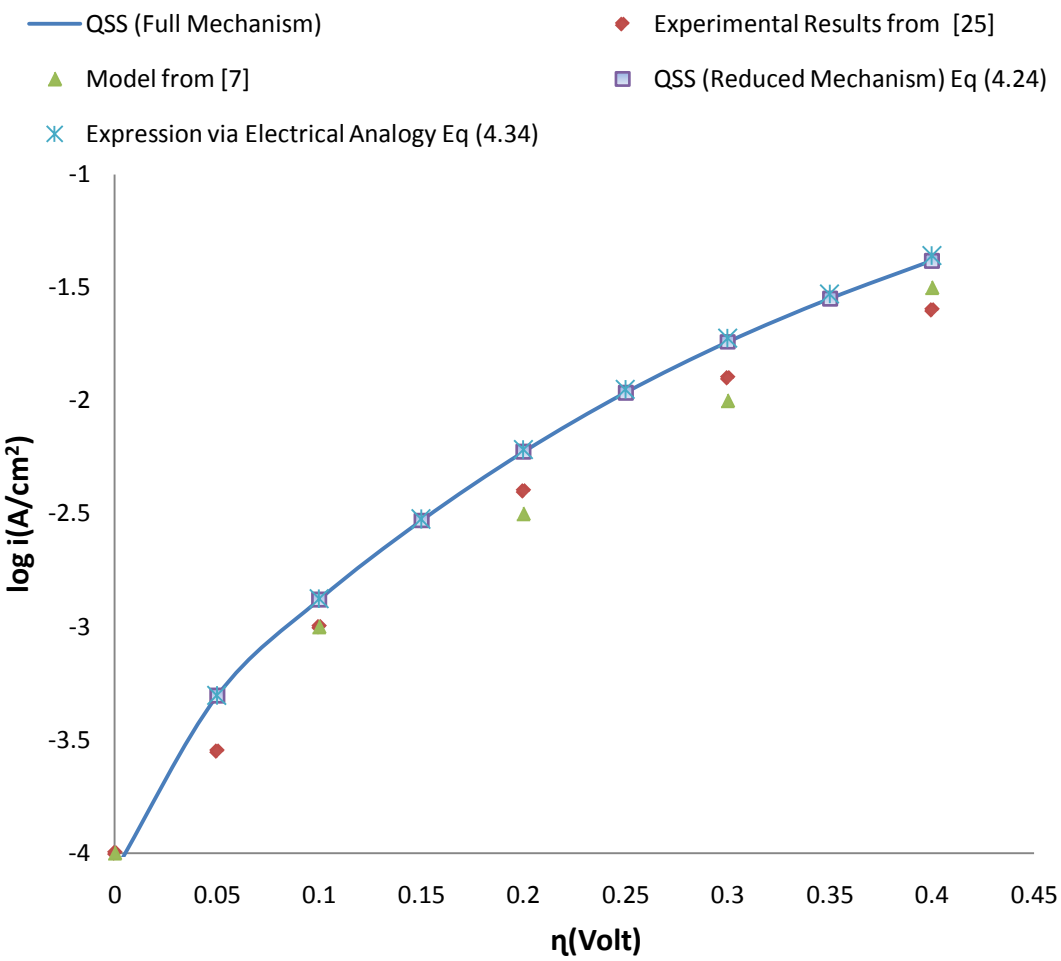

Figure 4.14: Comparison of the polarization curves with the experimental results and other studies

4.9. Conclusions

Through the use of RR graph scheme and its analogy with electrical circuit theory for hydrogen oxidation at Ni/YSZ SOFC anode, it was observed that there is one dominant pathway named as $FR_{1,}$ and hydrogen spill-over to oxide ion (S_9) is the rate limiting step governing the rate of over-all reaction, the same conclusion was also reported by Anderson et al. [69] and Vogler et al. [6, 7]. Further an explicit rate expression was also developed in terms of terminal species via new form of electrical analogy. A good quantitative agreement between numerical simulation based on QSS analysis and derived rate expressions with published literature in the form of polarization curves was also obtained, which strongly demonstrate the capability and effectiveness of the RR graph schematics.

Chapter 5

5.1. Conclusions

In this research work, a graph theoretic approach called the RR graph has been employed to investigate the kinetics of the hydrogen oxidation reaction at Ni/YSZ anode of an SOFC. An RR graph has been constructed for the hydrogen oxidation reaction mechanism, with the most promising elementary steps collected from across the literature. This graph reveals all the intertwined reaction pathways that lead to the overall reaction of hydrogen oxidation at the SOFC anode. Exploiting the electrical analogy, the step resistances were defined. Comparisons of the resistances of the competing pathways lead to a reduced graph. This reduced graph facilitated the derivation of an analytical expression for the overall reaction rate using the electrical analogy. The rate expression, obtained for the first time, was found to approximate the overall rate obtained using the conventional QSS methodology satisfactorily. Further, the graphical representation allows us to determine the pathway that is dominant in the mechanism. The pathway FR_1, containing the two hydrogen spill-over reactions was identified as the dominant one. Further investigation of this particular sequence of steps revealed that hydrogen spill-over to oxide ion (S_9) is the slowest reaction step with highest step resistance and governs the rate of over all reaction.

5.2. Recommendations for further work

The recommendations for further work in this area are given as follows.

- Although, the kinetic and thermodynamic data used in this study belongs to most consistent and holistic data set found in literature, they are based on fitting the parameters to some experimental curves. There is a need for experimental work to calculate rate parameters using fundamental methods. The accuracy of the predictions will be improved by using accurate rate parameters in the calculations.
- Only the anodic reaction of the SOFC was analysed in this work. However, there are indications that some of the cathodic reactions may be rate determining. Hence further studies should consider the fuel cell reaction as

a whole including both the anodic and the cathodic reactions to perform a more comprehensive study of their kinetics.

- Currently, there are no specific steps or methodology for the construction of the RR graph. Each mechanism has to be treated in a unique fashion. If some procedure could be developed for the graph construction, especially for non-minimal mechanisms, a lot of effort could be saved.

References

1. Hoogers, G., E. Chen, D. Thompsett, and M. Hogarth, eds. *FUEL CELL TECHNOLOGY HAND BOOK*. ed. G. Hoogers. 2003.
2. James Larminie, A.D., *Fuel Cell Systems Explained (second edition)*. 2003.
3. EG&G Services Parsons, I., *Fuel Cell Handbook (Fifth Edition)*. 2000, Morgantown, West Virginia.
4. Singhal, S.r. and K. Kendall, *High Temperature Solid Oxide Fuel Cells*. 2003.
5. Boer, B.d., *PhD Thesis, Hydrogen oxidation at porous nickel and nickel/yttriastabilised zirconia cermet electrodes*. 1998, University of Twente: Twente.
6. Vogler, M., *PhD Thesis, Elementary kinetic modelling applied to solid oxide fuel cell pattern anodes and a direct flame fuel cell system*. 2009, Ruperto-Carola University of Heidelberg.
7. Vogler, M., A. Bieberle-Hutter, L. Gauckler, J. Warnatz, and W.G. Bessler, *Modelling Study of Surface Reactions, Diffusion, and Spillover at a Ni/YSZ Patterned Anode.* Journal of The Electrochemical Society, 2009. 156(5): p. B663-B672.
8. Fishtik, I., C.A. Callaghan, and R. Datta, *Reaction Route Graphs. I. Theory and Algorithm.* The Journal of Physical Chemistry B, 2004. 108(18): p. 5671-5682.
9. Fishtik, I., C.A. Callaghan, and R. Datta, *Reaction Route Graphs. II. Examples of Enzyme- and Surface-Catalyzed Single Overall Reactions.* J. Phys. Chem., 2004. 108: p. 5683-5697.
10. Datta, R., C.A. Cllanghan., and F. Lllie, *Reaction Route Graphs. 3.Non-minimal Kinectic Mechanism.* J. Phys. Chem., 2005. 109(39-40): p. 2710-2722.
11. Vilekar, S.A., *PhD Thesis, Catalytic and Electrocatalytic Pathways in Fuel Cells*, in *Department of Chemical Engineering*. 2010, WORCESTER POLYTECHNIC INSTITUTE, USA.
12. A. Hammou and J. Guindet, *The CRC Handbook of Solid-State Electrochemistry*. 1997. p. 409-445.
13. Wikipedia. *Fuel cell*. 5 Feb 2011 at 18:27 [cited 2011 5-02]; Available from: http://en.wikipedia.org/wiki/Fuel_cell.
14. Ho, T.X., *PhD Thesis, Modeling of Transport, Chemical and Electrochemical Processes in Solid Oxide Fuel Cell* 2009, University of Bergen.
15. Goodridge, F. and K. Scott, *Electrochemical Process Engineering*. 1995, New York: Plenum Press.
16. Ugur, P. and W. Chao-Yang. *Computational fluid dynamics modeling of solid oxide fuel cells*. in *Proceedings of the Electrochemical Society (Solid oxide fuels cells VIII)*. 2003. Paris.
17. Bieberle, A. and L.J. Gauckler, *State-space modeling of the anodic SOFC system Ni, H2-H2O|YSZ.* Solid State Ionics, 2002. 146(1-2): p. 23-41.
18. J. Guindet, C. Roux, and A. Hammou. *Hydrogen oxidation at the Ni/Zirconia electrode*. in *Proc. of the 2nd Int. Symp. on Solid Oxide Fuel Cells*. 1991. Athens, Greece.
19. T. Norby, O.J. Velle, H. Leth-Olsen, and R. Tunold. *Reaction resistance in relation to three phase boundary length of Ni/YSZ electrodes*. in *Proc. Of the 3rd Int. Symp. On Solid Oxide Fuel Cells*. 1993. Honolulu, Hawaii.
20. P.A. Osborg and T. Norby. *Characterisation of a H2+H2O/Ni/YSZ point electrode system by impedance spectroscopy*. in *7th SOFC Workshop, theory and*

measurement of microscale processes in Solid Oxide Fuel Cells. 1995. Wadahl, Norway.

21. Mizusaki, J., H. Tagawa, T. Saito, T. Yamamura, K. Kamitani, K. Hirano, S. Ehara, T. Takagi, T. Hikita, M. Ippommatsu, S. Nakagawa, and K. Hashimoto, *Kinetic studies of the reaction at the nickel pattern electrode on YSZ in H2---H2O atmospheres.* Solid State Ionics, 1994. 70-71(Part 1): p. 52-58.
22. Mizusaki, J., H. Tagawa, T. Saito, K. Kamitani, T. Yamamura, K. Hirano, S. Ehara, T. Takagi, T. Hikita, M. Ippommatsu, S. Nakagawa, and K. Hashimoto, *Preparation of Nickel Pattern Electrodes on YSZ and Their Electrochemical Properties in H_2-H_2O Atmospheres.* Journal of The Electrochemical Society, 1994. 141(8): p. 2129-2134.
23. N. Nakagawa, H. Sakurai, K. Kondo, and K. Kato. *Study on the extension of reaction zone from Ni/YSZ interface by using fixed film electrodes*. in *Proc. of the 4th Int. Symp. On SOFC-IV*. 1995. Yokohama, Japan.
24. Bieberle, A. and L.J. Gauckler, *Reaction mechanism of Ni pattern anodes for solid oxide fuel cells.* Solid State Ionics, 2000. 135(1-4): p. 337-345.
25. Bieberle, A., L.P. Meier, and L.J. Gauckler, *The Electrochemistry of Ni Pattern Anodes Used as Solid Oxide Fuel Cell Model Electrodes.* Journal of The Electrochemical Society, 2001. 148(6): p. A646-A656.
26. Ehn, A., J. Hogh, M. Graczyk, K. Norrman, L. Montelius, M. Linne, and M. Mogensen, *Electrochemical Investigation of Nickel Pattern Electrodes in H[sub 2]/H[sub 2]O and CO/CO[sub 2] Atmospheres.* Journal of The Electrochemical Society, 2010. 157(11): p. B1588-B1596.
27. Mogensen, M. and S. Skaarup, *Kinetic and geometric aspects of solid oxide fuel cell electrodes.* Solid State Ionics, 1996. 86-88(Part 2): p. 1151-1160.
28. Primdahl, S. and M. Mogensen, *Oxidation of Hydrogen on Ni/Yttria-Stabilized Zirconia Cermet Anodes.* Journal of The Electrochemical Society, 1997. 144(10): p. 3409-3419.
29. Jiang, S.P. and S.P.S. Badwal, *Hydrogen Oxidation at the Nickel and Platinum Electrodes on Yttria-Tetragonal Zirconia Electrolyte.* Journal of The Electrochemical Society, 1997. 144(11): p. 3777-3784.
30. Jiang, S.P. and S.P.S. Badwal, *An electrode kinetics study of H2 oxidation on Ni/Y2O3-ZrO2 cermet electrode of the solid oxide fuel cell.* Solid State Ionics, 1999. 123(1-4): p. 209-224.
31. Jiang, S.P. and Y. Ramprakash, *H2 oxidation on Ni/Y-TZP cermet electrodes - polarisation behaviour.* Solid State Ionics, 1999. 116(1-2): p. 145-156.
32. Gewies, S., W.G. Bessler, V. Sonn, and E. Ivers-Tiffee, *Experimental and Modeling Study of the Impedance of Ni/YSZ Cermet Anodes.* ECS Transactions, 2007. 7(1): p. 1573-1582.
33. Horita, T., H. Kishimoto, K. Yamaji, Y. Xiong, N. Sakai, M.E. Brito, and H. Yokokawa, *Materials and reaction mechanisms at anode/electrolyte interfaces for SOFCs.* Solid State Ionics, 2006. 177(19-25): p. 1941-1948.
34. Williford, R.E. and L.A. Chick, *Surface diffusion and concentration polarization on oxide-supported metal electrocatalyst particles.* Surface Science, 2003. 547(3): p. 421-437.
35. Bessler, W.G., J. Warnatz, and D.G. Goodwin, *The influence of equilibrium potential on the hydrogen oxidation kinetics of SOFC anodes.* Solid State Ionics, 2007. 177(39-40): p. 3371-3383.
36. Marcel Vogler, W.G.B., Jürgen Warnatz, and A.B.-H.a.L.J. Gauckler. *Towards an Understanding of Ni Anodes in Solid Oxide Fuel Cells: Electrochemical Modeling and Experimental Validation Using Patterned Anodes*. in *I7th European SOFC Forum,*. 2006. Lucerne, Switzerland,.

37. Raz, S., K. Sasaki, J. Maier, and I. Riess, *Characterization of adsorbed water layers on Y2O3-doped ZrO2.* Solid State Ionics, 2001. 143(2): p. 181-204.
38. Vogler, M. and W.G. Bessler, *The Role of Interstitial Hydrogen Species in Ni/YSZ Patterned Anodes: A 2D Modeling Study.* ECS Transactions, 2009. 25(2): p. 1957-1966.
39. Bessler, W.G., S. Gewies, and M. Vogler, *A new framework for physically based modeling of solid oxide fuel cells.* Electrochimica Acta, 2007. 53(4): p. 1782-1800.
40. Mitterdorfer, A. and L.J. Gauckler, *Identification of the reaction mechanism of the Pt, O2(g)yttria-stabilized zirconia system: Part I: General framework, modelling, and structural investigation.* Solid State Ionics, 1999. 117(3-4): p. 187-202.
41. Setoguchi, T., K. Okamoto, K. Eguchi, and H. Arai, *Effects of Anode Material and Fuel on Anodic Reaction of Solid Oxide Fuel Cells.* Journal of The Electrochemical Society, 1992. 139(10): p. 2875-2880.
42. Kek, D., M. Mogensen, and S. Pejovnik, *A Study of Metal (Ni, Pt, Au)/Yttria-Stabilized Zirconia Interface in Hydrogen Atmosphere at Elevated Temperature.* Journal of The Electrochemical Society, 2001. 148(8): p. A878-A886.
43. Vayenas, C.G., S. Brosda, and C. Pliangos, *The double-layer approach to promotion, electrocatalysis, electrochemical promotion, and metal-support interactions.* Journal of Catalysis. 216(1-2): p. 487-504.
44. Metcalfe, I.S., *Electrochemical Promotion of Catalysis: I: Thermodynamic Considerations.* Journal of Catalysis, 2001. 199(2): p. 247-258.
45. Bultel, L., C. Roux, E. Siebert, P. Vernoux, and F. Gaillard, *Electrochemical characterisation of the Pt/YSZ interface exposed to a reactive gas phase.* Solid State Ionics, 2004. 166(1-2): p. 183-189.
46. Zhu, H., R.J. Kee, V.M. Janardhanan, O. Deutschmann, and D.G. Goodwin, *Modeling Elementary Heterogeneous Chemistry and Electrochemistry in Solid-Oxide Fuel Cells.* Journal of The Electrochemical Society, 2005. 152(12): p. A2427-A2440.
47. Cao, G.X., E. Nabighian, and X.D. Zhu, *Diffusion of Hydrogen on Ni(111) over a Wide Range of Temperature: Exploring Quantum Diffusion on Metals.* Physical Review Letters, 1997. 79(19): p. 3696.
48. Chebotin, V., M. Glumov, A. Neuimin, and S. Palguev, *Polarization of a hydrogen electrode on a solid oxide electrolyte.* Soviet Electrochemistry, 1971. 7: p. 55-60.
49. Holtappels, P., I.C. Vinke, L.G.J. de Haart, and U. Stimming, *Reaction of Hydrogen/Water Mixtures on Nickel-Zirconia Cermet Electrodes: II. AC Polarization Characteristics.* Journal of The Electrochemical Society, 1999. 146(8): p. 2976-2982.
50. Brown, M., S. Primdahl, and M. Mogensen, *Structure/Performance Relations for Ni/Yttria-Stabilized Zirconia Anodes for Solid Oxide Fuel Cells.* Journal of The Electrochemical Society, 2000. 147(2): p. 475-485.
51. Nowotny, J., C.C. Sorrell, and T. Bak, *Segregation in zirconia: equilibrium versus non-equilibrium segregation.* Surface and Interface Analysis, 2005. 37(3): p. 316-324.
52. Vels Jensen, K., S. Primdahl, I. Chorkendorff, and M. Mogensen, *Microstructural and chemical changes at the Ni/YSZ interface.* Solid State Ionics, 2001. 144(3-4): p. 197-209.
53. Hansen, K.V., K. Norrman, and M. Mogensen, *H[sub 2]-H[sub 2]O-Ni-YSZ Electrode Performance.* Journal of The Electrochemical Society, 2004. 151(9): p. A1436-A1444.
54. Sakai, N., K. Yamaji, T. Horita, Y.P. Xiong, H. Kishimoto, M.E. Brito, and H. Yokokawa, *Effect of water on electrochemical oxygen reduction at the interface between fluorite-type oxide-ion conductors and various types of electrodes.* Solid State Ionics, 2004. 174(1-4): p. 103-109.

55. Vijay, P., A.K. Samantaray, and A. Mukherjee, *Development of a thermodynamically consistent kinetic model for reactions in the solid oxide fuel cell.* Computers & Chemical Engineering, 2009. 34(6): p. 866-877.
56. Bessler, W.G., *A new computational approach for SOFC impedance from detailed electrochemical reaction-diffusion models.* Solid State Ionics, 2005. 176(11-12): p. 997-1011.
57. Goodwin, D.G., H. Zhu, A.M. Colclasure, and R.J. Kee, *Modeling Electrochemical Oxidation of Hydrogen on Ni--YSZ Pattern Anodes.* Journal of The Electrochemical Society, 2009. 156(9): p. B1004-B1021.
58. Mukherjee, J. and S. Linic, *First-Principles Investigations of Electrochemical Oxidation of Hydrogen at Solid Oxide Fuel Cell Operating Conditions.* Journal of The Electrochemical Society, 2007. 154(9): p. B919-B924.
59. Rossmeisl, J. and W.G. Bessler, *Trends in catalytic activity for SOFC anode materials.* Solid State Ionics, 2008. 178(31-32): p. 1694-1700.
60. Shishkin, M. and T. Ziegler, *Oxidation of H2, CH4, and CO Molecules at the Interface between Nickel and Yttria-Stabilized Zirconia: A Theoretical Study Based on DFT.* J. Phys. Chem., 2009: p. 21667–21678.
61. Ioselevich, A.S. and A.A. Kornyshev, *Phenomenological Theory of Solid Oxide Fuel Cell Anode.* Fuel Cells, 2001. 1(1): p. 40-65.
62. Janardhanan, V.M. and O. Deutschmann, *CFD analysis of a solid oxide fuel cell with internal reforming: Coupled interactions of transport, heterogeneous catalysis and electrochemical processes.* Journal of Power Sources, 2006. 162(2): p. 1192-1202.
63. Vilekar, S.A., I. Fishtik, and R. Datta, *Topological analysis of catalytic reaction networks: Methanol decomposition on Pt(111).* Journal of Catalysis, 2007. 252(2): p. 258-270.
64. Fishtik, I., C.A. Callaghan, J.D. Fehribach, and R. Datta, *A reaction route graph analysis of the electrochemical hydrogen oxidation and evolution reactions.* Journal of Electroanalytical Chemistry, 2005. 576(1): p. 57-63.
65. Vilekar, S., I. Fishtik, and R. Datta, *Kinetics of the Hydrogen Electrode Reaction.* ECS Meeting Abstracts, 2010. 1002(10): p. 979-979.
66. Vilekar, S.A., I. Fishtik, and R. Datta, *The steady-state kinetics of parallel reaction networks.* Chemical Engineering Science, 2009. 65(10): p. 2921-2933.
67. Cadence, D.S. *PSpice Schematics*. 2010 [cited 2010 09-10]; Available from: http://www.cadence.com.
68. Atkins, P.W., *Physical Chemistry (Fifth edition)*. 1994: Oxford University Press.
69. Anderson, A.B. and E. Vayner, *Hydrogen oxidation and proton transport at the Ni-zirconia interface in solid oxide fuel cell anodes: Quantum chemical predictions.* Solid State Ionics, 2006. 177(15-16): p. 1355-1359.